A Szilikátipari Tudományos Egyesület lapja

építőanyag

Journal of Silicate Based and Composite Materials

A TARTALOMBÓL:

2020/3

TURKEYTRIB 2020 3rd INTERNATIONAL CONFERENCE ON TRIBOLOGY

~~June 18-20 2020~~ POSTPONED TO DECEMBER 2020

CONFERENCE VENUE: Elite World Prestige Hotel
ADDRESS: Şehit Muhtar Caddesi No:40, 34435 Taksim Istanbul-TURKEY
WELCOME TO TURKEYTRIB 2020!

We are very pleased to announce that the 3rd International Conference on Tribology TURKEYTRIB 2020 will be held from 18 to 20 June 2020 at the Elite World Prestige Hotel Taksim-İstanbul-TURKEY. The scope of this conference embraces the state of art and future trends in tribology research and application, emphasizing the necessity of facilitation intellectual collaboration across both disciplinary and national-international boundaries. The main objective of the conference is to provide a unique opportunity of presenting and discussing recent developments in different aspects of Tribology and strengthen the linkage between academia and industry. The conference consists of scientific sessions, symposia on specific topics, exhibitions and various collateral events. Turkish and Foreign groups of experts will have chance to share information and get in touch with other groups in all part of Tribology. Nowadays these aspects are becoming more and more important both in respect of human life and environment.

– SPECIAL ISSUE (Web of Science Core Collection-Emerging Sources Citation Index): Selected high-quality papers (10) presented at the TurkeyTrib'20 conference will be selected and invited to submit their contributions for Special Issue publication in Építőanyag - Journal of Silicate Based and Composite Materials. (SCIE; Impact Factor 1.079 (2018). The submission due is 30 June 2020.

www.turkeytribconference.com/index.php/en/

TURKEYTRIB 2020
3rd INTERNATIONAL CONFERENCE TRIBOLOGY
18-20 JUNE
ELITE WORLD PRESTIGE HOTEL-TAKSIM
ISTANBUL-TURKEY

építőanyag

Journal of Silicate Based and Composite Materials

2020/3

TARTALOM

CONTENT

A finomkerámia-, üveg-, cement-, mész-, beton-, tégla- és cserép-, kő- és kavics-, tűzállóanyag-, szigetelőanyag-iparágak szakmai lapja
Scientific journal of ceramics, glass, cement, concrete, clay products, stone and gravel, insulating and fireproof materials and composites

A folyóiratot referálja · The journal is referred by:
MTA SZTAKI · ProQuest · Emerging Sources Citation Index · Google Scholar · INDEX COPERNICUS INTERNATIONAL · THOMSON REUTERS

A folyóiratban lektorált cikkek jelennek meg.
All published papers are peer-reviewed.
Kiadó · Publisher: Szilikátipari Tudományos Egyesület (SZTE)
Elnök · President: ASZTALOS István
1034 Budapest, Bécsi út 122–124.
Tel.: +36-1/201-9360 ▪ E-mail: epitoanyag@szte.org.hu
Tördelő szerkesztő · Layout editor: NÉMETH Hajnalka
Címlapfotó · Cover photo: GYURKÓ Zoltán

WWW.EPITOANYAG.ORG.HU
EN.EPITOANYAG.ORG.HU

Online ISSN: 2064-4477
Print ISSN: 0013-970x
INDEX: 2 52 50 ▪ 72 (2020) 79-116

Overview of ash as supplementary cementitious silicate-based composite and construction material

Salak építőanyagként és cement kiegészítő anyagként való alkalmazásának áttekintése

Kennedy Chibuzor ONYELOWE ▪ Department of Civil Engineering, Michael Okpara University of Agriculture, Nigeria ▪ konyelowe@mouau.edu.ng

Favour Adaugo Deborah ONYELOWE ▪ Department of Civil Engineering, Faculty of Engineering, Alex Ekwueme Federal University, Nigeria ▪ adaugofavour3@gmail.com

Duc BUI VAN ▪ Research Group of Geotechnical Engineering, Construction Materials and Sustainability, Hanoi University of Mining and Geology, Vietnam ▪ buivanduc@humg.edu.vn

Ifeyinwa I. OBIANYO ▪ Department of Material Science and Engineering, African University of Science and Technology, Nigeria

Sylvia E. KELECHI ▪ Department of Material Science and Engineering, African University of Science and Technology, Nigeria

Érkezett: 2019. 12. 31. ▪ Received: 31. 12. 2019. ▪ https://doi.org/10.14382/epitoanyag-jsbcm.2020.13

Abstract

The potential of ash as supplementary cementitious material with high silicate-based pozzolanic composition has been reviewed. Construction activities based on the utilization of ordinary cement have contributed hugely to the greenhouse emission due to the release of CO_2 into the atmosphere. The review was aimed at presenting the achievements that have been made using ash as a replacement for ordinary cement. Also, the source of ash from biomass and the biotechnological procedure involved in its usage have been reviewed. From the results so far reviewed, it has been observed that ash is an amorphous nonbiodegradable material with high aluminosilicates composition. This behavior makes it suitable for it to be utilized as alternative binder in problematic soils stabilization. Results also showed that the index and strength characteristics of expansive soils were improved substantially with increased proportion of ash, which included plasticity index, compaction, gradation, compression, California bearing ratio, resilient modulus and resistant value. Generally, it can be observed that ash is a good replacement for cement as a construction material.

Keywords: biomass, bio-based ash, solid waste recycling (SWR), biotech soil stabilization, supplementary cementitious materials (SCM), geotechnics, silicate based composite materials

Kulcsszavak: biomassza, bioalapú salak, szilárd hulladék újrahasznosítása, biotechnológiai talaj stabilizálás, cement kiegészítő anyagok, geotechnika, szilikát alapú kompozit anyagok

Kennedy Chibuzor ONYELOWE
is a senior lecturer and researcher at the department of civil engineering, Michael Okpara University of Agriculture, Umudike, Nigeria, an adjunct senior lecturer at the department of civil engineering, Alex Ekwueme Federal University, Ndufu Alike Ikwo, Abakaliki, Nigeria.

Favour Adaugo ONYELOWE
is an undergraduate student of the department of biotechnology, Ebonyi state university, Abakaliki, Nigeria.

Duc BUI VAN
is a lecturer at the Hanoi University of Mining and Geology, Hanoi, Vietnam and member of the research group of Geotechnical engineering, Construction Materials and sustainability, HUMG, Vietnam.

Ifeyinwa I. OBIANYO
PhD research candidates and Research Assistant of the Department of Material Science and Engineering, African University of Science and Technology, Abuja, Nigeria with emphasis in green and sustainable building and construction materials.

Sylvia E. KELECHI
PhD research candidates and Research Assistant of the Department of Material Science and Engineering, African University of Science and Technology, Abuja, Nigeria with emphasis in green and sustainable building and construction materials.

1. Introduction

Supplementary cementitious potentials found in ash amorphous in nature, is strongly due to the aluminosilicate composition contained in it [1, 2, 3]. For a material like ash to be considered cementitious or otherwise considered pozzolanic, the aluminosilicate composition i.e., the composition of Al_2O_3, SiO_2 and Fe_2O_3 must be greater than or equal to 70% in accordance with the American Society for Testing and Materials [1] for pozzolanas. By this composition, it can be seen that these materials are silicate-based composites utilized as construction materials [4, 5]. It is also important at this point to note that ash is only derived by direct combustion of biomass, lignocellulosic materials, agro-industrial wastes, household wastes and municipal wastes in a setup presented in *Fig. 1* and in a materials activity, cycle presented in *Fig. 2* [2, 3]. However, in a world faced with the dangers of global warming resulting from the emissions of carbon and its oxides, which contribute to the depletion of the ozone layer, it is only understandable that the future technological advancement should move quickly towards ways of solving this condition [2, 3, 6, 7, 8]. It is equally important to note that one of the many ways through which oxides of carbon are released into the atmosphere is through construction activities during the utilization of ordinary cement. Results from environmental impact assessment on the use of ordinary Portland cement and other conventional cements products in construction activities show that an equivalent amount of CO_2 is emitted into the atmosphere [3]. As a result, there have been technological effort to develop supplementary cementing or cementitious materials that would partially or totally replace ordinary and conventional cements. These supplementary cementitious materials (SCMs) are known to possess aluminosilicates at substantial amounts that enables them exhibit high pozzolanic properties enough to replace ordinary cements [3, 9]. They are divided into ash and powder materials. The ash materials are derived through the direct combustion of solid wastes while powder materials are derived through crushing or ball milling of selected solid waste materials [2, 3]. Research results have shown that ash materials are more efficient as supplementary binders than powder materials because ash materials are amorphous and nonbiodegradable while powder materials are biodegradable [10, 11, 12, 13, 14]. Further on this effort is the development of silicate-based composite materials with higher aluminosilicate contents because they are derived from the blending of more than one material [2, 3]. Geopolymer cements belong to this group of composite binders because they are developed by combining in proportions, which are dependent on the ash with the predominant aluminosilicates [15, 16]. These ashes of

different pozzolanic composition are mixed under the reactive influence of alkali activators as presented in Fig. 2 [2, 3, 17, 18]. It can be observed from previous findings that these materials of biomass and agro-industrial origin have shown to be good replacement for ordinary cement in construction operations. The aim and main objective of this work is reviewing relevant literatures that have shown that ash materials, as silicate-based materials are good replacements for cement as supplementary cementitious and composites materials for construction purposes. This is to bring an overview at a glance of the effects of these amorphous materials of ash and its associated composites on the mechanical properties of soils utilized as foundation and construction materials.

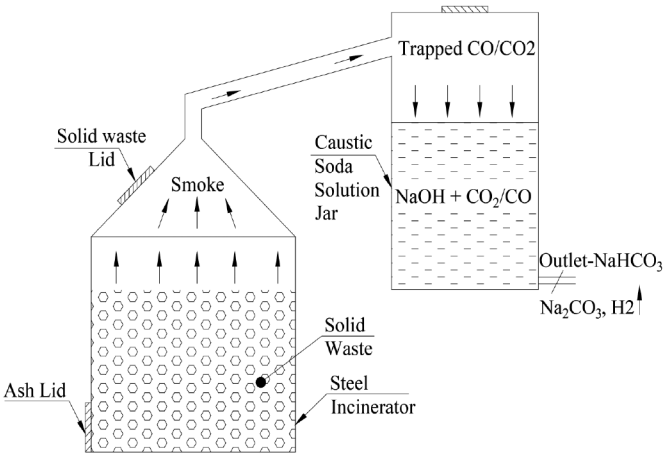

Fig. 1 Bio-waste controlled direct combustion setup [3]
1. ábra Biohulladék szabályozott elégetéséhez használt rendszer összeállítása [3]

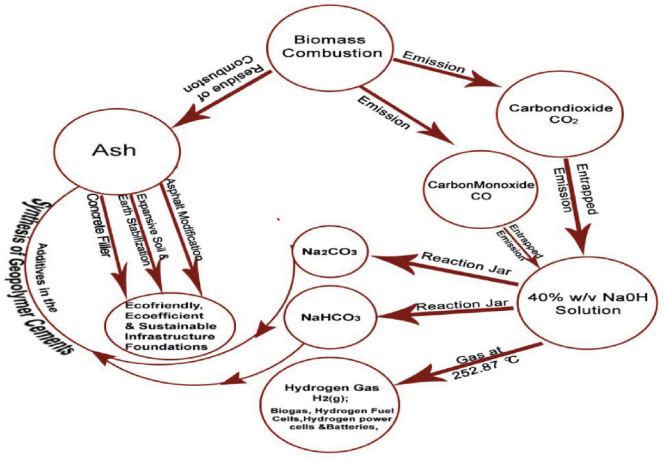

Fig. 2 Bio-waste valorization by combustion and the derivation of ash cycle [2]
2. ábra Biohulladék újrahasznosítása égetés által [2]

2. Overview of relevant resources

Ash has found been predominantly used as an admixture in the stabilization of soils to improve their geotechnical and mechanical properties for the purpose of foundation constructions and other civil engineering purposes. These also include concrete production and asphalt production as modifiers due to its constituents. This procedure has been successful due to the fact that; (i) ash particles are in the silt to sand size range, (ii) they are composed predominantly of amorphous alumina-silicate, (iii) the basic mineral found in waste ashes is silica, and (iv) ashes contain high percentages of 0-5% of clay size, 20-70% of silt size, 30-70% of sand size and 0-5% of gravel size making it suitable for homogenous mixture with soil during admixture stabilization of soils. An extensive look into the relevant resources available from previous findings from the use of ash as supplementary cementing material, will expand the horizon of knowledge on the successes recorded in this area of investigation. In the area of geotechnical engineering experimentations, soil, which is the major geomaterial used in various disciplines of the area are adapted into many forms either as a single material or treated coupled materials in composite forms. It is developed into a coupled material during stabilization or soil improvement for foundation purposes. Pavement foundations (airfield and highway), landscapes and parking lots underlain, embarkments, backfills, lateritic blocks, laterized marbles, etc. are geotechnical engineering activities that go on daily with soils. When these activities are suspected to be affected by problematic soils, a stabilization and ground improvement exercise is undertaken to enhance the properties of the soil to meet required standards. The binding effect and properties of the admixtures utilized during geotechnical engineering procedures have been harnessed over the years to substantially improve on the mechanical properties of soils used as foundation materials [2, 3]. It is important to note that the success of admixture or silicate-based binder stabilization rests on the ability of cations released from the oxides of the additive materials to migrate to the surface of the clayey soils being stabilized. This is where the diffused double layer or the adsorbed complex is formed, which gives rise to the formation of flocs; a resultant effect of hydration reaction, cation exchange reaction, carbonation, calcination and pozzolanic reaction as the case may be [10, 11, 12, 13, 14]. So, it is important that the mixing of the soils and the additive be done deeply to enhance reaction.

2.1 Review of selected ashes and their silicate-based potentials in accordance with ASTM C618, 1978

Rice husk is an agro-industrial waste discharged from rice farming and production. It has been observed through research that over 108 tons of rice husk is being generated annually across the world. The agro-industrial production of rice in Nigeria is over 2.0 million tons annually (see *Fig. 3*). While Niger state produces approximately 96.60 kilo-tons of rice, Ebonyi state produces well over 187.5 kilo-tons annually and this capacity has increased over the period due to increased demand for food. Moreover, the ash has been classified as a pozzolana, with silicon oxide component ranging between 67-70% with about 4.9% and 0.95% aluminum oxide and iron oxide respectively. The silicate-based composition of the pozzolanic ash is contained in amorphous state, which reacts with the ionized components of problematic soils throughout the hardening and strength gaining of the treated soils [19, 20].

Fig. 3 Rice husk
3. ábra Rizs héj

Fig. 4 Coconut shell
4. ábra Kókuszhéj

Fig. 5 Snail shells
5. ábra Csigaház

According to E. S. Nnochiri *et al.* [22], snail shells ash (SSA) with a specific gravity of 3.07, is a product of the combustion of snail shells (see *Fig. 5*) discharged as agricultural and household wastes disposed on landfills that hardly decay. They are burnt and pulverized to fineness and then used as additives in the stabilization of weak engineering soils. This has been classified as a supplementary cementing material because of its silicate-based component having aluminosilicates composition of more than 70% according to ASTM C618.

According to Nnochiri [23], periwinkle shell ash derived by combusting periwinkle shells (see *Fig. 6*) and pulverizing the residue. Periwinkle shells are agricultural, biological and household wastes found in the coastal region of Nigeria and across the world. They are disposed as wastes on landfills. The shells are v-shaped, hard, brittle and usually black. The ash has also been classified as pozzolanic because of the aluminosilicate composition, which satisfies the condition for materials to be classified as supplementary cementitious materials (SCM) in accordance to the ASTM C618.

Fig. 6 Periwinkle shells
6. ábra Tengeri csigaház

Fig. 7 Wood
7. ábra Fa

According to A. W. Otunyo and C. C. Chukuigwe [24], palm bunch ash and palm oil fuel ash are derived from the combustion of palm bunch as a biomass and a bio-based agricultural waste and the milling of palm oil from palm fruits respectively. Research results have shown also that this ash consists of aluminosilicates composition by weight over 70% thereby fulfilling the requirement for a material to be classified as a pozzolana. This composition makes palm bunch ash suitable as a construction material to supplement for cementation potentials.

According to B. D. Nath *et al.* [25], wood ash has been utilized in the modification of problematic soils for construction purposes. It is also the derivative of combusted wood materials in logs (see *Fig. 7*) or dusts, which are bio-based agricultural wastes. Wood ash contains high composition of aluminosilicates, which satisfies its utilization as a pozzolanic material in soft soils stabilization.

According to G. M. Ayininuola and A. O. Sogunro [26] and O. A. Adetayo *et al.* [27], bone ash was utilized in the modification of expansive soil to evaluate its effect on the shear properties of the soil. This was necessitated due to the calcium silicate based binding properties of the bone ash. Bone ash is an agricultural and household solid waste materials from animal bones (see *Fig. 8*). The high C-S composition satisfies the minimum pozzolanic requirements for use as a supplementary cementing construction material.

Fig. 8 Animal bones
8. ábra Állati csontok

Bello *et al.* [28] and Ramonu, J. A. L. *et al.* [29] had in different researches investigated the potential of cassava peel ash (CPA) and yam peel ash (YPA) as supplementary binders in soft and expansive soils stabilization. CPA and YPA are gotten from the peeling of the bark of cassava and yam peels (see *Fig. 9*) during garri and flour production. It was shown that CPA and YPA exhibited high composition of silicate based pozzolanic properties. This property enhanced the ashes suitability to be utilized as alternative binders in the stabilization of problematic soils.

Fig. 9 Cassava and yam peels
9. ábra Manióka és jam héj

According to Chou-Fu Liang and Hung-Yu Wang [30], G. M. Ayininuola and O. D. Afolayan [31] and Ubachukwu and Okafor [32], oyster shell (see *Fig. 10*) collected from the coastal regions of Nigeria- Rivers State, Delta State, Bayelsa State and across the world discharged as agricultural and bio-based waste has been studied for its potential property to be utilized as a supplementary binder in its ash and crushed form. Results of the investigations show that oyster shell ash and powder possess high composition of aluminosilicates, which makes it suitable to be utilized as a pozzolana in accordance with appropriate standards.

Fig. 10 Oyster shells
10. ábra Osztriga héj

According to Oriola and Moses [33], groundnut shell ash (GSA) potential for use as a pozzolanic material in the modification of the index and mechanical properties of plastic soils was investigated and encouraging results were achieved. Groundnut shells (see *Fig. 11*) are discharged after separating the edible nuts and leaving the littered shells as solid wastes. After sun drying, combustion and pulverization, the ash is obtained. The alumina-silicate-based composition of the ash has been determined to be more than the minimum standard for pozzolanas and suitable as a supplementary silicate-based binder.

Fig. 11 Groundnut shells
11. ábra Földimogyoró héjak

According to Sadeeq *et al.* [34], the potential of bagasse ash (BA) to be used as an alternative binder to replace ordinary cement has been studied. Bagasse ash derived from the combusted sugarcane biomass discharged after the extraction of the fluid. Bagasse (see *Fig. 12*) is an agro-industrial waste material discharged on landfills. It is predominantly common in the northern states of Nigeria where sugarcane farming is the trade of the people living in these areas. Research has shown that BA contains high amount by weight of the aluminosilicates responsible for cementation behavior of construction materials. Hence its potential utilization as a supplementary cementitious material in construction activities.

Fig. 12 Sugarcane farm
12. ábra Cukornád farm

3. Overview of results from relevant resources

3.1 Gradation characteristics of soils treated with ashes

Results of previous investigation on the potentials of ashes utilized as supplementary cementitious additives have shown that the gradation of the soils improved substantially and consistently with increased addition of ash by weight proportion of treated solids. This was due to the fineness of ash derived by drying-in most cases, combusting and pulverizing to fineness [35]. The texture of ash achieved through this procedure changes the particle size distribution of the treated soils blended with ashes. Gradation is a very important factor in construction materials' characterization and structural behavior [36].

3.2 Index and strength characteristics of soils treated with ashes

Index and strength characteristics of soils especially the expansive and problematic soils are very important factors considered in the design and performance monitoring of flexible pavements across the world. The overall performance and durability of these structures depend ultimately on the strength of the foundation. For instance, when pavements are laid on weak or expansive subgrade, the behavior of the entire structure is compromised. More importantly, if the structure is under a hydraulically bound condition like the pavement foundations subjected to the rise and fall of water table, it becomes even a more difficult problem due to the swell and shrink potentials of the compacted earth underlain. Over the years, ordinary cement has been used to improve on these properties of soils utilized as subgrade materials with its attendant greenhouse emissions. In recent developments in geo-environmental engineering, ash materials due to their amorphous nature and high composition of aluminosilicates have been utilized in single forms and in composite forms to modify weak soils. This was targeted at making the compacted earth suitable to withstand the adverse conditions it is subjected to in the sub structural level. Ash is environmentally friendly and possesses properties that are resistant to heat, moisture, sulfates, crack and shrinkage [2, 3, 35]. Because of these characteristics, soils treated with ash have shown to improve in their plasticity index condition, compaction behavior, and other strength properties like California bearing ratio, resilient modulus, resistant value, deviatoric stress and durability potentials.

4. Conclusions

The use of ash as supplementary cementitious material has been reviewed and the following remarks can be made; (i) ash is derived by combusting bio-based materials, (ii) because of its amorphous nature, ash doesn't decompose, (iii) ash is composed of silicate-based pozzolanic properties i.e. aluminosilicates and this makes it suitable as alternative cement, (iv) ash has proven to be an environmentally friendly cement with no greenhouse effects, (v) the addition of ash to soil as a mixed blend improves the mechanical properties of problematic soils in a stabilization protocol, (vi) ash from various sources is readily available and its utilization in construction works is highly sustainable and (vii) ash is a good alternative and appropriate replacement for ordinary cement in an environment yearning to be saved from hazards and global warming.

Acknowledgement

Vietnam Ministry of Education and Training for funding this research, based on Decision No. 5652/QD-BGDDT on December 28, 2018 with Grant No. MOET /2019 and with project number B2019-MDA-08.

References

[1] American Standard for Testing and Materials (ASTM) C618, 1978. Specification for Pozzolanas. ASTM International Annual Book of ASTM Standards, West Conshohocken, Philadelphia, USA.

[2] Onyelowe, K. C. – Onyelowe, Favour Deborah A. – Van, Duc Bui – Ikpa, Chidozie – Salahudeen, A. Bunyamin – Eberemu, Adrian O. – Osinubi, Kolawole J. – Onukwugha, Eze – Odumade, Adegboyega O. – Chigbo, Ikechukwu C. – Amadi, Agapitus A. – Igboayaka, Ekene – Obimba-Wogu, Jesuborn – Saing, Zubair – Amhadi, Talal (2020): Valorization and sequestration of hydrogen gas from biomass combustion in solid waste incineration NaOH oxides of carbon entrapment model (SWI-NaOH-OCE Model). Materials Science for Energy Technologies, Vol. 3, Pp. 250-254. https://doi.org/10.1016/j.mset.2019.11.003

[3] Onyelowe, K. C. – Van, Duc Bui – Ubachukwu, O. – Ezugwu, C. – Salahudeen, B. – Nguyen Van, M. – Ikeagwuani, C. – Amhadi, T. – Sosa, F. – Wu, W. – Duc, T. Ta – Eberemu, A. – Duc, T. Pham – Barah, O. – Ikpa, C. – Orji, F. – Alaneme, G. – Amanamba, E. – Ugwuanyi, H. – Sai, V. – Kadurumba, C. – Selvakumar, S. – Ugorji, B. (2019): Recycling and Reuse of Solid Wastes; a Hub for Ecofriendly, Ecoefficient and Sustainable Soil, Concrete, Wastewater and Pavement Reengineering. International Journal of Low-Carbon Technologies. Vol. 14(3), pp. 440-451. https://doi.org/10.1093/Ijlct/Ctz028

[4] Kotova, O. B. – Shushkov, D. A. – Gömze, L. A. – Kurovics, E. – Ignatiev, G. V. – Sitnikov, P. A. – Ryabkov, Y. I. – Vaseneva, I. N.: Composite materials based on zeolite-montmorillonite rocks and aluminosilicate wastes. Epitő anyag – Journal of Silicate Based and Composite Materials, Vol. 71 (4), 2019, Pp. 125–130. https://doi.org/10.14382/epitoanyag-jsbcm.2019.22

[5] El-Fakharany, M. E. – Ezzat, M. – Gad, A. – Ghafour, N. G. Abdel – Baghdady, A. R.: Performance of dolomitic cementitious mortars as a repairing material for normal concrete in Egypt. Építőanyag – Journal of Silicate Based and Composite Materials, Vol. 71 (2), 2019, Pp. 33–42. https://doi.org/10.14382/epitoanyag-jsbcm.2019.7

[6] Onyelowe, K. C. – Salahudeen, A. B. – Eberemu, A. O. – Ezugwu, C. N. – Amhadi, T. – Alaneme, G. (2020): Oxides of Carbon Entrapment for Environmentally Friendly Geomaterials Ash Derivation. In book: Recent Thoughts in Geoenvironmental Engineering, Proceedings of the 3rd GeoMEast International Congress and Exhibition, Egypt 2019 on Sustainable Civil Infrastructures – The Official International Congress of the Soil-Structure Interaction Group in Egypt (SSIGE), pp. 58-67. https://doi.org/10.1007/978-3-030-34199-2_4

[7] Onyelowe, K. C. – Salahudeen, A. B. – Eberemu, A. O. – Ezugwu, C. N. – Amhadi, T. – Alaneme, G. – Sosa, F. (2020): Utilization of Solid Waste Derivative Materials in Soft Soils Re-engineering. In book: Recent Thoughts in Geoenvironmental Engineering, Proceedings of the 3rd GeoMEast International Congress and Exhibition, Egypt 2019 on Sustainable Civil Infrastructures – The Official International Congress of the Soil-Structure Interaction Group in Egypt (SSIGE), pp. 49-57. https://doi.org/10.1007/978-3-030-34199-2_3

[8] Onyelowe, K. C. – Amhadi, T. – Ezugwu, C. N. – Onukwugha, E. – Ugwuanyi, H. – Jideoffor, I. – Ikpa, C. – U. Iro – Ugorji, B. (2020): Cemented Lateritic Soil as Base Material Improvement Using Compression. In book: Innovative Infrastructure Solutions using Geosynthetics, Proceedings of the 3rd GeoMEast International Congress and Exhibition, Egypt 2019 on Sustainable Civil Infrastructures – The Official International Congress of the Soil-Structure Interaction Group in Egypt (SSIGE), pp. 58-67. https://doi.org/10.1007/978-3-030-34242-5_4

[9] Boukhelkhal, A. – Benabed, B.: Fresh and hardened properties of self-compacting repair mortar made with a new reduced carbon blended cement Epitő anyag – Journal of Silicate Based and Composite Materials, Vol. 71 (4), 2019, Pp. 108–113. https://doi.org/10.14382/epitoanyag-jsbcm.2019.19

[10] Onyelowe, K. C. – Bui Van, D.: 2018. Durability of nanostructured biomasses ash (NBA) stabilized expansive soils for pavement foundation, International Journal of Geotechnical Engineering. https://doi.org/10.1080/19386362.2017.1422909

[11] Onyelowe, K. C. – Bui Van, D.: 2018. Predicting Subgrade Stiffness of Nanostructured Palm Bunch Ash Stabilized Lateritic Soil for Transport Geotechnics Purposes. Journal of GeoEngineering of Taiwan Geotechnical Society, 2018 (in press). http://140.118.105.174/jge/index.php

[12] Onyelowe, K. C. – Bui Van, D. (2018): Structural analysis of consolidation settlement behaviour of soil treated with alternative cementing materials for foundation purposes. Environmental Technology & Innovation, Vol. 11, Pp. 125-141. https://doi.org/10.1016/j.eti.2018.05.005

[13] Onyelowe, K. C. – Bui Van, D. (2018): Predicting Strength Behaviour of Stabilized Lateritic Soil- Ash Matrix using Regression Model for Hydraulically Bound Materials Purposes, International Journal of Pavement Research and Technology. https://doi.org/10.1016/j.ijprt.2018.08.004

[14] Onyelowe, K. C. – Bui Van, D. – Eberemu, A. O. – Xuan, M. N. – Salahudeen, A. B. – Ezugwu, C. – Van, M. N. – Orji, F. – Sosa, F. – Duc, T. T. – Amhadi, T. – Ikpa, C. – Ugorji, B. (2019): "Sorptivity, swelling, shrinkage, compression and durability of quarry dust treated soft soils for moisture bound pavement geotechnics". *Journal of Materials Research and Technology*, Vol. 8(4). Pp. 3529–3538. https://doi.org/10.1016/j.jmrt.2019.06.029

[15] Szabó R. 2019: Control of mechanical properties of lignite fly ash based geopolymers by vibrating compression. Építőanyag – Journal of Silicate Based and Composite Materials, Vol. 71 (2), 2019, Pp. 66–71. https://doi.org/10.14382/epitoanyag-jsbcm.2019.12

[16] Khater, Hisham Mustafa Mohamed: Preparation and characterization of lightweight geopolymer composites using different aluminium precursors. Építőanyag – Journal of Silicate Based and Composite Materials, Vol. 70 (6), 2018, Pp. 186–194. https://doi.org/10.14382/epitoanyag-jsbcm.2018.33

[17] Davidovits, J. (2013): Geopolymer Cement a review. Institute Geopolymer, F-02100 Saint-Quentin, France. [online]

[18] Hamidi, R. M. – Man, Z. – Azizli, K. A. (2016): Concentration of NaOH and the Effect on the Properties of Fly Ash Based Geopolymer. 4th International Conference of Process Engineering and Advanced Materials; Procedia Engineering, Vol. 148, Pp. 189-193. http://dx.doi.org/10.1016/j.proeng.2016.06.568

[19] Qasim, M. – Bashir, A. – Tanvir, M. – Anees, M. M. (2015): Effect of Rice husk ash on soil stabilization. Bulletin of Energy Economics, 3(1), 10-17.

[20] Candido, K. – Braga, Jener – Gutierrez II, Rodel – Tambal, Jeffrey – Orale, Ronald L. (2016): Fine-Grained Soil as Subgrades with Coconut Husk Ash. *Journal of Academic Research* 01:2 (2016), Pp. 19-26

[21] Oluremi, J. R. – Adedokun, S. I. – Osuolale, O. M. (2012): Stabilization of poor lateritic soils with coconut husk ash. International Journal of Engineering Research & Technology (IJERT) Vol. 1 Issue 8, October – 2012.

[22] Nnochiri, E. S. – Ogundipe, O. M. – Emeka, Helen O. (2018): Effects of Snail Shell Ash on Lime Stabilized Lateritic Soil. Malaysian Journal of Civil Engineering 30(2):239-253

[23] Nnochiri, E. S. (2017): Effects of Periwinkle Shell Ash on Lime-Stabilized Lateritic Soil. J. Appl. Sci. Environ. Manage., Vol. 21 (6) 1023-1028. https://dx.doi.org/10.4314/jasem.v21i6.4

[24] Otunyo, A. W. – Chukuigwe, C. C. (2018): Investigation of The Impact of Palm Bunch Ash on The Stabilization of Poor Lateritic Soil. Nigerian Journal of Technology (NIJOTECH), Vol. 37, No. 3, July 2018, pp. 600 – 604. http://dx.doi.org/10.4314/njt.v37i3.6

[25] Nath, B. D. – Sarkar, Grytan – Siddiqua, Sumi – Rokunuzzaman, Md. – Islam, Md. Rafiqul (2018): Geotechnical Properties of Wood Ash-Based Composite Fine-Grained Soil. Advances in Civil Engineering, Vol. 2018. https://doi.org/10.1155/2018/9456019

[26] Ayininuola, G. M. – Sogunro, A. O. (2013): Bone Ash Impact on Soil Shear Strength. World Academy of Science, Engineering and Technology International Journal of Environmental and Ecological Engineering Vol.7 (11). Pp. 793-797.

[27] Adetayo, O. A. – Amu, O. O. – Ilori, A. O. (2019): Cement Stabilized Structural Foundation Lateritic Soil with Bone Ash Powder as Additive. Arid Zone Journal of Engineering, Technology & Environment, Vol. 15 (2). Pp. 479-487.

[28] Bello, A. A. – Adebayo Ige, Joseph – Ayodele, Hammed (2015): Stabilization of Lateritic Soil with Cassava Peels Ash. British Journal of Applied Science & Technology, Vol. 7(6). Pp. 642-650.

[29] Ramonu, J. A. L. et al., (2018): Geotechnical properties of lateritic soil stabilized with yam peel ash for subgrade construction. International Journal of Civil Engineering and Technology (IJCIET), Vol. 9 (13), Pp. 1666-1681.

[30] Liang, Chou-Fu – Wang, Hung-Yu (2013): Feasibility of Pulverized Oyster Shell as a Cementing Material. Advances in Materials Science and Engineering, Volume 2013. http://dx.doi.org/10.1155/2013/809247

[31] Ayininuola, G. M. – Afolayan, O. D. (2018): Potential of Oyster Shell Ash Activated with Cement as soil Stabilizer for Road Construction. International Journal of Engineering and Advanced Technology (IJEAT), Vol. 7 (5). Pp. 118-126.

[32] Ubachukwu, O. A. – Okafor, F. O. (2019): Investigation of the Supplementary Cementitious Potentials of Oyster Shell Powder for Eco-Friendly and Low-cost Concrete. *Electronic Journal of Geotechnical Engineering*, Vol. 24 (5), Pp 1297-1306.

[33] Oriola, F. – Moses, G. (2010): Groundnut Shell Ash Stabilization of Black Cotton Soil. Electronic Journal of Geotechnical Engineering, Vol. 15, Pp. 415-428.

[34] Sadeeq, J. A. – Ochepo, J. – Salahudeen, A. B. – Tijjani, S. T. (2015). Effect of Bagasse Ash on Lime Stabilized Lateritic Soil. Jordan Journal of Civil Engineering, Vol. 9 (2), Pp. 203-213.

[35] Nigerian General Specification, 1997. Specification for Construction of Roads and Bridges, Nigeria.

[36] Roads and Maritime Services, 2012. Erodibility of stabilized road construction materials: Test Method T186, New South Wales.

Ref.:
Onyelowe, Kennedy Chibuzor – **Onyelowe**, Favour Adaugo Deborah – **Bui Van**, Duc – **Obianyo,** Ifeyinwa I. – **Kelechi** Sylvia E. : *Overview of ash as supplementary cementitious silicate-based composite and construction material*
Építőanyag – Journal of Silicate Based and Composite Materials, Vol. 72, No. 3 (2020), 80–85. p.
https://doi.org/10.14382/epitoanyag-jsbcm.2020.13

Resilient modulus and deviatoric stress of cemented soils treated with crushed waste ceramics (CWC) for pavement subgrade construction

Útalapozás készítéséhez alkalmazott zúzott hulladékkerámiával (CWC) kezelt cementált talajok rugalmassági mudulusa és deviátoros feszültsége

Kennedy Chibuzor ONYELOWE ▪ Department of Civil Engineering, Michael Okpara University of Agriculture, Nigeria ▪ konyelowe@mouau.edu.ng

Duc BUI VAN ▪ Faculty of Civil Engineering and Member, Research Group of Geotechnical Engineering, Construction Materials and Sustainability, Hanoi University of Mining and Geology, Vietnam

Chidozie IKPA, Department of Civil Engineering, Faculty of Engineering, Alex Ekwueme Federal University, Nigeria

Kolawole OSINUBI ▪ Faculty of Engineering, Ahmadu Bello University, Nigeria

Adrian EBEREMU ▪ Faculty of Engineering, Ahmadu Bello University, Nigeria

A. Bunyamin SALAHUDEEN ▪ Department of Civil Engineering, Faculty of Engineering, University of Jos, Nigeria

Oscar C. NNADI ▪ Department of Civil Engineering, College of Engineering & Engineering Technology, Michael Okpara University of Agriculture, Nigeria

Moses C. CHIMA ▪ Department of Civil Engineering, College of Engineering & Engineering Technology, Michael Okpara University of Agriculture, Nigeria

Jesuborn OBIMBA-WOGU ▪ Department of Civil Engineering, College of Engineering & Engineering Technology, Michael Okpara University of Agriculture, Nigeria

Kizito IBE ▪ Department of Civil Engineering, College of Engineering & Engineering Technology, Michael Okpara University of Agriculture, Nigeria

Benjamin UGORJI ▪ Department of Civil Engineering, College of Engineering & Engineering Technology, Michael Okpara University of Agriculture, Nigeria

Érkezett: 2019. 12. 12. ▪ Received: 12. 12. 2019. ▪ https://doi.org/10.14382/epitoanyag-jsbcm.2020.14

Abstract

The behavior of resilient modulus of cemented lateritic soils treated with crushed waste ceramics and utilized as pavement underlain has been investigated under laboratory conditions. This is the measure of the rigidity of soils used as foundation materials. The rampant failures of pavements due to undesirable characteristics exhibited by the foundations have spurred this research work to enable a better understanding of the behavior of soils used as foundation materials and how best they can be handled or treated to ensure stability and durability of the structures. The soils were first characterized and found to belong to A-7, A-7-6, A-7 and A-7-5 group of soils according to the AASHTO classification method. Also, they were found, from basic experiments, to be highly plastic soils with high clay contents. The soils were treated with crushed waste ceramics in the proportion of 10%, 20%, 30%, 40%, 50%, 60%, 70%, 80%, 90%, 100%, 110% and 120% by weight of solid with a constant addition of 2.5% by weight ordinary cement. The results of the examination showed that the resilient modulus increased substantially with increased rate of crushed waste ceramics. This showed that crushed ceramic waste is a good pozzolanic material for soils stabilization in the construction of pavement foundations.

Keywords: resilient modulus, deviatoric stress, cemented soils, crushed waste ceramics, solid wastes, geomaterials, pavement foundation

Kulcsszavak: rugalmassági modulus, deviátoros feszültség, cementált talajok, zúzott hulladék-kerámiák, szilárd hulladék, geoanyagok, útburkolat alapozás

Kennedy Chibuzor ONYELOWE
is a senior lecturer and researcher at the department of civil engineering, Michael Okpara University of Agriculture, Umudike, Nigeria, an adjunct senior lecturer at the department of civil engineering, Alex Ekwueme Federal University, Ndufu Alike Ikwo, Abakaliki, Nigeria and Visiting Scholar to the Department of Mechanical and Civil Engineering, Kampala International University, Kampala, Uganda

Duc BUI VAN
is a lecturer at the Hanoi University of Mining and Geology, Hanoi, Vietnam and member of the research group of Geotechnical engineering, Construction Materials and sustainability, HUMG, Vietnam.

Chidozie IKPA
is currently a technologist in the department of civil engineering laboratory of the Alex Ekwueme University, Ndufu Alike Ikwo, Nigeria.

Kolawole J. OSINUBI
is an astute professor of geoenvironmental engineering at the Ahmadu Bello University, Zaria, Nigeria.

Adrian O. EBEREMU
is an Associate Professor at the Ahmadu Bello University, Zaria, Nigeria with research experience in geotechnical and geoenvironmental engineering.

A. Bunyamin SALAHUDEEN
is senior lecturer and researcher at the University of Jos, Nigeria.

Oscar C. NNADI
is a graduate of civil engineering from the Michael Okpara University of Agriculture, Umudike, Nigeria with research interest in soil stabilization and construction materials.

Moses C. CHIMA
is a graduate of civil engineering from the Michael Okpara University of Agriculture, Umudike, Nigeria with research interest in soil stabilization and construction materials.

Jesuborn OBIMBA-WOGU
is a graduate assistant at the department of civil engineering, Michael Okpara University of Agriculture, Umudike, Nigeria with research interest in geotechnical engineering.

Kizito IBE
is a graduate assistant at the Michael Okpara University of Agriculture, Umudike, Nigeria with interests in structural engineering.

Benjamin UGORJI
is a graduate assistant at the Michael Okpara University of Agriculture, Umudike, Nigeria with interests in geotechnical engineering.

1. Introduction

The unbounded aggregate layer and unsaturated state upon which pavement foundations are constructed play an important role in the performance of pavements more especially with the hydraulically bound conditions where rise and fall of moisture due to suction plays another role [1, 2, 3, 4, 5]. It is wrong to assume that pavement layers are under steady saturated conditions and this assumption affects the design and eventually the stiffness and stability of the pavement foundations [6, 7]. According to Ba *et al.* [8] it is noted that moisture migration and percolation into the pavement layers either through suction and surface water seepage affects the resilient modulus and stability of subgrade materials, which commonly are constructed with compacted lateritic soils. It has been proven through research that moisture affects the carrying capacity and strength of clayey soils due to the loss of strength on immersion [7, 9]. The behavior of soils under suction is

directly corresponding with the resilient modulus of such soils especially when subjected to the effect of moisture [10, 11]. This behavior brings about the failure of pavements when they are underlain with unsuitable and expansive soils, which behave in undesirable pattern under the influence of matric suction [2, 12]. Due to the fluctuations in the water conditions of the subgrade, the pavement foundations are designed for the most critical exposure conditions [13, 14, 15]. Soils stabilization has been adopted to improve on the inadequate properties of the soils utilized as subgrade materials [2-5, 10]. This is achieved through the use of chemical compounds like the ordinary Portland cement or biobased or lignocellulose materials, which are environmentally friendly geomaterials [10, 16, 17, 18]. The biobased or lignocellulose materials are derived through controlled direct combustion to have ash or through crushing to achieve powder with good gradation. In this work, crushed waste ceramics is derived by crushing waste ceramic materials collected from dumpsites. This material is used as a geomaterial in the stabilization of soils for use as subgrade materials because of its pozzolanic properties [18]. Due to the high content of aluminosilicates in the CWC, its blend with soft lateritic soils produce compacted stabilized subgrade soils with high rigidity, density and stability. This behavior gives rise to the improvement of the resilient modulus of the treated material at optimum molding moisture conditions [1]. The objectives of this work were to evaluate the effect of crushed ceramics wastes on the deviatoric stress and resilient modulus of the treated soils.

2. Materials

2.1 Soils

Four borrow pits in four different locations in Abia State, Nigeria were the source of the soil samples. These borrow pits are located on coordinates 5°29'16" North and 7°28'58" East (for Olokoro location soil), 5°27'0" North and 7°31'60" East (for Amaba location soil), 5°31'0" North and 7°26'0" East (for Ohiya location soil) and 4°53'14" North and 7°21'26" (for Akwete location soil). The samples were sundried for 7 days, 500 grams each was measured and prepared for use.

2.2 Crushed waste ceramics

The ceramics were collected from dumpsites within Umuahia urban area, sundried for two days and crushed by ball milling. The crushed ceramic waste was characterized and sieved to determine its gradation and particle distribution. Afterwards, it was stored for use in the stabilization exercise.

2.3 Ordinary Portland cement

Portland cement was used at a steady rate of 2.5%, that meets the requirements of ASTM C618 [18], as a binder as shown in the chemical oxide composition presented in *Table 2*. The preliminary characterization exercises were conducted on the test materials to determine their gradation and chemical oxide composition (aluminosilicates content). These test admixtures were utilized in the percentages of 10% to 120% in an incremental rate of 10% to treat the soils.

3. Methods

The particle size distribution, compaction, Atterberg limits, shrinkage limits, free swell index, and specific gravity were generally conducted on the test soils in accordance with BS 1377 [19]. This was carried out to determine the characterization and basic properties of the test soils. Similarly, chemical oxide composition and particle size distribution tests were conducted to determine the aluminosilicate content and gradation respectively in accordance with ASTM C618 [18] and BS 1377 [19] respectively. Of particular interest to this work was the stiffness of the treated soils as subgrade or pavement materials, which was determined with the resilient modulus test carried out on the CWC treated soils in accordance with AASHTO [10] , AASHTO T 22-03 [1], and BS 1924 [20]. Specifically, the resilient modulus of both the control specimen and treated test soils was determined under the laboratory conditions. This represented the simulated physical and stress conditions of geomaterials treated soils A, B, C and D overlain by flexible pavements subjected to dynamic traffic loads. A cyclic axial stress of fixed magnitude under deviatoric stress, load duration of 0.1s, and cyclic duration of 3s is applied to prepared cylindrical test specimens in a modified triaxial compression set up. The final recoverable axial deformation response (recoverable strain) and the deviatoric stress of the test specimens were measure and the resilient moduli at different proportions of the additives were determined with Eq. 1.

$$M_R = \frac{\rho_d}{\varepsilon_r} \tag{1}$$

where:
M_R = resilient modulus, ρ_d = deviatoric stress, ε_r = strain

4. Results and analytical remarks

4.1 Classification Characteristics of Test Materials

The basic properties of the test soils are presented in *Table 1*, *Fig. 1* and *Table 2*. The test soil were observed to possess 2.85%, 10%, 4.6% and 7.6% passing sieve No. 200, and classified as A-7, A-7-6, A-7 and A-7-5 respectively according to AASHTO classification method. Test soils A, B, C and D were classified as poorly graded according to unified soil classification system. The results of the consistency protocol show that the test soils are highly plastic soils (> 17%) with high free swell index. The basic results of the resilient modulus show that the soils fall under clayey subgrade (0.345E+05 to 1.034E+05 kN/m^2) [16]. The chemical oxides composition test results presented in *Table 2* show that the test materials possess high aluminosilicates responsible for the pozzolanic, calcination and hydration reactions that take place in a stabilization process.

Property description of test soils and units	Values			
	Test soil (A)	Test soil (B)	Test soil (C)	Test soil (D)
% Passing Sieve, No 200	2.85	10	4.6	7.6
NMC (%)	12.1	13.49	14	16
LL (%)	40	46	64	65
PL (%)	18	21	36	33
PI (%)	22	25	28	32
SL (%)	8	8	7	10
FSI (%)	250	234	275	296
G_S	2.6	2.43	2.12	2.08
AASHTO Classification	A-7	A-7-6	A-7	A-7-5
USCS	GP, CH	GP	GP, CH	GP, CH
MDD (g/cm3)	1.76	1.85	1.80	1.56
OMC (%)	13.1	16.2	13.13	15.4
CBR (%)	12	13	8	7
R-Value	11.74	11.70	11.70	11.50
MR (kN/m2)	0.42E+05	0.42E+05	0.42E+05	0.72E+05
Color	Reddish Brown	Reddish Gray	Reddish Ash	Ash

Table 1 Basic properties of test soils
1. táblázat A vizsgált talajok alapvető tulajdonságai

Materials	Oxides Composition (content wt %)												
	SiO_2	Al_2O_3	CaO	Fe_2O_3	MgO	K_2O	Na_2O	TiO_2	LOI	P_2O_5	SO_3	IR	Free CaO
Soil A	76.56	15.09	2.30	2.66	0.89	2.10	0.33	0.07	-	-	-	-	-
Soil B	77.57	14.99	3.11	1.78	0.86	1.45	0.23	0.01	-	-	-	-	-
Soil C	77.73	16.65	1.42	3.22	0.07	0.89	0.02	-	-	-	-	-	-
Soil D	72.34	17.30	5.40	2.32	0.34	2.13	0.17	-	-	-	-	-	-
CWC	64.45	24.14	0.25	1.3	0.28	3.69	2.51	0.18	1.09	-	2.11	-	-
DOPC	21.45	4.45	63.81	3.07	2.42	0.83	0.20	0.22	0.81	0.11	2.46	0.16	0.64

**IR is Insoluble Residue, LOI is Loss on Ignition, CWC: Crushed Waste Ceramics*
DOPC: Dangote Ordinary Portland cement

Table 2 Chemical oxides composition of the materials used in this paper
2. táblázat A felhasznált anyagok kémiai oxidos összetétele

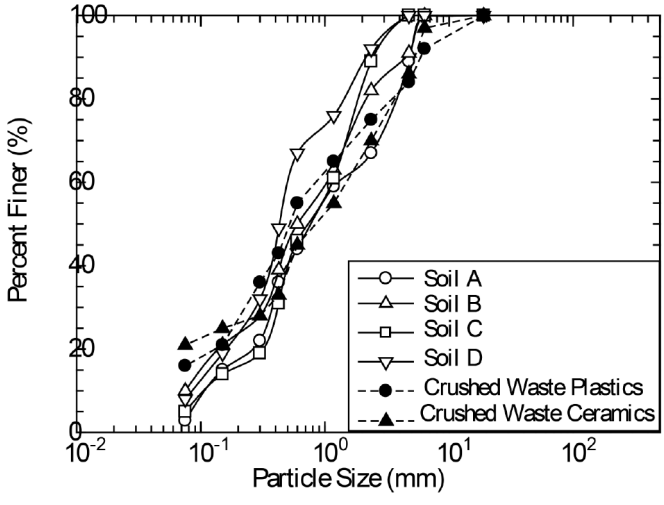

Fig. 1 Grain size distribution of studied materials
1. ábra A vizsgált anyagok szemcseméret eloszlása

4.2 Deviatoric stress and resilient modulus (M_R) of the treated cemented soils

The results of the resilient modulus of the CWC treated soils used to characterize the treated matrix as a subgrade material is presented in *Figs. 2* and *3*. The applied deviator stress and the recoverable strain of the modified triaxial test on the treated specimens were used. The four test soils behaved in almost the same pattern with similar reactions with increased crushed waste ceramics (CWC). The deviatoric stress consistently increased with increase in the proportion of the admixture for test soils A, B, C and D. It is important to note at this point that the additive CWC is a highly aluminosilicate compound according to the requirements of American Standard for Testing and Materials [18], with a crystal texture prior to its utilization in the stabilization procedure. These compounds are responsible for pozzolanic reaction, and strengthening by forming silicates of calcium hydrates and aluminates. These further forms floc, which condense to the strength buildup of the treated materials. Test soils A, B and C had an improvement index of about 21%, while test soil D had an improvement index of 25%. The higher improvement index recorded with test soil D is in line with its natural soil high resilient modulus of 0.72E+05, which was improved upon. The hydration reaction between compounds of strengthening from the additive and the dissociated soil ions

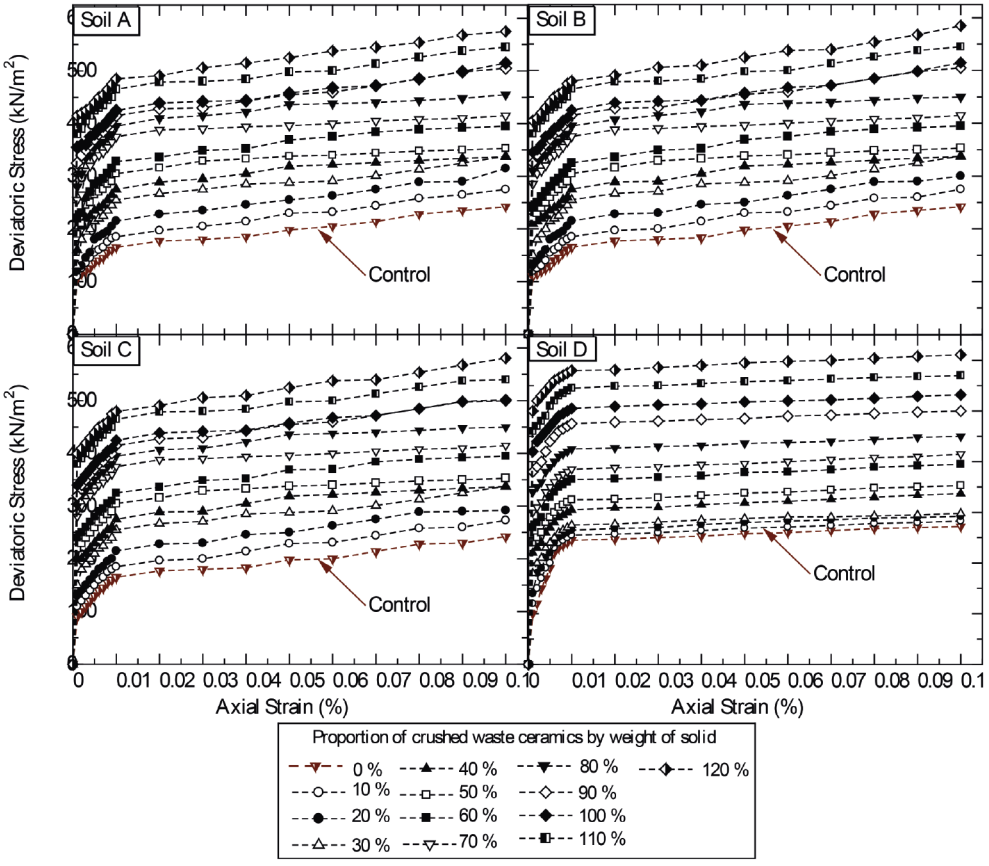

Fig. 2 Effects of CWC on deviatoric stress of the treated cemented soils
2. ábra CWC hatása a cementált talajok deviátoros feszültségére

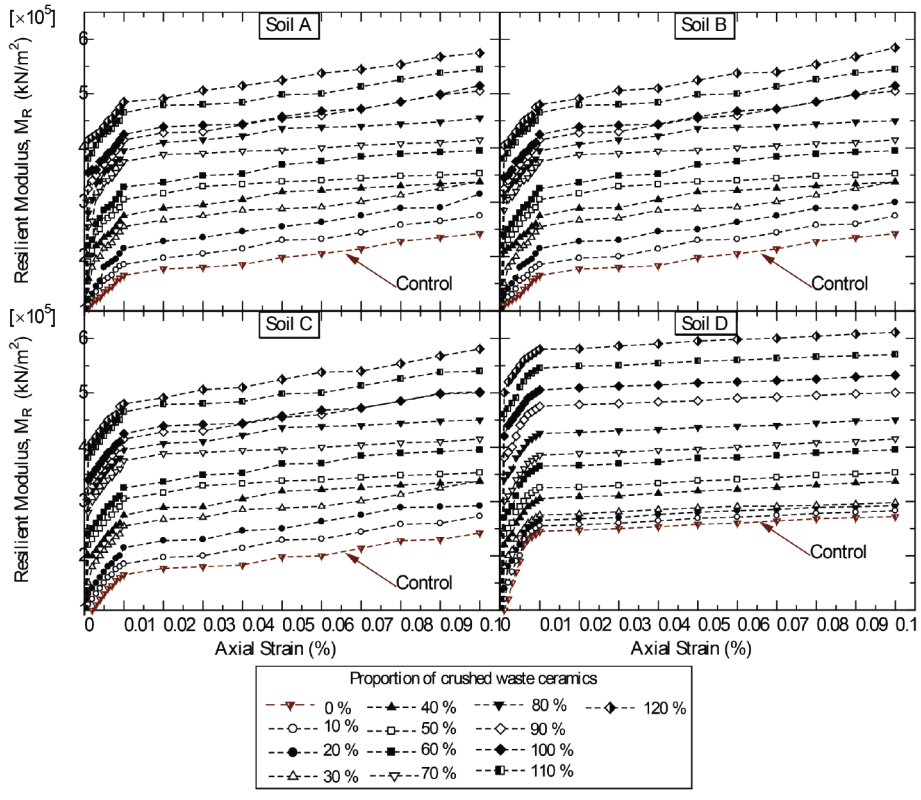

Fig. 3 Effects of CWC on resilient modulus, M_R, of the treated cemented soils
3. ábra CWC hatása a cementált talajok rugalmassági modulusára (M_R)

in contact with moisture caused the improvement on both deviatoric stress and resilient modulus of the treated soils. In addition, the cation exchange reaction between the dipole ions of the additive when in contact with molding moisture and those of soils caused the improved properties of the test soils [21, 22]. These results were recorded under cyclic loading on specimens subjected to testing sequences. The physical conditions that affect the resilient modulus (moisture and unit weight) were influenced by the introduction of the highly aluminosilicate CWC hence improving the strength behavior of the treated soils.

5. Conclusions

The experimental results of the treatment of soils with crushed waste ceramics have been observed and tabulated. The following remarks can be made; (i) the crushed waste ceramics was characterized and sampled as a silicate-based geomaterial with similarly particle gradation with the test soils and results show that the prepared materials contains binding properties that make it useful as a supplementary cementitious material. (ii) the soils were also tested for their basic properties which showed that they belong to A-2-7, A-2-6, A-7 and A-7-5 groups according to the American Association of State Highway and Transportation Officials classification method. Further characterization exercise on the soils shows that the soils are highly plastic soils, which implies that they are problematic and need modification to meet the requirements for use as construction materials. (iii) the soils were treated with the crushed waste ceramics at the rate of 10% to 120% by weight of solid in a steady increment of 10% by mixing and compacting to maximum dry density at an optimum moisture. (iv) the resilient modulus of the soils

was tested and results show that it improved consistently and substantially with increased rate of crushed waste ceramics. (v) the crushed waste ceramics showed that it can be utilized as a supplementary cementing construction material with its high content of aluminosilicates to improve the properties of soils used as pavement subgrade materials.

Acknowledgement

Vietnam Ministry of Education and Training for funding this research, based on Decision No. 5652/QD-BGDDT on December 28, 2018 with Grant No. MOET /2019 and with project number B2019-MDA-08.

References

[1] American Administration of State Highway and Transportation Officials (2014). Standard Method of Test for Compressive Strength of Cylindrical Concrete Specimens: AASHTO T 22–03, Washington DC.

[2] Onyelowe, K. C. – Bui Van, D. (2018a): Durability of nanostructured biomasses ash (NBA) stabilized expansive soils for pavement foundation, International Journal of Geotechnical Engineering. https://doi.org/10.1080/19386362.2017.1422909

[3] Onyelowe, K. C. – Bui Van, D. (2018b): Predicting Subgrade Stiffness of Nanostructured Palm Bunch Ash Stabilized Lateritic Soil for Transport Geotechnics Purposes. Journal of GeoEngineering of Taiwan Geotechnical Society, 2018 (in press). http://140.118.105.174/jge/index.php

[4] Onyelowe, K. C. – Bui Van, D. (2018c): Structural analysis of consolidation settlement behaviour of soil treated with alternative cementing materials for foundation purposes. Environmental Technology & Innovation, Vol. 11, pp. 125-141. https://doi.org/10.1016/j.eti.2018.05.005

[5] Onyelowe, K. C. – Bui Van, D. (2018d): Predicting Strength Behavior of Stabilized Lateritic Soil- Ash Matrix using Regression Model for Hydraulically Bound Materials Purposes, International Journal of Pavement Research and Technology. https://doi.org/10.1016/j.ijprt.2018.08.004

[6] Eberemu, A. O. – Afolayan, Joseph O.– Abubakar, Idris – Osinubi, Kolawole J. (2014): Reliability Evaluation of Compacted Lateritic Soil Treated With Bagasse Ash as Material for Waste Land Fill Barrier. Geo-Congress 2014 Technical Papers, GSP 234, 911-920.

[8] Mei Fong, Chong – Kah Peng, Lee – Hui Jiun, Chieng – Ramli, Syazwani Binti – Izyan, Ili (2009): Removal of boron from ceramic industry wastewater by adsorption-flocculation mechanism using palm oil mill boiler (POMB) bottom ash and polymer. Water Research, vol. 43 (13), Pp. 3326-3334. https://doi.org/10.1016/j.watres.2009.04.044

[9] Ba, M. – Nokkaew, K. – Fall, M. – Tinjum, J. M. (2013): Effect of Matric Suction on Resilient Modulus of Compacted Aggregate Base Courses. Geotechnical and Geological Engineering, An International Journal, Vol. 31 (3). https://doi.org/10.1007/s10706-013-9674-y

10] K. C. Onyelowe, – Duc Bui Van, – Obiekwe Ubachukwu, – Charles Ezugwu, – Bunyamin Salahudeen, – Manh Nguyen Van, – Chijioke Ikeagwuani, – Talal Amhadi, – Felix Sosa, – Wei Wu, – Thinh Ta Duc, – Adrian Eberemu, – Tho Pham Duc, – Obinna Barah, – Chidozie Ikpa, Francis Orji, – George Alaneme, – Ezenwa Amanamba, – Henry Ugwuanyi, – Vishnu Sai, – Chukwuma Kadurumba, – Subburaj Selvakumar – Benjamin Ugorji (2019): Recycling and Reuse of Solid Wastes; a Hub for Ecofriendly, Ecoefficient and Sustainable Soil, Concrete, Wastewater and Pavement Reengineering. International Journal of Low-Carbon Technologies. Vol. 14(3), pp. 440-451. https://doi.org/10.1093/Ijlct/Ctz028

[11] American Administration for State Highway Officials., (1993). Guide for Design of Pavement Structures, AASHTO, California, USA

[12] Osinubi, K. J. – Eberemu, A. O. (2019): Compatibility and Attenuative Properties of Blast Furnace Slag Treated Laterite. Journal of Solid Waste Technology and Management, 35(1 8), P*p. 7-16.*

[13] Atahu, M. K. – Saathoff, F. – Gebissa, A. (2019): Mechanical behaviors of expansive soil treated with coffee husk ash. Journal of Rock Mechanics and Geotechnical Engineering. https://doi.org/10.1016/j.jrmge.2018.11.004

[14] Onyelowe, K. C. – Salahudeen, A. B. – Eberemu, A. O. – Ezugwu, C. N. – Amhadi, T. – Alaneme, G. (2020a): Oxides of Carbon Entrapment for Environmental Friendly Geomaterials Ash Derivation. In book: Recent Thoughts in Geoenvironmental Engineering, Proceedings of the 3rd GeoMEast International Congress and Exhibition, Egypt 2019 on Sustainable Civil Infrastructures – The Official International Congress of the Soil-Structure Interaction Group in Egypt (SSIGE), pp. 58-67. https://doi.org/10.1007/978-3-030-34199-2_4

[15] Onyelowe, K. C. – Salahudeen, A. B. – Eberemu, A. O. – Ezugwu, C. N. – Amhadi, T. – Alaneme, G. – Sosa, F. (2020b): Utilization of Solid Waste Derivative Materials in Soft Soils Re-engineering. In book: Recent Thoughts in Geoenvironmental Engineering, Proceedings of the 3rd GeoMEast International Congress and Exhibition, Egypt 2019 on Sustainable Civil Infrastructures – The Official International Congress of the Soil-Structure Interaction Group in Egypt (SSIGE), pp. 49-57. https://doi.org/10.1007/978-3-030-34199-2_3

[16] Onyelowe, K. C. – Amhadi, T. – Ezugwu, C. N. – Onukwugha, E. – Ugwuanyi, H. – Jideoffor, I. – Ikpa, C. – Iro, U. – Ugorji, B. (2020c). Cemented Lateritic Soil as Base Material Improvement Using Compression. In book: Innovative Infrastructure Solutions using Geosynthetics, Proceedings of the 3rd GeoMEast International Congress and Exhibition, Egypt 2019 on Sustainable Civil Infrastructures – The Official International Congress of the Soil-Structure Interaction Group in Egypt (SSIGE), pp. 58-67. https://doi.org/10.1007/978-3-030-34242-5_4

[17] Tan, Y. – Hu, M. – Li, D. (2016). Effect of agglomerate size on California bearing ratio of lime treated lateritic soils. International Journal of Sustainable Built Environment, Vol. 5 (1), Pp. 168-175. https://doi.org/10.1016/j.ijsbe.2016.03.002

[18] Boukhelkhal, A. – Benabed, B.: Fresh and hardened properties of self-compacting repair mortar made with a new reduced carbon blended cement Epitő anyag – Journal of Silicate Based and Composite Materials, Vol. 71 (4), 2019, Pp. 108–113. https://doi.org/10.14382/epitoanyag-jsbcm.2019.19

[19] American Standard for Testing and Materials (ASTM) C618 (1978). Specification for Pozzolanas. ASTM International, Philadelphia, USA.

[20] BS 1377 - 2, 3. (1990). Methods of Testing Soils for Civil Engineering Purposes, British Standard Institute, London.

[21] BS 1924. (1990). Methods of Tests for Stabilized Soil, British Standard Institute, London

[22] El-Fakharany, M. E. – Ezzat, M. – Gad, A. – Ghafour, N. G. Abdel, – Baghdady, A. R.: Performance of dolomitic cementitious mortars as a repairing material for normal concrete in Egypt. Építőanyag – Journal of Silicate Based and Composite Materials, Vol. 71 (2), 2019, Pp. 33–42. https://doi.org/10.14382/epitoanyag-jsbcm.2019.7

[23] Onyelowe, K. C. – Bui Van, D. – Eberemu, A. O. – Xuan, M. N. – Salahudeen, A. B. – Ezugwu, C. – Van, M. N. – Orji, F. – Sosa, F. – Duc, T. T. – Amhadi, T. – Ikpa, C. – Ugorji, B. (2019): "Sorptivity, swelling, shrinkage, compression and durability of quarry dust treated soft soils for moisture bound pavement geotechnics". *Journal of Materials Research and Technology*, 8(4):3529–3538. https://doi.org/10.1016/j.jmrt.2019.06.029

Ref.:
Onyelowe, Kennedy Chibuzor – **Bui Van**, Duc – **Ikpa**, Chidozie – **Osinubi**, Kolawole – **Eberemu**, Adrian – **Salahudeen**, A. Bunyamin – **Nnadi**, Oscar C. – **Chima**, Moses C. – **Obimba-Wogu**, Jesuborn – **Ibe**, Kizito – **Ugorji**, Benjamin: *Resilient modulus and deviatoric stress of cemented soils treated with crushed waste ceramics (CWC) for pavement subgrade construction*
Építőanyag – Journal of Silicate Based and Composite Materials, Vol. 72, No. 3 (2020), 86–90. p.
https://doi.org/10.14382/epitoanyag-jsbcm.2020.14

The formation of phases with low or negative linear thermal expansion coefficient in porous mullite ceramics

Alacsony vagy negatív lineáris hőtágulási együtthatóval rendelkező fázisok kialakulása porózus mullit kerámiákban

Ludmila MAHNICKA-GOREMIKINA ▪ Institute of Silicate Materials, Riga Technical University, Latvia ▪ mahnicka@inbox.lv
Ruta SVINKA ▪ Institute of Silicate Materials, Riga Technical University, Latvia
Visvaldis SVINKA ▪ Institute of Silicate Materials, Riga Technical University, Latvia
Liga GRASE ▪ Institute of Silicate Materials, Riga Technical University, Latvia
Vadims GOREMIKINS ▪ Institute of Structural Engineering and Reconstruction, Riga Technical University, Latvia

Érkezett: 2019. 02. 19. ▪ Received: 19. 02. 2019. ▪ https://doi.org/10.14382/epitoanyag-jsbcm.2020.15

Abstract

Mullite ceramic has a low linear thermal expansion coefficient compared to other ceramics, such as alumina or zirconia ceramics. Applying porous mullite ceramics as modern refractory materials requires an extra reduction of linear thermal expansion. The main purposes of the investigation are the modification of porous mullite ceramic with WO_3 and differently stabilized ZrO_2 as well as in situ formation of crystalline phases with low or negative linear thermal expansion in such ceramic. Modified porous mullite ceramics were formed by slip casting the concentrated slurry of raw materials and were sintered at 1600 °C for 1 hour. Porosity of mullite ceramics obtained due to hydrogen gas evolution as a result of the reaction between the used aluminium paste and water. Using yttria stabilized zirconia (YSZ, 8 mol% Y_2O_3), magnesia stabilized zirconia (MSZ, 2.8 mol% MgO), WO_3, α- and γ-Al_2O_3, amorphous SiO_2 and kaolin allowed sintering the mullite ceramics with additional in situ formed crystalline phase of $ZrSiO_4$ and $Al_2(WO_4)_3$, which decreased the linear thermal expansion of certain porous mullite ceramics' samples. Used synthesis conditions allow to achieve stability of $ZrSiO_4$ and $Al_2(WO_4)_3$ phases The differently stabilized zirconia additive had influence on the formation of $ZrSiO_4$. Doubling the WO_3 content in the mixture of components increased the formation of $Al_2(WO_4)_3$ with a negative linear thermal expansion coefficient.

Keywords: powders, solid-state reaction, thermal expansion, mullite, $Al_2(WO_4)_3$
Kulcsszavak: porok, szilárd állapotbeli reakciók, hőtágulás, mullit, $Al_2(WO_4)_3$

Ludmila MAHNICKA-GOREMIKINA
Dr. sc. ing. Lead researcher at Institute of Silicate Materials in Faculty of Materials Science and Applied Chemistry of Riga Technical University, Latvia. Research interests: porous technical ceramic.

Ruta Svinka
Dr. sc. ing. Lead researcher and associate professor at Riga Technical University, Faculty of Material Science and Applied Chemistry, Institute of Silicate Materials, Latvia. Author and co-author of 185 scientific publications, h-index in SCOPUS 4. Expert of Latvian Science Council, member of board of Latvian Material Research Society, Ceramic Society. Research interests: minerals and synthetic nanopowders for obtaining of porous ceramic, modification of ceramic materials, new clay ceramic materials, catalysis and catalytic processes.

Visvaldis SVINKA
Dr. hab. sc. ing. Lead researcher and associate professor at Riga Technical University, Faculty of Material Science and Applied Chemistry, Institute of Silicate Materials, Latvia. Author and co-author of 135 scientific publications, h-index in SCOPUS 4. Expert of Latvian Science Council, member of Promotion Council P-02, member of Latvian Material Research Society, member of German Ceramic Society. Research interests: ceramic filters, porous lightweight ceramic, refractory ceramic, ceramic sorbents, clay minerals.

Liga GRASE
Dr. sc. ing. Lead researcher and assistant professor at Riga Technical University, Faculty of Material Science and Applied Chemistry, Institute of Silicate Materials, Latvia. Research interests: investigation of microstructure of silicate materials and interaction of laser radiation with semiconductors.

Vadims GOREMIKINS
Dr. sc. ing. Lead researcher at Institute of Structural Engineering and Reconstruction of Riga Technical University, Latvia. Author and co-author of 21 scientific publications. Research interests: structural fire design, composite structures, cable structures, suspension bridges.

1. Introduction

Mullite-based ceramic is an important type of refractory ceramic. Relatively low linear thermal expansion is very important for mullite ceramic application in conditions of rapidly changing temperatures [1]. The literature reports linear thermal expansion coefficient (LTEC) values for porous mullite ceramics ranging from 4.0 to $5.9 \cdot 10^{-6} \cdot °C^{-1}$ (average between 30 °C and 1000 °C) [2]. The average LTEC of mullite ceramics can be decreased by adding materials with a low or negative linear thermal expansion coefficient or the in situ formation of additional crystalline phases with low LTEC during the ceramic sintering time. Previous research investigated whether the thermal expansion of mullite ceramics can be effectively decreased by modification with cordierite ($\alpha_{cord.} \approx 0.5 \cdot 10^{-6} \cdot °C^{-1}$) [3], aluminium titanate ($\alpha_{alum.\ tit} \approx 1 \cdot 10^{-6} \cdot °C^{-1}$) [4, 5] and zircon ($\alpha_{zircon} \approx 4.1 \cdot 10^{-6} \cdot °C^{-1}$) [6] due to low linear thermal expansion coefficient of these phases. The influence of phases with negative LTEC on the properties of mullite ceramics has not been well studied. Research on materials with a negative LTEC has been of high interest since the mid-20th century and continues to now [7-9]. Crystalline phases such as aluminium tungstate ($Al_2(WO_4)_3$) and zirconium tungstate ($Zr(WO_4)_2$) have an average negative linear thermal expansion coefficient. The LTEC of aluminium tungstate is $-1.5 \cdot 10^{-6} \cdot °C^{-1}$ in the temperature range from 25 to 850 °C [8], and the LTEC of zirconium tungstate is $-8.6 \cdot 10^{-6} \cdot °C^{-1}$ from 0 to 777 °C [9]. According to the literature data, $Al_2(WO_4)_3$ formation can be observed by the co-precipitation reaction method, by the sol-gel method and from solid-state synthesis. The $Al_2(WO_4)_3$ formation temperature is in the 620–1050°C range, and depends on the sintering method. The holding time at the formation temperature varies from 5 hours to much longer, about 30–40 hours [10, 11]. The particle size and the morphology of $Al_2(WO_4)_3$ depends on the treatment temperature and holding time. In the case of the co-precipitation reaction method, crystalline $Al_2(WO_4)_3$ formation occurred after firing the Al-W-precipitated composition at temperatures of 430 °C [12], 630 °C, 700 °C [13], 800 °C [11] and 830 °C [12] for 5 hours. The particle size of synthesized $Al_2(WO_4)_3$ powder was increased from 20 to 300 nm [12] or from 50 to 150 nm [13, 14] with increasing temperature. Koseva and Nikolov had concluded that in the case of the sol-gel modified Pechini method, the particle size of pure phase $Al_2(WO_4)_3$ was between 50 nm (at 620 °C for 12 hours) and 200 nm (at 830 °C for 36 hours) [10, 14]. Achary et al. [8] synthesized $Al_2(WO_4)_3$ by the solid-state reaction from Al_2O_3 and WO_3 at 900 °C for 42 hours followed by 1000 °C for 30 hours with

intermittent grinding. Later Nikolov et al. [14] also synthesized pure $Al_2(WO_4)_3$ by this method at similar temperatures, but with a shorter holding time, respectively at 930 °C for 16 hours, at 990 °C and 1050 °C for 8 hours. Romao et al. prepared ZrW_2O_8/$Al_2W_3O_{12}$ ceramics composites by the solid-state reaction from yttria stabilized zirconia, monoclinic ZrO_2, Al_2O_3 and WO_3 during sintering at 1200 °C, with holding times varying from 6 to 21 hours [15]. A ZrW_2O_8 phase, in turn, can be synthesized by the combustion method [16], by hydrothermal synthesis of raw compounds at 160 °C for 36 hours with further sintering at 570 °C for 1 hour [17, 18], by the co-precipitation reaction with drying at 60–80 °C and firing at 1150 °C for 10 hours, and by the sol-gel method with firing at 600 °C for 10 hours [18]. From the literature, ZrW_2O_8 is stable in a narrow temperature range from 1105 to 1257 °C, but this phase decomposes to ZrO_2 and WO_3 at about 700–850 °C, respectively. The melting temperature of this phase is above 1257 °C [15-18].

The aim and novelty of this work is to investigate the use of ZrO_2 and WO_3 additives for the in situ formation of phases with negative LTEC, ($Al_2(WO_4)_3$ and ZrW_2O_8), in porous mullite ceramics sintered from powder raw materials by a solid-state reaction method.

2. Materials and methods

2.1 Raw materials and sample preparation

Materials	Average particle size, d_{50} (μm)	Name, Manufacturer
α-Al_2O_3	2.0	Nabalox NO 725, Nabaltec AG, Germany
γ-Al_2O_3	80.0	Nabalox NO 201, Nabaltec AG, Germany
SiO_2 amorphous	3.0–5.0	GetNanoMaterials, France
Kaolin (SiO_2 – 56.5 wt%, Al_2O_3 – 31.0 wt%)	1.5	MEKA, Amberger Kaolinwerke, Germany
ZrO_2 stabilized by 8 mol% Y_2O_3	0.5	GetNanoMaterials, France
ZrO_2 stabilized by 2.8 mol% MgO	0.8	Goodfellow, United Kingdom
WO_3	5.0	GetNanoMaterials, France
Aluminium paste (solid content of 70 ± 2%)	12.0	Aquapor-9008, Schlenk Metallic Pigments GmbH, Germany

Table 1 Raw material specifications
1. táblázat A felhasznált alapanyagok pontos megnevezése

Commercially available raw powders, such as α-Al_2O_3, γ-Al_2O_3, amorphous SiO_2, kaolin, two types of ZrO_2 and WO_3 were used for ceramics materials samples preparation. *Table 1* summarises the raw materials specifications. In all compositions, the amount of kaolin was 30 wt%, the ratio of Al_2O_3 to SiO_2 was 2.57:1 and the ratio of α-Al_2O_3 to γ-Al_2O_3 was 1:3. The ratio of Al_2O_3 to SiO_2 corresponded to the mullite stoichiometric composition, $3Al_2O_3{\cdot}2SiO_2$. The ratio of α-Al_2O_3 to γ-Al_2O_3 was determined as effective in previous studies [19]. Yttria stabilized zirconia (YSZ, 8 mol% Y_2O_3), magnesia stabilized zirconia (MSZ, 2.8 mol % MgO) and WO_3 were used as modification additives. 5 wt% of each type of zirconia was used, both separately as well as in a mixture with WO_3 in a 1:1 and 1:2 ratio. Aluminium paste (0.18 wt%) was used as a pore-forming agent to prepare porous mullite ceramic.

Slip casting the concentrated slurry of raw materials was used for samples preparation. The water content of the concentrated slurry was 38–40 wt%. The method and process of samples preparation were described in more detail in previous articles [19-21]. The dried samples were sintered at 1600 °C with a 250 °C/h (4.2 °C/min) heating rate and the holding time at maximum temperature was 1 hour. The fired samples cooling process was as slow as the heating process.

2.2 Characterisation

Appropriate equipment was used to analyse the crystallographic phases, different phase transformations and reactions in the samples at the heating treatment time and the sintered sample microstructure. X-ray powder diffraction (XRD) was carried out with a Rigaku Ultima+ (Japan) using Cu K_a radiation and operating at 30 kV and 20 mA. XRD patterns were scanned in the 5–60 2θ° measurement angle range with a 0.02° step and a 2°/min goniometer scanning rate. Differential thermal analysis was done using „SETSYS Evolution TGA-DTA/TMA SETARAM". The heating for DTA was 12 °C per minute at a temperature range from 0 to 1300 °C with air as the carrier gas. The samples microstructures were analysed using two scanning electron microscopes (SEM), -Hitachi TableTop Microscope TM3000 and high-resolution field emission low vacuum scanning electron microscope (FEI Nova NanoSEM 650). The samples were observed in low vacuum mode eliminating the need for metal coating sputtering. The sample elemental composition was determined using energy-dispersive X-ray spectroscopy (EDX) with an X-ray fluorescence spectrometer (Apollo X SDD) created by TEAM™ Integrated EDX. The shrinkage after ceramics' sintering and bulk density of the samples was calculated mathematically. The determination of apparent porosity and water uptake was based on the Archimedes principle according to the European standard EN 623-2. The temperature dependence of the linear thermal expansion coefficient for sintered samples was determined by high temperature horizontal dilatometer L76/1600 D (Linseis, Selb, Germany).

3. Results and discussion

3.1 X-ray diffraction

The X-ray diffraction patterns in *Fig. 1* represent the phase compositions of samples with yttria stabilized zirconia and magnesia stabilized zirconia additives. The mullite phase was the dominant phase of the samples for both raw material compositions, which were sintered at 1600 °C. The ZrO_2 phase was mainly expressed in monoclinic modification in both samples. Cubic ZrO_2 was detectable in samples with yttria stabilized zirconia, but tetragonal ZrO_2 modification observed in samples with magnesia stabilized zirconia. The corundum phase was found in the samples with YSZ additive (*Fig. 1 (a)*) as opposed to samples with MSZ (*Fig. 1 (b)*).

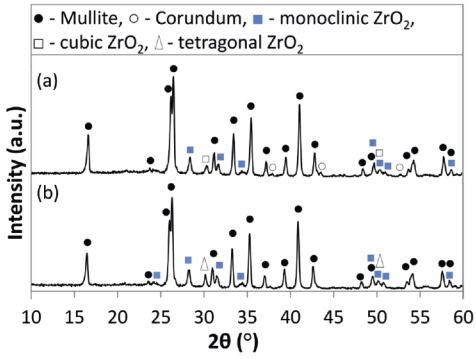

Fig. 1 *XRD patterns of the samples with ZrO_2 additives: (a) with YSZ, (b) with MSZ*
1. ábra *ZrO_2-t tartalmazó minták röntgen diffrakciós analízisének eredménye: (a) YSZ-t tartalmazó, (b) MSZ-t tartalmazó*

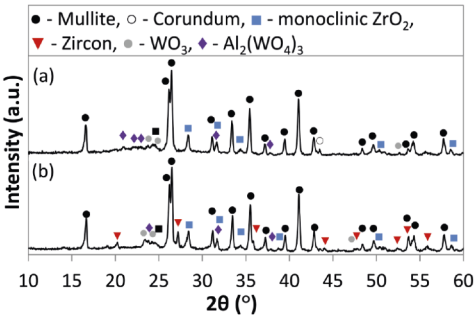

Fig. 2 *XRD patterns of the samples with ZrO_2 and WO_3 additives in the ratio of 1:1: (a) with YSZ and WO_3, (b) with MSZ and WO_3*
2. ábra *ZrO_2-t és WO_3-t 1:1 arányban tartalmazó minták röntgen diffrakciós analízisének eredménye: (a) YSZ-t és WO_3-t tartalmazó, (b) MSZ-t és WO_3-t tartalmazó*

Fig. 2 shows the XRD patterns of the samples with YSZ or MSZ addition in a 1:1 ratio in the mixture with WO_3, sintered at 1600 °C. The mullite and monoclinic ZrO_2 were the main phases of these samples. Tetragonal ZrO_2 and corundum phases were not detectable. The intensity peaks of WO_3 were less definite for samples with YSZ and WO_3 (1:1) than for samples with MSZ and WO_3 (1:1). The XRD pattern in *Fig. 2* (b) shows that zircon was formed as an additional phase after firing in samples with MSZ and WO_3 (1:1). In the samples with the addition of only YSZ or MSZ (*Fig. 1 (a)* and *(b)*) and with the YSZ:WO_3=1:1 (*Fig. 2 (a)*), the zircon phase was not observed. This is because the presence of stabilizers such as Y_2O_3 and MgO, respectively from YSZ and MSZ, led to the forming a liquid phase in the Y_2O_3-Al_2O_3-SiO_2 system at 1550 °C and MgO-Al_2O_3-SiO_2 at 1450–1550 °C that promoted zircon dissociation with subsequent mullite phase formation [22]. In the case using YSZ, this influence was much more pronounced due to the higher amount of Y_2O_3 as a stabilization additive rather than MgO, respectively 8 mol% and 2.8 mol%. Using the WO_3 prevented liquid formation in the MgO-Al_2O_3-SiO_2 system, and zircon was retained in the phase composition of synthesized mullite ceramics with MSZ and WO_3 (1:1), unlike the samples with YSZ and WO_3 (1:1).

The XRD patterns in the 2θ° range from 20° to 24° (*Fig. 2 (a)* and (b)) show the mixture of crystalline and amorphous phases for both samples with ZrO_2 and WO_3 (1:1). The presence of separate peaks on the XRD patterns of these compositions in the 2θ° range from 20° to 24°, at 32°, 35° and 43° corresponded to the aluminium tungstate phase.

Doubling the WO_3 amount contributed to the zircon and aluminium tungstate formation in both sample compositions with two types of stabilized ZrO_2 (*Fig. 3 (a)* and *(b)*). In the case of these samples, the number of intensity peaks ZrO_2 phase decreased due to ZrO_2 participation in forming $ZrSiO_4$. The location of t-ZrO_2 in the neighbourhood of amorphous SiO_2 promoted zircon formation at a lower temperature by a diffusion reaction. Zircon formation in the corresponding ceramic samples was proposed to occur via several successive reactions. First, $ZrSiO_4$ began forming by reacting t-ZrO_2 with amorphous SiO_2 at about 1200 °C. Then, zircon formation continued by the reaction of t-ZrO_2 with cristobalite at 1400–1470 °C owing to the crystallization and corresponding modification of SiO_2. Complete formation of this phase occurred by the reaction of m-ZrO_2 with cristobalite after ~1580 °C due to t-ZrO_2 gradually transforming into m-ZrO_2 with an increase in temperature because of the decrease in excess surface energy [23-26]. In turn, increasing the WO_3 amount also prevented liquid formation and zircon dissipation in the case of samples with YSZ and WO_3 (1:2). 1600 °C was not high enough for decomposing $ZrSiO_4$ to ZrO_2 and SiO_2 according to the literature [23]. The mullite phase also remained dominant in these samples, but the intensity of this phase's diffraction maximums decreased (*Fig. 3*) because the Al_2O_3 and SiO_2 mullite components were used forming phases such as aluminium tungstate and zircon. The intensity of aluminium tungstate phase diffraction maximums increased in samples with ZrO_2 and WO_3 additives (1:2) due to the increasing WO_3 amount. The ZrW_2O_8 phase was not observed in sintered samples compositions. The XRD pattern of the ceramic material with YSZ:WO_3 (1:2) shows the significant presence of WO_3 phase than in samples with MSZ:WO_3 (1:2).

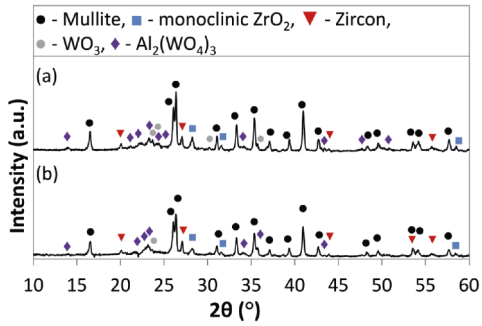

Fig. 3 *XRD patterns of the samples with ZrO_2 and WO_3 additives in the ratio of 1:2: (a) with YSZ and WO_3, (b) with MSZ and WO_3*
3. ábra *ZrO_2-t és WO_3-t 1:2 arányban tartalmazó minták röntgen diffrakciós analízisének eredménye: (a) YSZ-t és WO_3-t tartalmazó, (b) MSZ-t és WO_3-t tartalmazó*

3.2 Differential thermal analysis

The DTA curves for heating and cooling the MEKA kaolin and the non-sintered sample compositions are shown, respectively, in *Fig. 4* and *Fig. 5*. In the DTA plots (*Fig. 4*) for all samples, the first endothermic peak at about 180 °C represented the elimination of free water absorbed between the particles. In the case of kaolin (*Fig. 4 (a)*), the second strong endothermic peak at 530 °C corresponded to the dehydroxylation of kaolinite and the formation of metakaolinite [27]. The dehydroxylation

process should be considered a crystal-chemical process of the kaolinite's bilayer lattice changing with the absorption of a significant amount of heat [28-31]. The exothermic effect in the 647 to 660 °C temperature range defined the crystallization of some amorphous phase [32]. The sharp exothermic peak within 1000 °C was due to the formation of new crystalline phases such as a Si-containing γ-Al_2O_3 with spinel structure plus amorphous SiO_2 or a 2:1 mullite plus amorphous SiO_2 [30, 31]. Then, the mullite phase ($3Al_2O_3{\cdot}2SiO_2$) formation and cristobalite were followed at about 1235–1245 °C, which is represented as a gently sloping exothermic peak [30, 31].

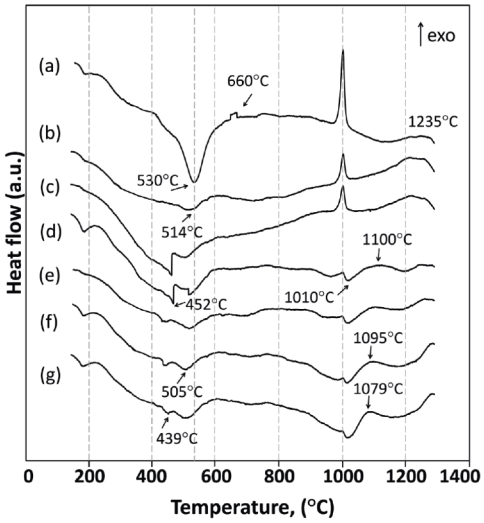

Fig. 4 DTA for samples, heating curves: (a) kaolin, (b) with YSZ, (c) with MSZ, (d) with YSZ:WO_3 (1:1), (e) with MSZ:WO_3 (1:1), (f) with YSZ:WO_3 (1:2), (g) with MSZ:WO_3 (1:2)

4. ábra Differenciális termoanalízisből származó fűtési görbék egyes mintákra: (a) kaolin, (b) YSZ-t tartalmazó, (c) MSZ-t tartalmazó, (d) YSZ:WO_3 (1:1) arányban tartalmazó, (e) with MSZ:WO_3 (1:1) arányban tartalmazó, (f) with YSZ:WO_3 (1:2) arányban tartalmazó, (g) with MSZ:WO_3 (1:2) arányban tartalmazó

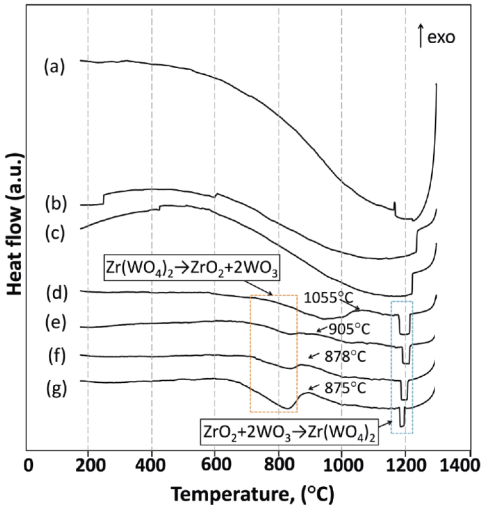

Fig. 5 DTA for samples, cooling curves: (a) kaolin, (b) with YSZ, (c) with MSZ, (d) with YSZ:WO_3 (1:1), (e) with MSZ:WO_3 (1:1), (f) with YSZ:WO_3 (1:2), (g) with MSZ :WO_3 (1:2)

5. ábra Differenciális termoanalízisből származó hűtési görbék egyes mintákra: (a) kaolin, (b) YSZ-t tartalmazó, (c) MSZ-t tartalmazó, (d) YSZ:WO_3 (1:1) arányban tartalmazó, (e) with MSZ:WO_3 (1:1) arányban tartalmazó, (f) with YSZ:WO_3 (1:2) arányban tartalmazó, (g) with MSZ:WO_3 (1:2) arányban tartalmazó

The DTA thermal behaviour of the samples compositions with YSZ and MSZ demonstrated processes similar to those seen in heating pure kaolin: the dehydroxylation of kaolinite at about 514 °C, spinel structure or primary mullite formation with amorphous SiO_2 at 1000 °C and secondary mullite ($3Al_2O_3{\cdot}2SiO_2$) formation at about 1200 °C. The DTA curves of the samples with a mixture of ZrO_2 and WO_3 in a 1:1 and 1:2 ratio showed an endothermic peak at about 400–460 °C (*Fig. 4 (d–g)*), which indicated the WO_3 phase transformation from the monoclinic modification to the orthorhombic [33-35]. The exothermic peak within 1000 °C for all samples with a ZrO_2 and WO_3 mixture was smaller than for kaolin and samples without WO_3. It is important to note that after this small exothermic peak at 1000 °C, an endothermic peak immediately followed at 1015–1090 °C, which was also characteristic of all samples with a mixture of ZrO_2 and WO_3. This can be explained by the combination of two processes that came at relatively the same time in the 950–1090 °C range. Therefore, the exothermic peak at 1000 °C corresponded to one of the stages of the thermal conversion of kaolin, which was described above, and the subsequent endothermic peak was associated with the formation of zirconium tungstate from ZrO_2 and WO_3 [16, 17, 36]. This was also confirmed by the behaviour of the cooling curves (*Fig. 5 (d–g)*). The elongated endothermic peak of the cooling curves at the 1185–1200 °C region was due to the formation of zirconium tungstate at the samples cooling as verified by the ZrO_2 and WO_3 system phase diagram [37] and the works of Dedova and Lommens [17, 36], and is not typical behaviour of an unmodified mullite ceramic DTA cooling curve. The ZrW_2O_8 phase intensity peaks were not observed in the XRD patterns after sample sintering because ZrW_2O_8 melting occurs above 1257 °C [17, 33], which is lower than the sample sintering temperature. ZrW_2O_8 was not present after slowly cooling the samples due to the decomposition of this phase into ZrO_2 and WO_3 within the narrow 770–825 °C temperature range [16, 36, 37]. ZrW_2O_8 decomposing into oxides caused a smooth rise in the DTA cooling curves from 825 °C to lower temperatures (*Fig. 5 (d–g)*).

The $Al_2(WO_4)_3$ formation is shown in the sample heating DTA curves (*Fig. 4 (d–g)*) as an exothermic effect at 1075–1100°C. The mullite phase formed at temperatures higher than 1200°C in the case of a mixture of differently stabilized zirconia and WO_3 in a 1:1 and 1:2 ratios. The wide exothermic peak of the cooling curves (*Fig. 5 (d–g)*) for samples with YSZ and WO_3 (1:1) at 1055 °C was due to the formation of aluminium tungstate while cooling, as verified by the Al_2O_3-WO_3 system phase diagram [38, 39]. For samples with the addition of MSZ:WO_3=1:1, YSZ:WO_3=1:2 and MSZ:WO_3=1:2, the $Al_2(WO_4)_3$ formation also occurred while cooling but at lower temperatures, respectively at ~905 °C, ~878 °C and ~875 °C. The $Al_2(WO_4)_3$ formation temperature was lower in case of mullite ceramics with MSZ and WO_3 mixture of both ratios.

3.3 Scanning electron microscopy

SEM micrographs showing the microstructure of samples with the YSZ additive are presented in *Fig. 6*. The structure of these samples was composed of densely packed, elongated mullite crystals, which are located in a glassy phase (*Fig. 6 (a)*

and (b)). The glassy phase was formed with the participation of yttrium oxide and increased the sintering of the samples. Sample fracture occurred in the glassy phase at the time of sample preparation for the SEM (samples were broken in half), which is visible in *Fig. 6 (c)*. The SEM micrograph from the TableTop SEM Microscope TM3000 (*Fig. 6 (a)*) shows large and small white inclusions, which confirm the presence of ZrO_2.

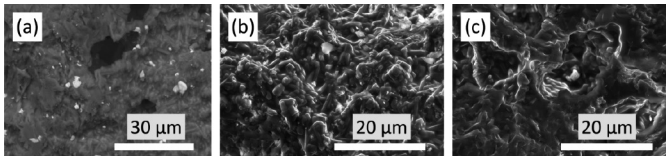

Fig. 6 SEM micrographs of the microstructure of sintered samples with YSZ
6. ábra Az YSZ-t tartalmazó szinterelt mintákról mikroszerkezetéről pásztázó elektronmikroszkóppal készített felvételek

The structure of ceramics samples with the MSZ additive was similar to the structure of the samples with YSZ (*Fig. 7 (a)* and (b)). The white particles in the SEM micrographs (*Fig. 7 (a)*) for samples with MSZ showed that m-ZrO_2 particles have a smaller size and are more uniformly distributed in the sample structure after sintering.

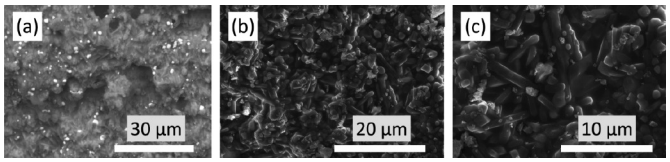

Fig. 7 SEM micrographs of the microstructure of sintered samples with MSZ
7. ábra Az MSZ-t tartalmazó szinterelt mintákról mikroszerkezetéről pásztázó elektronmikroszkóppal készített felvételek

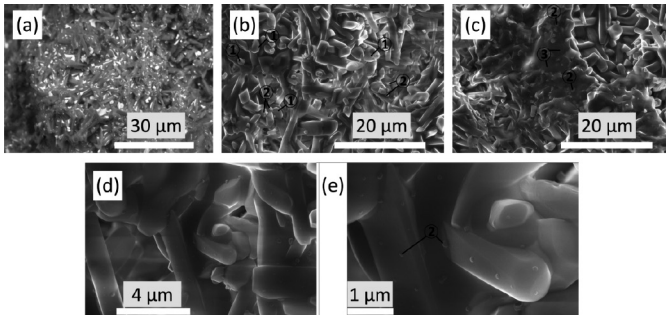

Fig. 8 SEM micrographs of the microstructure of sintered samples with YSZ and WO_3 additive in a 1:1 ratio
8. ábra Az YSZ-t és WO_3-at 1:1 arányban tartalmazó szinterelt mintákról mikroszerkezetéről pásztázó elektronmikroszkóppal készített felvételek

The sample structure changed with the use of a ZrO_2 and WO_3 mixture in the case of both ratios of these oxides. The structure of samples with YSZ:WO_3=(1:1) was formed from needle-like mullite crystals. Parts of the mullite crystals were covered by a continuous glassy phase that was white in the SEM micrograph from the TableTop SEM (*Fig. 8 (a)*). The structure of these samples also contained granular inclusions.

Table 2 presents the elemental compositions of samples' certain areas after EDX point analysis. EDX analysis results showing that some grains were ZrO_2, other grains were aluminium tungstate, respectively EDX points 1 and 2 in *Fig. 8 (b)* and in *Table 2*. The mullite crystals were distinguishable at the larger magnification (*Fig. 8 (b–e)*) after using the high-resolution SEM (FEI Nova NanoSEM 650). The EDX results (EDX point 3) in *Fig. 8 (c)* and data in *Table 2* show that the existing amorphous phase contained a higher weight per cent of elements such as O, Al, Si, W and a lower weight percent of Zr and Y, which can correspond to the alumina-silica glassy phase [40] and alumina-tungstate glassy phase with dissolved ZrO_2 and Y_2O_3. This amorphous part of the samples contained crystalline grains (*Fig. 8 (c)*, EDX point 2), which were identified as aluminium tungsten crystalline grains after the EDX analysis. Some mullite crystals contained relatively small white points (*Fig. 8 (a)*), which were another phase. The SEM micrographs at the higher magnification (*Fig.8 (d)* and *(e)*) demonstrated small crystals on the surface of the mullite crystals. These crystals were identified as aluminium tungstate crystals by the results of the EDX point analysis (point 2) in *Table 2*.

Fig. 9 shows the structure of the samples with MSZ and WO_3 in a 1:1 ratio. Relatively fine particles (marked in light grey in *Fig. 9. (a)*) were distributed in the sample structure. These faceted crystals were zircon, by the EDX analysis (EDX point 4 and 5) (*Fig. 9. (a–c)* and *Table 2*). The prismatic mullite crystals in these samples are relatively thinner and longer than mullite crystals of the YSZ:WO_3=(1:1) samples.

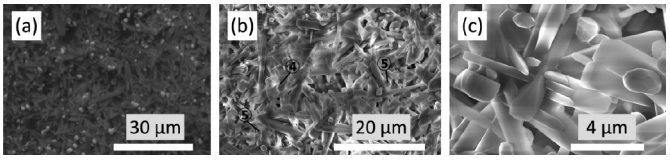

Fig. 9 SEM micrographs of the microstructure of sintered samples with MSZ and WO_3 additive in a 1:1 ratio
9. ábra Az MSZ-t és WO_3-at 1:1 arányban tartalmazó szinterelt mintákról mikroszerkezetéről pásztázó elektronmikroszkóppal készített felvételek

Element	Point 1		Point 2		Point 3		Point 4		Point 5	
	Weight %	Atom %	Weight %	Atom %	Weight %	Atom %	Weight %	Atom %	Weight %	Atom %
O	37.1	72.7	39.3	61.7	39.1	66.6	34.9	66.5	46.4	69.1
Al	4.9	5.6	30.8	28.6	15.9	16.1	-	-	13.3	11.8
Si	2.3	2.6	7.1	6.3	11.3	11.0	16.7	18.5	14.6	12.4
W	-	-	22.9	3.4	26.9	4.0	-	-	-	-
Zr	55.7	19.1	-	-	2.8	1.1	48.4	15.0	25.7	6.7
Y	-	-	-	-	4.0	1.2	-	-	-	-

Table 2 The elemental compositions of samples' certain plots after EDX point analysis
2. táblázat Az EDX (energia diszperzív röntgensugár) analízis egyes pontjaiban a minták elemi összetételei

The structures of samples with YSZ:WO_3 and MSZ:WO_3 in a 1:2 ratio were formed from crystal agglomerates of mullite and aluminium tungstate crystals. The aluminium tungstate crystals were located on and between the mullite crystals (*Fig. 10* and *Fig. 11*). Comparing the SEM micrographs of samples with YSZ:WO_3 mixtures in ratios of (1:1) and (1:2) in *Fig. 8* and *Fig. 10*, the quantity of aluminium tungstate crystals increased with increasing WO_3 quantity. In turn, thinner mullite crystals were randomly located among the larger mullite crystals. The presence of aluminium tungstate crystals in samples with MSZ:WO_3 also became noticeable after increasing the WO_3 quantity (*Fig. 11. (b)* and *(c)*).

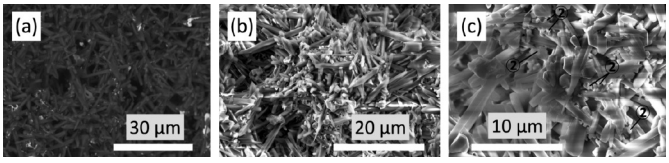

Fig. 10 SEM micrographs of the microstructure of the sintered samples with YSZ and WO_3 additive in a 1:2 ratio
10. ábra Az YSZ-t és WO_3-at 1:2 arányban tartalmazó szinterelt mintákról mikroszerkezetéről pásztázó elektronmikroszkóppal készített felvételek

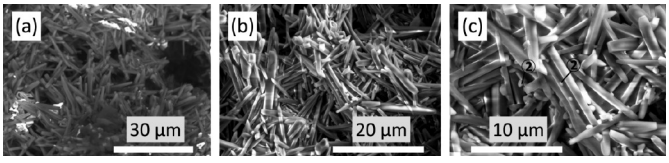

Fig. 11 SEM micrographs of the microstructure of the sintered samples with MSZ and WO_3 additive in a 1:2 ratio
11. ábra Az MSZ-t és WO_3-at 1:2 arányban tartalmazó szinterelt mintákról mikroszerkezetéről pásztázó elektronmikroszkóppal készített felvételek

The possible growth of aluminium tungstate crystals on the mullite crystals occurred from the Al_2O_3 and WO_3 solid-state reaction during sintering and from the alumina-tungstate liquid phase during cooling. The nucleation and growth of aluminium tungstate crystals proceeded in possible defect sites on mullite crystals. Supersaturation of the alumina-tungstate liquid phase occurred with increasing WO_3 in samples with YSZ:WO_3 (1:2) and MSZ:WO_3 (1:2) mixtures and aluminium tungstate crystalline grains continued to grow.

3.4 Shrinkage, bulk density and apparent porosity of the sintered samples

The ceramics samples, modified only with YSZ or MSZ, have shrinkage higher than 35±1% and bulk density 1.55±0.05 g/cm^3 (*Fig. 12*). Using the mixture of stabilized ZrO_2 and WO_3 additive decreases the shrinkage and bulk density of the samples. The results of the bulk density decrease with increasing of the samples apparent porosity (*Fig. 13*). The apparent porosity of all samples compositions is higher than 40% and maximum porosity is 66–73%. The samples with YSZ:WO_3 (1:1) and MSZ:WO_3 (1:2) have porosity about 63-66% and the bulk density of 1.24±0.05 g/cm^3. Modifying of the porous mullite ceramics with mixture of magnesia stabilized zirconia and WO_3 has higher influence on the apparent porosity and water uptake of the samples than the yttria stabilized zirconia in mixture with WO_3. The mixture of MSZ and WO_3 in a 1:1 ratio caused increasing of the apparent porosity of ≈15%, but these oxides mixture in a 1:2 ratio caused increasing of the apparent porosity of ≈11%, respectively in comparison with YSZ:WO_3 (1:1) and YSZ:WO_3 (1:2). Doubling the WO_3 amount slightly decreases the porosity.

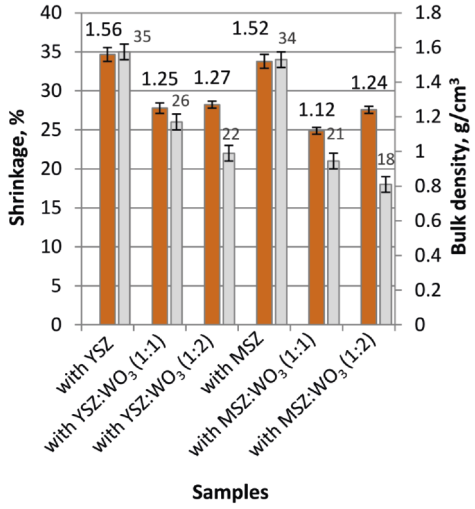

Fig. 12 Shrinkage and bulk density of the sintered samples
12. ábra A szinterelt minták zsugorodása és testsűrűsége

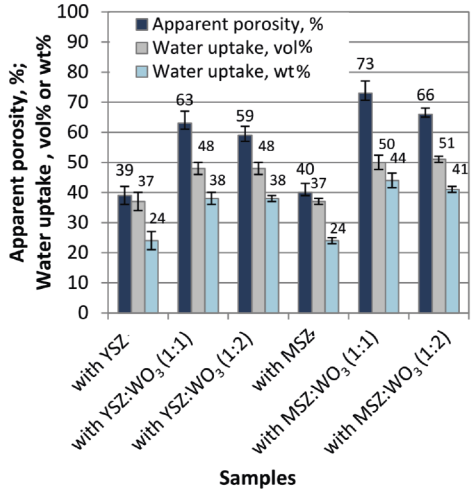

Fig. 13 Apparent porosity and water uptake of the samples
13. ábra A minták látszólagos porozitása és és vízfelvétele

3.5 Linear thermal expansion of the sintered samples

The analysis of the thermal property in *Fig. 14* shows that samples only with YSZ or MSZ have the similar linear thermal expansion as the pure mullite ceramics due to the mullite phase dominance in these samples. The presence of such phases as zircon (α_{zircon} = 4.1·10^{-6}·°C^{-1}) [6] and aluminium tungstate ($\alpha_{aluminium\ tungstate}$ = −1.5·10^{-6}·°C^{-1}) [8] decreased the linear thermal expansion of samples with YSZ:WO_3 mixture in a 1:1 ratio and with MSZ:WO_3 in a 1:2 ratio. At the same time, samples with YSZ:WO_3 mixture in a 1:2 ratio and with MSZ:WO_3 in a 1:1 ratio, containing unreacted WO_3 (confirmed by XRD results), have higher expansion due to the high linear expansion coefficient of WO_3 ($\alpha_{tungsten\ oxide}$= 13–15·10^{-6}·°C^{-1}) [8, 9]. The expansion of samples with the ZrO_2 and WO_3 mixture decreases in the temperature range approximately from

950 to 1020 °C due to the formation of zirconium tungstate ($\alpha_{\text{zirconium tungstate}} = -8.6 \cdot 10^{-6} \cdot °C^{-1}$) [9] from ZrO_2 and WO_3 during the heating and at these temperatures the ceramic materials have an effect of contracting.

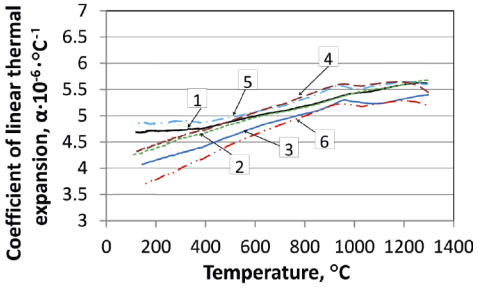

Fig. 14 Temperature dependence of the linear thermal expansion coefficient for sintered samples: 1 - with YSZ, 2 - with MSZ, 3 - with YSZ:WO_3 (1:1), 4 - with MSZ:WO_3 (1:1), 5 - with YSZ:WO_3 (1:2), 6 - with MSZ:WO_3 (1:2)

14. ábra A szinterelt minták lineáris hőtágulási együtthatójának hőmérséklet függése: 1 – YSZ-t tartalmazó, 2 – MSZ-t tartalmazó, 3 – YSZ-t és WO_3-at 1:1 arányban tartalmazó, 4 – MSZ-t és WO_3-at 1:1 arányban tartalmazó, 5 – YSZ-t és WO_3-at 1:2 arányban tartalmazó, 6 – MSZ-t és WO_3-at 1:2 arányban tartalmazó

4. Conclusions

Modified porous mullite ceramics were fabricated by slip casting a concentrated slurry of raw materials and were sintered at 1600 °C for 1 h with a slow cooling process. It was established that the in situ formation of crystalline phases with low or negative LTEC in mullite ceramics can be found after adding YSZ (8 mol% Y_2O_3) or MSZ (2.8 mol% MgO with WO_3 mixture in a 1:1 and 1:2 ratio at the correspond sintering conditions. These synthesis conditions are much simpler than the applicable methods and long holding time considered above from literature date, which is an advantage for obtaining porous mullite ceramics. Only $Al_2(WO_4)_3$ or two crystalline phases, $ZrSiO_4$ and $Al_2(WO_4)_3$, were formed into the porous mullite ceramics after its modification with metal oxides such as differently stabilized zirconia and WO_3. The $Zr(WO_4)_2$ phase was not detectable due to the not appropriate firing-cooling process, which does not allow remaining this phase in phase composition of investigated mullite ceramics. The 8 mol% Y_2O_3 stabilized zirconia additive has higher influence on decreasing temperature of $ZrSiO_4$ dissociation than 2.8 mol% MgO stabilized zirconia. Using the certain amount of WO_3 prevent the $ZrSiO_4$ dissociation in mullite ceramic modified with ZrO_2 and WO_3. Addition of the 2.8 mol% MgO stabilized zirconia in mixture with WO_3 increases the porosity of mullite ceramic. Sintered porous mullite ceramics with YSZ:WO_3 mixture in a 1:1 ratio and with MSZ:WO_3 in a 1:2 ratio have the potential application in conditions of elevated temperatures ≥1200 °C as thermal insulator with lowered linear thermal expansion.

Acknowledgements

This work has been supported by the European Regional Development Fund within the Activity 1.1.1.2 "Post-doctoral Research Aid" of the Specific Aid Objective 1.1.1 "To increase the research and innovative capacity of scientific institutions of Latvia and the ability to attract external financing, investing in human resources and infrastructure" of the Operational Programme "Growth and Employment" (No.1.1.1.2/VIAA/1/16/121).

References

[1] Ilić, S. – Zec, S. – Miljković, M. – Poleti, D. – Pošarac-Marković, M. – Janaćković, Dj. – Matović, B.: Sol–gel synthesis and characterization of iron doped mullite. J. Alloys Compd. 612 (2014) 259–264. https://doi.org/10.1016/j.jallcom.2014.05.204

[2] Foo, C. T. – Salleh, M. A. M. – Ying, K. K. – Matori, K. A.: Mineralogy and thermal expansion study of mullite-based ceramics synthesized from coal fly ash and aluminum dross industrial wastes. Ceram.Int. 45 (6) (2019) 7488–7494. https://doi.org/10.1016/j.ceramint.2019.01.041

[3] Belogurova, O. A. – Grishin, N. N.: Modified mullite-cordierite materials. Refract. Ind. Ceram. 50 (5) (2009) 368–371. https://doi.org/10.1007/s11148-010-9216-6

[4] Violini, M. A. – Hernandez, M. F. – Gauna, M. – Suarez, G. – Conconi, M. S. – Rendtorff, N. M.: Low (and negative) thermal expansion Al_2TiO_5 materials and Al_2TiO_5 - $3Al_2O_3{\cdot}2SiO_2$ - $ZrTiO_4$ composite materials. Processing, initial zircon proportion effect, and properties. Ceram.Int. 44 (17) (2018) 21470–21477. https://doi.org/10.1016/j.ceramint.2018.08.208

[5] Ewais, E. M. M. – Besisa, N. H. A. – Ahmed, A.: Aluminum titanate based ceramics from aluminum sludge waste. Ceram. Int. 43 (2017) 10277–10287. https://doi.org/10.1016/j.ceramint.2017.05.057

[6] Rendtorff, N. M. – Garrido, L. B. – Aglietti, E. F.: Thermal shock resistance and fatigue of Zircon–Mullite composite materials. Ceram. Int. 37 (2011) 1427–1434. https://doi.org/10.1016/j.ceramint.2011.01.004

[7] Lind, C.: Two decades of negative thermal expansion research: Where do we stand? Materials. 5 (2012) 1125–1154. https://doi.org/10.3390/ma5061125

[8] Achary, S. N. – Mukherjee, G. D. – Tyagi, A. K. – Vaidya, S. N.: Preparation, thermal expansion, high pressure and high temperature behaviour of $Al_2(WO_4)_3$. J. Mater. Sci. 37 (2002) 2501–2509. https://doi.org/10.1023/A:1015487406446

[9] Evans, J. S. O.: Negative thermal expansion materials. J. Chem. Soc. 19 (1999) 3317–3326. https://doi.org/10.1039/a904297k

[10] Koseva, I. I. – Nikolov, V. S.: Preparation of aluminum tungstate $Al_2(WO_4)_3$ using sol-gel modified Pechini method. Bul. Chem. Com. 42 (4) (2010) 300–304.

[11] Zhecheva, E. – Stoyanova, R. – Ivanova, S. – Nikolov, V.: On the preparation of nanosized $Al_2(WO_4)_3$ by a precipitation method. Solid State Sci. 12 (2010) 2010–2014. https://doi.org/10.1016/j.solidstatesciences.2010.08.018

[12] Maczka, M. – Nikolov, V. – Hermanowicz, K. – Yordanova, A. – Kurnatowska, M. – Hanuza, J.: Optical and phonon properties of nanocrystalline $Al_2(WO_4)_3$ doped with chromium(III) prepared by co-precipitation method. Opt. Mater. 34 (2012) 1048–1053. https://doi.org/10.1016/j.optmat.2011.12.016

[13] Shi, N. – Liu, Q. – He, X. – Cen, H. – Ju, R. – Zhang, Y. – Ma, L.: Production of lactic acid from cellulose catalysed by easily prepared solid $Al_2(WO_4)_3$. Biores. Tech. Rep. 5 (2019) 66–73. https://doi.org/10.1016/j.biteb.2018.12.005

[14] Nikolov, V. – Koseva, I. – Stoyanova, R. – Zhecheva, E.: Conditions for preparation of nanosized $Al_2(WO_4)_3$. J. Alloys Compd. 505 (2010) 443–449. https://doi.org/10.1016/j.jallcom.2010.06.100

[15] Romao, C. P. – Marinkovic, B. A. – Werner-Zwanziger, U. – White, M. A.: Thermal expansion reduction in alumina-toughened zirconia by incorporation of zirconium tungstate and aluminum tungstate. J. Am. Ceram. Soc. 98 (9) (2015) 2858–2865. https://doi.org/10.1111/jace.13675

[16] Yang, X. – Cheng, X. – Yan, X. – Yang, J. – Fu, T. – Qiu, J.: Synthesis of ZrO_2/ZrW_2O_8 composites with low thermal expansion. Comp. Sci. and Tech. 67 (2007) 1167–1171. https://doi.org/10.1016/j.compscitech.2006.05.012

[17] Dedova, E. S. – Shadrin, V. S. – Gubanov, A. I. – Kulkov, S. N.: The preparation and structural features of zirconium tungstate possessing abnormal thermal properties. Inorg. Mat.: Appl. Res. 5 (5) (2014) 471–475. https://doi.org/10.1134/S2075113314050074

[18] Kameswari, U. – Sleight, A. W. – Evans, J. S. O.: Rapid synthesis of ZrW_2O_8 and related phases, and structure refinement of $ZrWMoO_8$. Int. J. Inorg. Mat. 2 (2000) 333–337. https://doi.org/10.1016/S1466-6049(00)00029-5

[19] Mahnicka, L. – Svinka, R. – Svinka, V. : Influence of kaolin and firing temperature on the mullite formation in porous mullite-corundum materials. (2011) 1–9. IOP Conf. Ser.: Mater. Sci. Eng. 25 012008 https://doi.org/10.1088/1757-899X/25/1/012008

[20] Mahnicka-Goremikina, L. – Svinka, R. – Svinka, V.: Influence of metal oxides additives on the porous mullite ceramics. Key Eng. Mater. 604 (2014) 293–296. https://doi.org/10.4028/www.scientific.net/KEM.604.293

[21] Juettner, T. – Moertel, H. – Svinka, V. – Svinka, R.: Structure of kaolin–alumina based foam ceramics for high temperature applications. J. Eur. Ceram. Soc. 27 (2007) 1435–1441. https://doi.org/10.1016/j.jeurceramsoc.2006.04.029

[22] Awaad, M. – Zawrah, M. F. – Khalil, N.M.: In situ formation of zirconia–alumina–spinel–mullite ceramic composites. Ceram. Int. 34 (2008) 429–434. https://doi.org/10.1016/j.ceramint.2006.11.002

[23] Kaiser, A. – Lobert, M. – Telle, R.: Thermal stability of zircon ($ZrSiO_4$). J. Eur. Ceram. Soc. 28 (2008) 2199–2211. https://doi.org/10.1016/j.jeurceramsoc.2007.12.040

[24] Kanno, Y.: Thermodynamic and crystallographic discussion of the formation and dissociation of zircon. J. Mater. Sci. 24 (1989) 2415–2420. https://doi.org/10.1007/BF01174504

[25] Zhukov, I. – Buyakova, S. P. – Kulkov, S.S.: Properties of ZrO_2–Al_2O_3 ceramics produced from different powder mixtures of zirconia and aluminum hydroxide. Építőanyag – JSBCM. 68 (3) (2016) 74–78. http://dx.doi.org/10.14382/epitoanyag-jsbcm.2016.13

[26] Rodríguez Torres, G. M. – Zarate Medina, J. – Contreras García, M. E.: Synthesis and characterization of Zirconia-Yttria nanoparticles in t' phase by sol-gel and spray drying. Építőanyag – JSBCM. 68 (4) (2016) 120–123. http://dx.doi.org/10.14382/epitoanyag-jsbcm.2016.21

[27] Kurovics, E. – Gömze, L. A. – Ibrahim, J-E. F. M. – Gömze, L. N.: Effect of composition and heat treatment on porosity and microstructures of technical ceramics made from kaolin and IG-017 additive. IOP Conf. Ser.: Mater. Sci. Eng. 613 (2019) 012025. http://dx.doi.org/10.1088/1757-899X/613/1/012025

[28] Kurovics, E. – Kotova, O. B. – Gömze, L. A. – Shushkov, D. A. – Ignatiev, G. V. – Sitnikov, P. A. – Ryabkov, Y. I. – Vaseneva, I. N. – Gömze, L. N.: Preparation of particle-reinforced mullite composite ceramic materials using kaolin and IG-017 bio-origin additives. Építőanyag – JSBCM. 71 (4) (2019) 114–119. https://doi.org/10.14382/epitoanyag-jsbcm.2019.20

[29] Esharghawi, A. – Penot, C. – Nardou, F.: Contribution to porous mullite synthesis from clays by adding Al and Mg powders. J. Eur. Ceram. Soc. 29 (2009) 31–38. https://doi.org/10.1016/j.jeurceramsoc.2008.05.036

[30] Lee, S. – Kim, Y. J. – Moon, H. S.: Phase transformation sequence from kaolinite to mullite investigated by an energy-filtering transmission electron microscope. J. Am. Ceram. Soc. 82 (10) (1999) 2841–2848. https://doi.org/10.1111/j.1151-2916.1999.tb02165.x

[31] Souza, A. E. – Teixeira, S. R. – Santos, G. T. A. – Longo, E.: Addition of sedimentary rock to kaolinitic clays: influence on sintering process. Cerâmica. 59 (2013) 147–155. http://dx.doi.org/10.1590/S0366-69132013000100017

[32] Stubna, I. – Trnik, A. – Vozar, L.: Thermomechanical analysis of quartz porcelain in temperature cycles. Ceram. Int. 33 (2007) 1287–1291. https://doi.org/10.1016/j.ceramint.2006.04.024

[33] Schieder, M. – Lunkenbein, T. – Martin, T. – Milius, W. – Auffermann, G. – Breu, J. : Hierarchically porous tungsten oxide nanotubes with crystalline walls made of the metastable orthorhombic polymorph. J. Mater. Chem. A. 1 (2013) 381–387. https://doi.org/10.1039/c2ta00169a

[34] Cazzanelli, E. – Vinegoni, C. – Mariotto, G. – Kuzmin, A. – Purans, J.: Raman study of the phase transitions sequence in pure WO_3 at high temperature and in H_xWO_3 with variable hydrogen content. Solid State Ionics. 123 (1999) 67–74. https://doi.org/10.1016/S0167-2738(99)00101-0

[35] Thummavichai, K. – Wang, N. – Xu, F. – Rance, G. – Xia, Y. – Zhu, Y.: In situ investigations of the phase change behaviour of tungsten oxide nanostructures. R. Soc. Open Sci. 5 (4) (2018) 1–10. https://doi.org/10.1098/rsos.171932

[36] Lommens, P. – De Meyer, C. – Bruneel, E. – De Buysser, K. – Driessche, I.V. – Hoste, S.: Synthesis and thermal expansion properties of ZrO_2/ZrW_2O_8 composites. J. Eur. Ceram. Soc. 25 (16) (2004) 3605–3610. https://doi.org/10.1016/j.jeurceramsoc.2004.09.015

[37] Jacob, S. – Javornizky, J. – Wolf, G. H. – Angell, C. A.: Oxide ion conducting glasses: Synthetic strategies based on liquid state and solid state routes. Int. J. Inorg. Mat. 3 (3) (2001) 241–251. https://doi.org/10.1016/S1466-6049(01)00024-1

[38] Waring, J. L.– Amer, J.: Phase equilibria in the system aluminum oxide-tungsten oxide. Ceram. Soc. 48 (1965) 493–494. https://doi.org/10.1111/j.1151-2916.1965.tb14809.x

[39] Matthews, S.: Plasma spraying of Al_2O_3–WO_3 composite coatings. Surf. and Coat. Tech. 206 (2012) 3323–3331. https://doi.org/10.1016/j.surfcoat.2012.01.043

[40] Kurovics, E. – Shmakova, A. – Kanev, B. – Gömze, L. A.: Development ceramic composites based on Al_2O_3, SiO_2 and IG-017 additive. IOP Conf. Ser.: Mater. Sci. Eng. 175 (2017) 012013. https://doi.org/10.1088/1757-899X/175/1/012013

Ref.:
Mahnicka-Goremikina, Ludmila – **Svinka**, Ruta – **Svinka**, Visvaldis – **Grase**, Liga – **Goremikins**, Vadims: *The formation of phases with low or negative linear thermal expansion coefficient in porous mullite ceramics*
Építőanyag – Journal of Silicate Based and Composite Materials, Vol. 72, No. 3 (2020), 91–98. p.
https://doi.org/10.14382/epitoanyag-jsbcm.2020.15

Alagúttüzek hatása az alagútfalazat és kőzetkörnyezet teherbírására

2. rész (vágatstatikai számítás)

Effects of tunnel-fire on load bearing capacity of tunnel-lining and surrounding rock mass

Part 2 (Sectional Calculation)

Csanády Dániel ▪ Budapesti Műszaki és Gazdaságtudományi Egyetem ▪ csanady.daniel@epito.bme.hu
Fenyvesi Olivér ▪ Budapesti Műszaki és Gazdaságtudományi Egyetem ▪ fenyvesi.oliver@epito.bme.hu
Megyeri Tamás ▪ Budapesti Műszaki és Gazdaságtudományi Egyetem ▪ tamas.megyeri@noma-consulting.com
Érkezett: 2019. 02. 21. ▪ Received: 21. 02. 2019. ▪ https://doi.org/10.14382/epitoanyag-jsbcm.2020.16

Abstract

The effect of tunnel-fire can cause significant changes in the strength of the tunnel-lining and its rock environment. This structural damage is a potential threat after fire load. The condition of the structure can be estimated if some concrete specimens exist from the mixture of the tunnel wall. These specimens should be loaded by the same temperature that affected the tunnel in fire during different heating and cooling treatments. According to the test results, the inner and outer part of the lining can be modelled under fire.

The change of compressive strength and Young's modulus can be obtained from compressive strength tests. These processes were explained in details in our previous article, titled "Effects of tunnel-fire on load bearing capacity of tunnel-lining and surrounding rock mass". The ratios of the initial and instantaneous material properties give reduction factors. If the maximum temperature during a fire is known the overheating of the lining wall can be modelled by numerical methods, from which isothermal zones can be determined. From the thickness of these zones and the reduction factors (compressive-, tensile strength and Young's modulus) the present condition of the tunnel wall can be estimated by the model. The damaged wall can be modelled with a wall with equivalent stiffness to the damaged one with the use of the reduction factors. The created numerical model gives an opportunity for a fast structural evaluation of the tunnel after fire.

This initial model was validated by comparison of model results from different software products tested with different boundary conditions. In present paper two software and three types of beam-spring models (2D, 3D, node and surface support) were compared. All of these model types gave very close results, so it can be concluded, that they can be applied for tunnel modelling under increased temperatures without the further laboratory test of concrete specimens of the tunnel wall.

Locations of partial failure (after fire) can be determined from the model which generates plastic hinges in the tunnel wall. In this step the model has to be recalculated to evaluate the final condition. From the different stresses and material properties of the wall the necessary provisional support system can be designed and constructed. This support system provides the required safety under the early stage of reconstruction. Besides this, the necessary thickness of reparation can also be estimated from the model results.

Kulcsszavak: Alagúttűz, gerenda-rugó modell, beton, nyomószilárdság, rugalmassági modulus
Keywords: Tunnel fire, beam-spring model, concrete, compressive strength, modulus of elasticity

CSANÁDY Dániel
Okl. építőmérnök, doktorandusz a BME Építőanyagok és Magasépítés Tanszékén. A Szilikátipari Tudományos Egyesület tagja. Fő érdeklődési körök: építőanyagok tűzzel szembeni viselkedése, új típusú betonok fejlesztése, környezetbarát építőanyagok, biomimetika, hőszigetelés, hangszigetelés, új építőanyagok fejlesztése.

Dr. FENYVESI Olivér
(1981), okl. építőmérnök (BME 2005), PhD (BME 2012), műemlékvédelmi szakmérnök (BME 2017), adjunktus a BME Építőanyagok és Magasépítés Tanszékén. Fő kutatási területei: betonok korai (autogén+száradási) zsugorodása, korai zsugorodási repedések normál és könnyűbetonokban, szálerősített betonok, szálerősített könnyűbetonok, könnyűbetonok tartóssága, önterülő könnyűbetonok, épületdiagnosztika, épített örökség védelme. A Szilikátipari Tudományos Egyesület Beton Szakosztályának titkára illetve Kő és kavics szakosztályának tagja, a fib (Nemzetközi Betonszövetség) Magyar Tagozatának tagja, a Magyar Mérnöki Kamara tagja.

MEGYERI Tamás
Okl. Építőmérnök (Noma Consulting, 2017), alagutak és földmegtámasztó szerkezetek tervezésével foglalkozó geotechnikus mérnök.

1. Bevezetés

A beton alagútfalazatok és a kőzetkörnyezet anyagtulajdonságainak vizsgálatát cikkünk előző részében mutattuk be [1]. Jelen cikkünk a korábbi eredményeke épülő modellkészítésről és ebből levont következtetésekről szól.

Az alagúttüzekből származó hőhatás jelentős változásokat eredményezhet az alagútfalazat és a kőzetkörnyezet szilárdsági és merevségi tulajdonságaiban, esetlegesen teljesen tönkre is teheti a szerkezeti elemeket. A tűzhatáson túl a szerkezeti károsodások is potenciális veszélyforrást jelentenek. Az alagút betonjából célszerű előzetesen próbatesteket készíteni és tűzteher hatására az anyagtulajdonságaiban bekövetkező változásait megvizsgálni. A vizsgálat eredményeit egy modellbe építhetjük, a modell közelítőleg korrekt képet adhat az alagút tűz utáni állapotáról, növeli a mentés és a megerősítés alatti biztonságot.

Beton alagútfalazatok nyomószilárdságának és elszíneződésének laboratóriumi vizsgálatával foglalkozott [2]. A gerenda-rugó modellek vizsgálatával foglalkozott [3]. Talajok nyomásának számításánál nagyobb biztonságot követel meg a tervezés (mint például magasépítésben ahol pontosabban leírható az erőjáték és a megtámasztási viszonyok), ezért fontos hogy az alagutat körülvevő kőzetek anyagtulajdonságait (és változásait hőteher hatására) megfelelően pontosan vegyük fel és az alagútfalazatra ható terheket jól határozzuk meg. A témával részletesen foglalkozott és vizsgálta a gránitos kőzetek hő hatására történő szilárdságváltozását [4]. Az alagútfalazatra és kőzetre nem csak alagúttüzek esetén juthat hőteher, hanem például nukleáris hulladéklerakókban lejátszódó bomlási folyamatok által is. Nukleáris hulladéklerakó alagútját vizsgálta [5].

2. Célkitűzések

Munkánk során alapvetően a tűz tartószerkezetre gyakorolt hatásaival foglalkoztunk, kiemelve a vasbeton alagútfalazatban a beton anyagtulajdonságaiban okozott változásokat visszahűlt állapotban (ezzel a biztonság oldaláról közelítve az anyagtulajdonságokat, továbbá a helyreállítás során ezen állapotok érvényesek). Az alagúttűz következményeinek reprodukcióját laboratóriumi környezetben és az alagútfalazat károsodásának vizsgálatát (mik a károsodások okai) az *„Alagúttüzek hatása az alagútfalazat és kőzetkörnyezet teherbírására”* című cikkünk első részében mutattuk be. A kapott eredmények felhasználásával végeselemes programban épített síkbeli és térbeli gerenda-rugó („beam-spring”) modell segítségével mutatjuk be a szilárdsági tulajdonságok változásainak hatását az alagút erőjátékára. Választ kerestünk arra a kérdésre, hogy az alagútfalazat különböző részeinek teherbírása megfelel-e a tűzeset után, illetve kialakulnak-e képlékeny csuklók a falazatban. Majd a csuklókat beépítve a modellbe ellenőriztük, hogy képlékeny nyomatékátrendeződés után megfelelő teherbírású marad-e a falazat. Végül általános javaslatot adtunk a helyreállítás menetére. A síkbeli modell eredményeit összevetettük a térbeli modell eredményeivel, ha az egyezés megfelelő mértékű, elégséges lehet a síkbeli modell használata. A síkbeli gerenda-rugó modell előnye, hogy egyszerűen felépíthető, gyorsan szolgáltat eredményeket, ami alapján meghatározhatók az alagúttal kapcsolatos azonnali intézkedések illetve eldönthető, hogy a sérült alagútfalazat hosszútávon alkalmas-e a ráháruló terhek viselésére, vagy meg kell erősíteni, és ha igen, mely részeken és milyen módon.

3. A „beam-spring” modell

A gerenda-rugó modell vasbeton alagútfalazatok méretezése során kis takarású vasbeton elemek esetén használatos. Ez a végeselemes modell csak a beton falazatot veszi figyelembe. A falazat deformációja az alagút hossztengelyének irányában közel nulla (ε_z=0) a keresztirányú alakváltásokat (ε_x, ε_y) figyelembe vesszük. Az alagutat körülvevő talajnyomást a gerendaelemek csomópontjaiban ható külső erőhatásként veszi figyelembe a modell. A falazat talajba/kőzetbe való rugalmas ágyazását a csomópontokba csatlakozó rugóelemek adják. A csatlakozó rugók merevsége a körülvevő talaj rugalmassági/összenyomódási modulusától E (MPa) és Poisson tényezőjétől ν (-) függ. Kör keresztmetszetű alagutaknál a sugárirányú elmozdulások u (m) a következők szerint alakulnak (1):

$$u = \left(\frac{1+\nu}{\mathrm{E}}\right) \times R \times p \qquad (1)$$

ahol

- p (MPa) a talaj/kőzet nyomása
- R (m) az alagút sugara
- E (MPa) a körülvevő talaj rugalmassági modulusa
- ν (-) a körülvevő talaj Poisson tényezője

A rugóban ébredő erő értéke (2) egyenlet alapján számítható (N), ami azt jelenti, hogy az ébredő erő a radiális elmozdulások (u) függvénye (3)

$$F = A \times p \qquad (2)$$

$$F = \left(\frac{E}{1+\nu} \times \frac{A}{R}\right) \times u. \qquad (3)$$

ahol

- R (m) a kör keresztmetszetű alagút sugara
- E (MPa) a körülvevő talaj rugalmassági modulusa
- ν (-) a körülvevő talaj Poisson tényezője

A (m^2) az egy rugóelemhez tartozó alagútfalazat-terület (általában a csomóponthoz csatlakozó gerendaelemek fél hosszainak összege szorozva a figyelembe vett szélességgel).

A rugóelem rugóállandója (4) egyenlet alapján

$$K = \left(\frac{E}{1+\nu} \times \frac{A}{R}\right) \text{(N/m)} \qquad (4)$$

Az előző képletek kör keresztmetszetű alagutakra érvényesek, viszont az alagutak keresztmetszete több eltérő ívből is állhat, amikhez különböző sugarak tartoznak. Ilyen alagút-keresztmetszet esetén R helyére $R_{átl}$ kerül, ami az alagút keresztmetszet átlagos sugara.

Tapasztalatok szerint több ívből álló szerkezeti formák esetén az esetek döntő többségében számolhatunk a helyettesítő sugárral, amelyből számítható kör keresztmetszeti területe azonos a tényleges alagút keresztmetszeti területével. A rugók húzó- és nyomó- rugómerevsége eltérő, csak nyomás esetén vesznek fel terhelést, húzás esetén rugómerevségük nulla [6], [7], [8], [9]. Elsőként síkbeli modellel foglalkoztunk, majd a modellből kapott eredményeket összehasonlítottuk a térbeli modellből kapott eredményekkel.

4. Vágatstatikai számítás

Az alagút modelljeit két végeselemes programban is elkészítettük (*1. ábra*), mert a „program 1” (amit a terhek számítására is használtunk a „program 2”-ben készített modelltől eltérő módon számítja a terheket. Így az eredmények ellenőrizhetőek és, megfelelő egyezés esetén kijelenthető, hogy az eredmények nem függnek a használt szoftvertől. Szilárd, tagolt kőzetkörnyezetben készült alagutak vágatstatikai számításait mutatja be [10], végeselemes és diszkrét elemes módszerrel [5]. Az alagút betonfalazatát és a mögötte lévő kőzet kölcsönhatásait vizsgálta laboratóriumi körülmények között [11], a modellekben való pontosabb kapcsolati jellemző felvétele érdekében. Több síkbeli és egy térbeli modellt építettünk, így elemezhetjük, hogy a síkbeli modellből kapott eredmények mennyire pontosan közelítik meg a valósághoz közelebb álló térbeli modell eredményeit.

A vizsgált minta-alagút nyomvonala tektonikai lemezek határához közel fekszik, ezért a területen jellemző a túlnyomórészt magmás kőzetek (gránit) jelenléte. Az alagút feletti fedés 40 m. A területen talajvizet nem találtak a fúrások során. A kőzet paramétereit az *1. táblázat* tartalmazza.

Megnevezés	Testsűrűség [kg/m^3]	Egyirányú nyomószilárdság [MPa]	Rugalmassági modulus [MPa]	Poisson tényező [-]	Kohézió [MPa]	Belső surlódási szög [°]	GSI [-]
Monzo gránit	2570	120	4500	12	0,091	36,61	10

1. táblázat Kőzetfizikai paraméterek
Table 1 Rock Strength Parameters

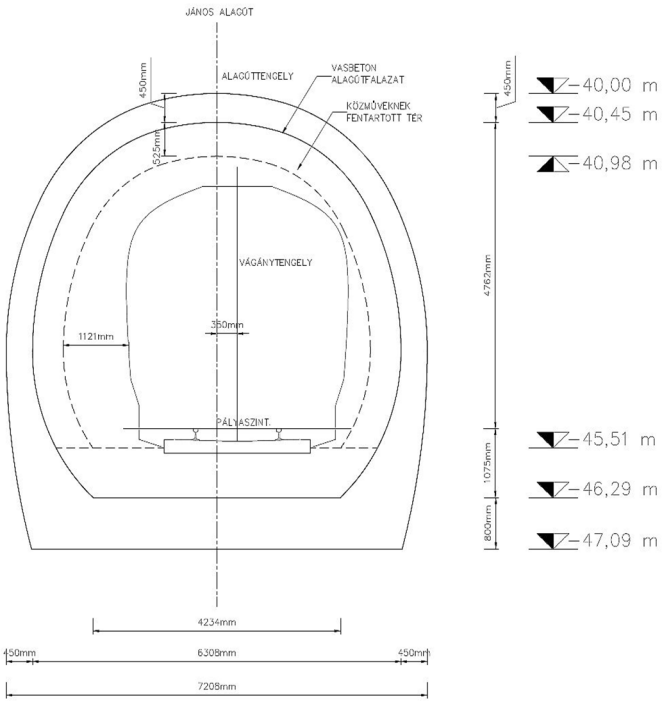

1. ábra Az alagútszelvény méretei
Fig. 1 Dimensions of the tunnel section

5. Mértékadó hőhatás meghatározása

Alagutak tűzvizsgálata esetén a szénhidrogén és a módosított szénhidrogén görbék használata a jellemző, a létesítmény adottságai, alakja és az égő anyag összetétele miatt (pl. közlekedési járművek üzemanyaga). A szénhidrogének égése során a szabványos tűzgörbétől eltérő karakterisztikájú jelenségeket tapasztalhatunk. Mind a görbe lefutása, mind a maximuma eltér a magasépítési gyakorlatban alkalmazott szabványos tűztől. A szénhidrogének gyorsabb belobbanása meredekebb hőmérsékletemelkedést, míg nagyobb hőfejlesztésük magasabb maximális hőmérsékletet eredményez (5).

A görbe egyenlete:

$$T[°C] = 20 + 1080 \times \left(1 - 0{,}325 \times e^{-0{,}167 \times t\,[min]} - 0{,}675 \times e^{-2{,}5 \times t\,[min]}\right). \quad (5)$$

Az alagút keresztmetszetében feltételezett hőmérséklet eloszlást a következőkre alapoztuk. A szénhidrogén tűzgörbe gyors emelkedése miatt, egyszerűsített tűzmodell esetén a lokalizált tűz elhanyagolható és a teljesen kifejlett tűz gyorsan kialakul. Másrészt a fejlett tűzmodellek közül az egyzónás modell indokolt használata támasztja alá a feltételezést. Ugyan mindkettő említett tűzmodellt (*egyszerűsített, fejlett*) általában a magasépítésben használják, de alagutak esetében is alkalmazható mindkettő modelltípus második szakasza. A keresztmetszet geometriája miatt előáll az a teljesen kifejlett tűzhöz hasonló eset, amikor a lángok beborítják az alagút teljes keresztmetszetét, ami egyenletes léghőmérséklet kialakulását vonja maga után. A kezdeti léghőmérséklet-eloszlást az alagút hossztengelyében vizsgálva, megállapítható, hogy a tűzfészek környezetében uralkodó magas hőmérséklet a távolsággal arányosan csökken [13]. Később az egyenletes léghőmérséklet eloszlás kialakulását az alagútban lévő erős ventilláció is elősegíti. Ezen kívül az idő múlásával, a tűzfészektől távolabbi, éghető anyagok is lángra kaphatnak, aminek következtében a hőmérséklet-eloszlás maximumhelyei térben széthúzódhatnak és az alagút falazatának mind nagyobb szakaszát érheti a maximális hőterhelés [12], tehát egyenletesebbé válhat a hőmérséklet eloszlása a keresztmetszetben és a hossz mentén is. Feltételezésünk szerint a teljes alagút keresztmetszete mentén egyenletes a léghőmérséklet eloszlás, így a falazat vastagsága mentén egyenletesen melegszik át a keresztmetszet. Emellett az alagút hosszirányában is viszonylag egyenletes a hőmérséklet eloszlás, mivel az alagútban lévő erős ventilláció a tűz terjedésével egyre intenzívebb lesz, ami áramlásával közvetíti az energiát az alagút távolabbi részeibe. A hőmérsékletemelkedésnek és az ebből származó fluxusnak a ventillációval való összefüggését [14] vizsgálta.

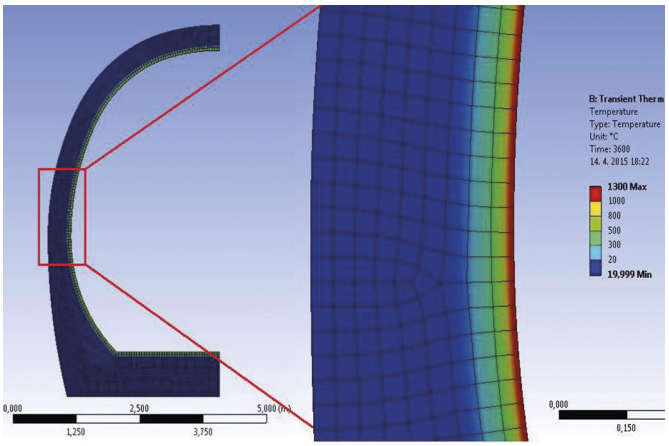

2. ábra A modellezett fél keresztmetszet (balra), 1 órás tűzhatás alatt átmelegedett falazat (jobbra)
Fig. 2 Modelled half-section (left), overheated cross-section right after 1 hour long fire (right)

A falazat átmelegedését végeselemes programmal határoztuk meg 1 óra időtartamú tűz hatására, a módosított szénhidrogén tűzgörbe egyenlete alapján (T_{max}=1300 °C). Az 1300 °C az 1000 °C-os terheléssel azonosnak tekinthető, mert a próbatestek már 1000 °C-on elveszítik teljes szilárdságukat). A programba szimmetria megadásával a fél keresztmetszetet vittük be és egyenletes hőmérséklet eloszlást feltételeztünk. Így megkaptuk az egyes hőmérsékleti tartományokhoz tartozó zónákat, amikhez később hozzárendelhettük a mért szilárdsági és merevségi értékeket (*2. ábra*).

6. A numerikus modellek felépítése

Két síkbeli és egy térbeli modellt készítettük („program 2”-ben). A síkbeli modellek és a térbeli modell is gerenda-rugó elméleten alapulnak. Az első síkbeli modell egy „klasszikus”, csomópontjaiban megtámasztott gerenda-rugó modell, a második egy módosított változat, ahol csomóponti támaszok helyett vonalmenti támaszokat használtunk. A térbeli modell is gerenda-rugó modell alapjául szolgáló, az alagút boltozat ívét közelítő sokszög keresztmetszet alapján készült, mivel a program nem tud görbült felületeket modellezni. A modell héjelemekből áll, mert szegmensei mind középsíkjukkal párhuzamosan, mind erre merőlegesen terheltek és a valós

alagútfalazat egyszer görbült felületszerkezet (*3. ábra*). A szegmensek egymáshoz merev módon kapcsolónak (mint ahogy a gerenda-rugó modellnél a gerendák), talajba/kőzetbe való rugalmas ágyazásukat felületre merőleges felületi támaszokkal vettük figyelembe. A térbeli modellt három, tíz méter hosszú részre osztottuk, ezek közül a középsőben maximális 1300 °C-ot feltételeztünk, a két szélső tíz méteres szakaszban 800 °C-ot. A tíz méteres szakaszokra való felosztás az eltérő maximális hőmérsékletekhez tartozó, a falazatban bekövetkező változások közti eltérést hivatott szemléltetni. Térben az alagútfalazat keresztmetszetét (a fal belső felületétől kifelé haladva) 1300 °C, 1000 °C, 800 °C, 500 °C, 300 °C-os zónákra bontottuk fel. A 300 °C-nál alacsonyabb hőmérsékletű zónák 20 °C-os betonként jelennek meg a szendvicsmodellben, mivel 300 °C-ig jelentős változás nem lép fel a beton szilárdságában. Ezekhez a zónákhoz rendeltük hozzá a kísérletekből kapott anyagjellemzők értékeit. Így a kapott szendvicsmodell különböző zónáihoz (zónánként eltérő inercia és rugalmassági modulus) tartozó merevségek összegzett értéke alapján számítható a helyettesítő vastagság. Az így számított vastagságú falazat a modellben a nem hőterhelt, 20 °C-os beton anyagtulajdonságaival (szilárdság, rugalmassági modulus) rendelkezik, de merevsége megegyezik a hőterhelt falazatéval. Alapvető feltételezés, hogy a belső oldali betonfedés réteges, korai leválása miatt tönkrement, így a belső oldali vasalás is elvesztette tapadását, majd felmelegedés után a szilárdságának nagy részét. Progresszív réteges leválás nem történt, a levált betontakarást megtartotta a belső oldali vasalás, de a kialakuló repedések lehetőséget adtak arra, hogy a felmelegedett levegő közvetlen érintkezésbe kerüljön a betontakarás mögötti zónákkal. A réteges leválás miatt a betonfedés mögötti felületet a maximális hőmérséklet közvetlenül éri, így ez a zóna melegszik át leginkább. Így a végeselemes modellből kapott átmelegedett zónavastagságokat eltoltuk a levált betonfedés vastagságával (kb. 5 cm) a falazat külső része felé, ezzel is rontva a teherbírást és növelve a biztonságot a számításban. A nyomatéki maximumok helyén (a boltozat és az ellenbolt találkozásánál) a keresztmetszetben kiékelés található, hogy a falazat képes legyen viselni a nagy igénybevételeket, ezt a modellben a gerendamagasság növelésével vettük figyelembe.

7. Eredmények ismertetése

A terhek számítására használt végeselemes programból (program 1) kapott terhekre a „program 2”-ben is lefuttattuk a modelleket, hogy lássuk, megfelelő mértékben egyeznek-e a két szoftverből kapott igénybevételek, illetve az eredmények a síkbeli és a térbeli modell esetén. A különböző számítási módokkal kapott eredmények mind a normálerők mind a nyomatékok tekintetében 10-15%-os eltérést mutatnak (*4. ábra*). Néhány kritikus keresztmetszetekben ébredő igénybevétel, különböző szoftverből vagy modelltípusból származó tűzeset előtti, illetve utáni értékeinek összehasonlítása a *5-6 és 12-13. ábrákon* láthatóak. A normál hőmérsékletű, tűzeset előtti alagútfalazat igénybevételeit és ellenállási értékeit egyszerűsített teherbírási görbén ábrázoltuk és így igazoltuk az alagútfalazat teherbírási megfelelőségét a kiindulási állapotban. (*7. ábra*). Az alagúttervezési gyakorlatban a nyíróerők és azok felvétele jellemzően nem okoz problémát, ezért a jelen cikk keretein belül ezt nem vizsgáltuk. Ahol értékük jelentősen megnövekszik a falazatban, ott az ellenbolt megtámasztja a falazatot és ahol az ellenboltban növekszik jelentős mértékűre a nyíróerő, ott a falazat kiékelt része támasztja meg az ellenboltozatot.

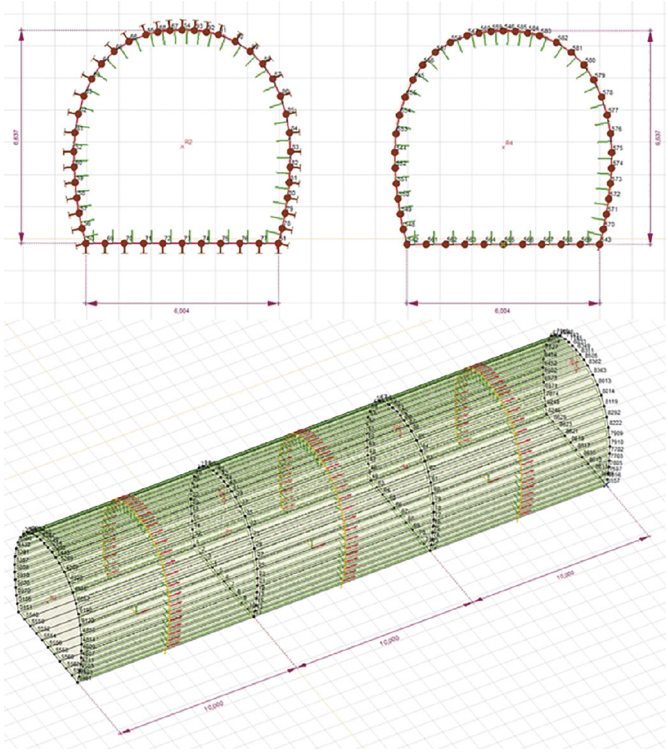

3. ábra A gerenda-rugó modellek felépítése. Síkbeli (fent) térbeli (lent)
Fig. 3 Structure of beam-spring modell. 2D (above) 3D (below)

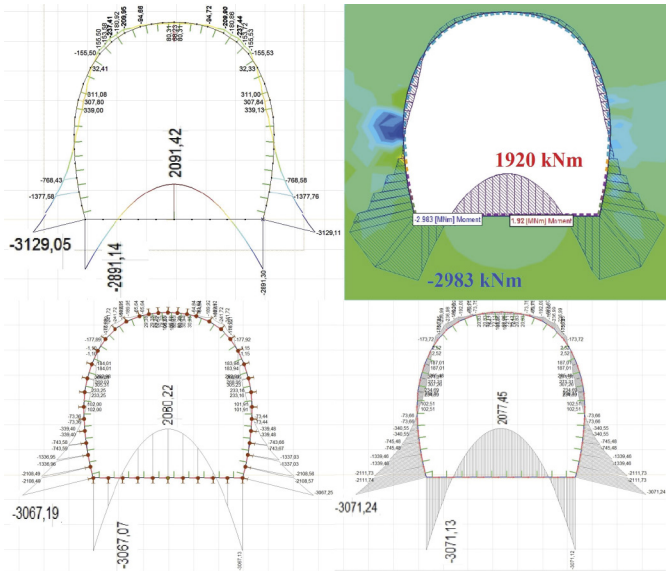

4. ábra A kőzetnyomásból ébredő nyomatékok összehasonlítása: térbeli modell (bal felső), a terheket számító végeselemes program (jobb felső) csomóponti megtámasztású modell (bal alsó) és vonalmenti megtámasztású modell (jobb alsó)
Fig. 4 Comparison of bending moment calculated by different softwares

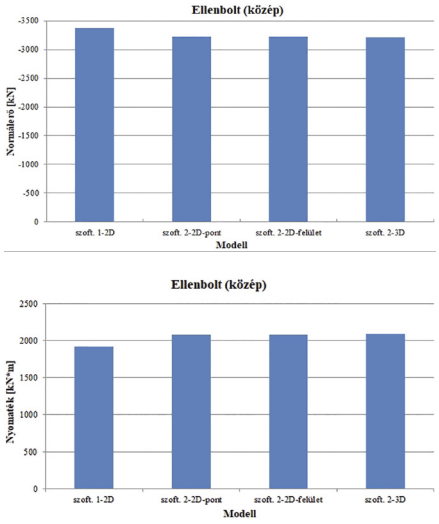

5. ábra Az ellenbolt közepén ébredő, különböző szoftverekből vagy modelltípusból származó normálerők összehasonlítása (felül). Az ellenbolt közepén ébredő, különböző szoftverekből vagy modelltípusból származó nyomatékok összehasonlítása (alul).

Fig. 5 Comparison of normal force in the middle of the invert from different softwares or modell types (above). Comparison of bending moments in the middle of the invert from different softwares or modell types (below).

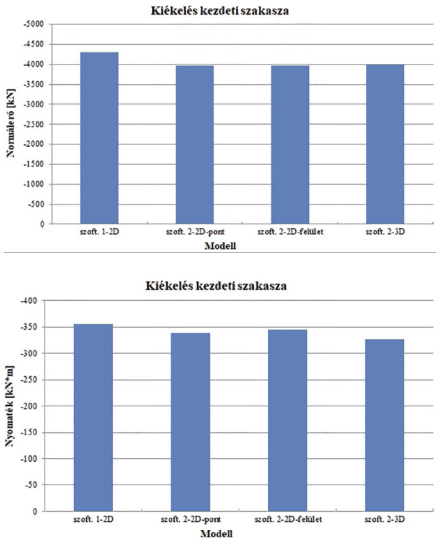

6. ábra A kiékelés kezdeti szakaszánál ébredő, különböző szoftverekből vagy modelltípusból származó normálerők összehasonlítása (felül). A kiékelés kezdeti szakaszánál ébredő, különböző szoftverekből vagy modelltípusból származó nyomatékok összehasonlítása (alul).

Fig. 6 Comparison of normal force in the joint of the wall and invert from different softwares or modell types (abowe). Comparison of bending moments in the joint of the wall and invert from different softwares or modell types (belowe).

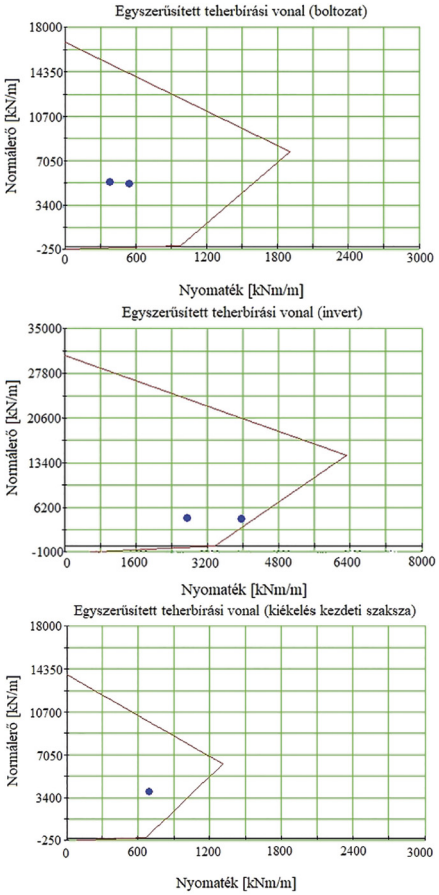

7. ábra Teherbírási görbék hőterhelés előtt

Fig. 7 Load-bearing curves before fire load

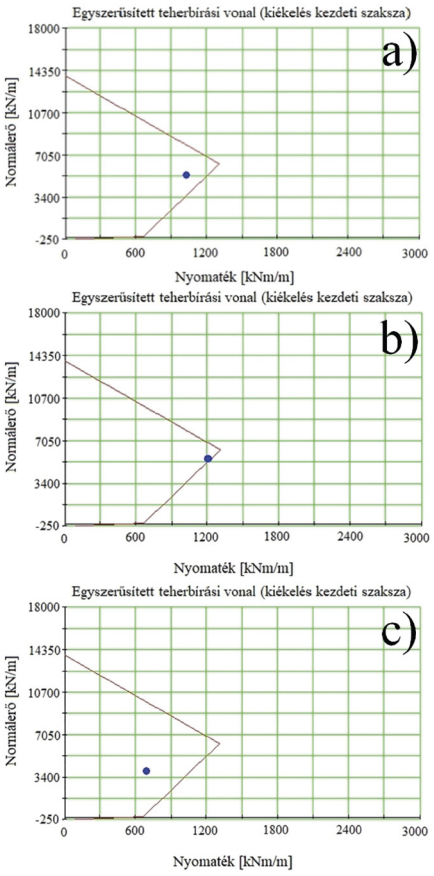

8. ábra A kritikus keresztmetszet teherbírási görbéi hőterhelés utáni T_{max}=1300°C nyomatékátrendeződés előtt és után. a: képlékeny csukló nélkül, b: képlékeny csuklókkal, c: dúccal

Fig. 8 Critical cross-section load-bearing curves before and after bending-moment rearrangement after T_{max} = 1300 °C. a: without plastic hinges, b: with plastic hinges, c: with struts

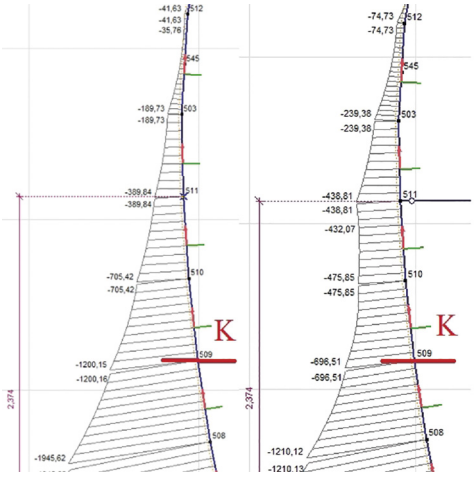

9. ábra A kritikus keresztmetszet tehermentesítése dúc alkalmazásával

Fig. 9 Load reduction of the critical cross-section by using a strut

A hőterhelés utáni esetekben az alagútfalazatot két-három mértékadó helyen vizsgáltuk meg, melyek közül a kiékelés kezdeti szakasza volt a kritikus keresztmetszet. Az alagútfalazat belső oldaláról kieső vasak miatt a keresztmetszet nyomási teherbírási pontjának eltolódását nem vettük figyelembe, mert az eltolódás mértéke elhanyagolhatóan kicsi, a szerkezeti vastagságokhoz képest a falazatban 1,38 mm és az ellenboltban 5,93 mm. A *8. ábra* az 1300°C-os hőterhelés után a kritikus keresztmetszet teherbírási görbéit mutatja eltérő állapotokban. A teherbírási görbéket elkészítettük 1300 °C, 1000 °C, 800 °C,

500 °C, 300 °C-os zónákra is (terjedelmi okok miatt csak a kezdeti és magasabb hőmérsékleti értékeket ábrázoltuk). A tűzeset utáni a hossztengely mentén változó alagútfal merevséget a *10. ábrán* mutatjuk be 20, 800 és 1000 °C-os hőterhelés hatására.

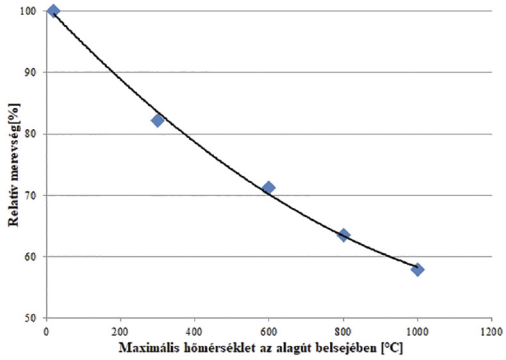

10. ábra Az alagútfalazat merevségének változása a hőmérséklet függvényében
Fig. 10 Change in stiffness of tunnel wall at different temperatures

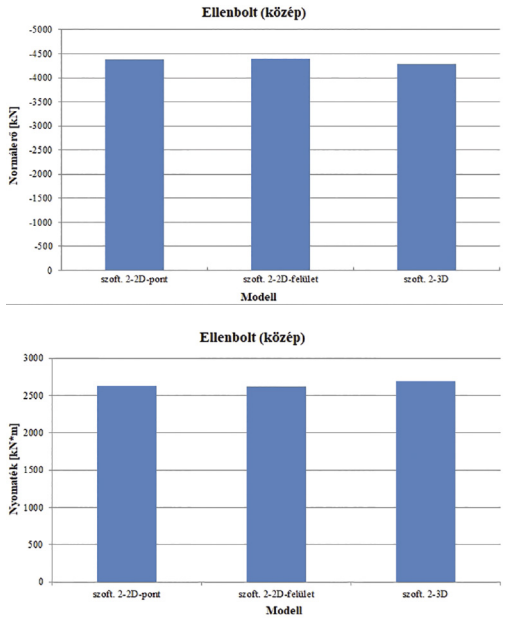

11. ábra Az ellenbolt közepén ébredő, különböző modellekből származó normálerők összehasonlítása, a tűzeset után (felül). Az ellenbolt közepén ébredő, különböző modellekből származó nyomatékok összehasonlítása, a tűzeset után (alul).
Fig. 11 Comparison of normal force after fire in the middle of the invert from different modell types (abowe). Comparison of bending moments after fire in the middle of the invert from different modell types (below).

Ahol a maximális léghőmérséklet elérte az 1300 °C –ot, ott a falazat a belső oldali húzást egyértelműen nem tudta tovább felvenni. A képlékeny nyomatékátrendeződés utáni számítások eredményei alapján kijelenthető, hogy ennek ellenére az alagútfalazat állékony marad. Azonban a kiékelés kezdeti szakaszán, ugyan nem alakul ki képlékeny csukló, mivel a falazat külső oldalon húzott, de keresztmetszet csökkenése és a nyomaték-átrendeződés miatt közel 100%-ban kihasznált (*8. ábra*). Ezért a tönkremenetelhez közeli keresztmetszet felett (50-100 cm-el) ki kell dúcolni az alagútfalazatot, ekkor az említett keresztmetszetben a nyomaték 60%-ára esik vissza (*9. ábra*). A 800 °C-ra felmelegedett keresztmetszetekben az előző esettel analóg módon kell cselekedni. Miután a dúcolás megtörtént megkezdődhetnek a megerősítési munkálatok, minek során el kell távolítani minden olyan sérült betonréteget, amely elérte a 300 °C-ot. A bontási munkálatokat csak kis szélességű, egymástól eltolt zónákban, több ütemben lehet végrehajtani. Ezt követően a felületet meg kell tisztítani és kellően érdesíteni (szükség esetén együttdolgoztató csapokkal ellátni), hogy a megerősítő betonrétegek megfelelően együtt tudjanak dolgozni a régi szerkezettel. A betonréteg felhordása előtt a vasalást rögzíteni kell a falazaton ügyelve arra, hogy a szakaszos megerősítéseknél a vasalás elegendő toldási hosszúságban túlnyúljon a lőtt felületen, hogy a toldások kialakíthatóak legyenek. A megerősítés során célszerű visszaállítani legalább azt a teherbírást, amivel a szerkezet a tűzesetet megelőzően rendelkezett.

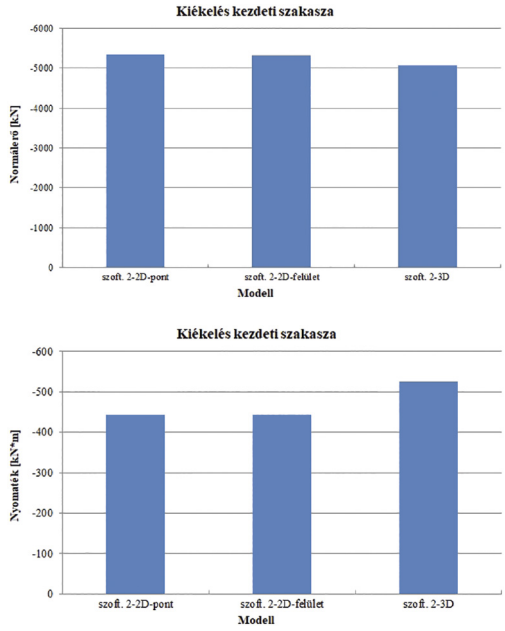

12. ábra A kiékelés kezdeti szakaszán ébredő, különböző modellekből származó normálerők összehasonlítása, a tűzeset után (felül). kiékelés kezdeti szakaszán ébredő, különböző modellekből származó nyomatékok összehasonlítása, a tűzeset után (alul).
Fig. 12 Comparison of normal force after fire in the joint of the wall and invert from different modell types (abowe). Comparison of bending moments after fire in the joint of the wall and invert from different modell types (below).

8. Összefoglalás

A modellkísérletek során egy alagútfalazat tűzterhelés előtti és utáni viselkedését vizsgáltuk. A modellek bemenő adatait az „*Alagúttüzek hatása az alagútfalazat és kőzetkörnyezet teherbírására*”, [1] című cikkünk tartalmazza.

1. Ellenőriztük a ható kőzetnyomást „kézi módszerrel” és végeselemes programban. Az eredmények 99 %-ban egyeztek.
2. Vertikálisan terhelt, kör keresztmetszetű ellenőrző alagút modellen igazoltuk a gerenda-rugó modell beállításinak helyességét.
3. Az alagútfalazat igénybevételeit két végeselemes programban is meghatároztuk. Az eredmények megfelelően közel estek egymáshoz, reálisnak tekinthetők. A második programban két gerenda-rugó elven működő síkbeli és egy térbeli modellt készítettünk.

Ép alagútfalazat esetén a modellek eredményeinek eltérése 10-15 %-on belüli (a biztonság javára), tehát elégséges a síkbeli modellek alkalmazása.

4. Kiszámítottuk a hőterhelés utáni alagútfalazat helyettesítő vastagságát. A hőterhelés utáni alagútfalazat két- és háromdimenziós modelljének igénybevétel eloszlásai és maximális értékei közel estek egymáshoz. Sürgős esetben megengedhető az elhanyagolás.
5. A modelleket képlékeny csuklók kialakulása előtt és után is vizsgáltuk. Az alagút igénybevételeit és teherbírását minden állapotban egyszerűsített teherbírási görbével ábrázoltuk. Az alagútfalazat képlékeny nyomatékátrendeződés után megfelel, de szinte 100%-ban kihasznált, a biztonság csekély. A megerősítési munkálatok csak a falazat dúcolása után kezdődhetnek meg.
6. A megerősítés során a sérült (300°C-nál jobban átmelegedett) betonrétegeket el kell távolítani, a felületet meg kell tisztítani, kellően érdesíteni és nedvesíteni, hogy a megerősítő betonrétegek tapadását biztosítsuk. A megerősítéssel vissza kell állítani az eredeti teherbírást.
7. Az eltérő modelltípusok azonos keresztmetszeteinek igénybevételeit oszlopdiagramok segítségével szemléltettük. Az eredmények közel estek egymáshoz, tehát a jelen kutatás eredményei alapján gyors intézkedés szükségessége esetén kellő biztonsággal alkalmazhatók a kétdimenziós modellek is (ennek végleges bizonyítására további nagyszámú vizsgálat szükséges.) (*11-12. ábra*).
8. Az alagútfalazat hő hatására időben változó merevségét diagramon ábrázoltuk (*10. ábra*). A falazat teljes vastagságának csak kis része melegszik át, mégis nagymértékű merevségcsökkenést szenved a szerkezet.

Irodalomjegyzék

[1] Csanády, D. – Fenyvesi, O. – Lublóy, É. –Megyeri, T. (2018): Effects of tunnel-fire on load bearing capacity of tunnel-lining and surrounding rock mass, Journal of Silicate Based and Composite Materials, Vol. 70, pp. 54-61, https://doi.org/10.14382/epitoanyag-jsbcm.2018.11

[2] Du, S. – Zhang, Y. – Sun, Q. – Gong, W. – Geng, J. – Zhang, K. (2018): Experimental study on color change and compression strength of concrete tunnel lining in a fire, Tunnelling and Underground Space Technology, Vol. 71, pp. 106-114, https://doi.org/10.1016/j.tust.2017.08.025.

[3] Hao, W. – Biao, T. – Zhen, X. – Kai, Z. – Ya, Z. (2012): The Sensitivity Analysis of Beam-Spring Model for Shield Tunnel Segment, Applied Mechanics and Materials, Vol. 256-259, pp. 1263-1269, https://doi.org/10.4028/www.scientific.net/AMM.256-259.1263

[4] Török, A. – Török, Á. – Görög, P. (2015): „The effect of temperature on the physical properties of Mauthausen Granite (Austria)", In: MG Winter, DM Smith, PJL Eldred, DG Toll (szerk.), Geotechnical Engineering for Infrastructure and Development: XVI European Conference on Soil Mechanics and Geotechnical Engineering. 4800 p., Edinburgh, Skócia, 2015.09.13-2015.09.17. London: ICE Publishing, 2015. pp. 3401-3406., ISBN: 9780727760678

[5] Borbély, D. – Megyeri, T. – Görög, P. (2014): Numerical modelling of an underground low and medium level radioactive waste repository in fractured rockmass. In: Ioannis Bakogiannis (szerk.) 2nd Eastern European Tunnelling Conference: Tunnelling in a Challenging Environment, Athens, Görögország, 2014.09.28-2014.10.01. Paper o41. 10 p.

[6] Savov, K. – Lackner, R. – Mang, H. A. (2005): Stability assessment of shallow tunnels subjected to fire load, Fire safety journal, Vol. 40., pp. 10-11., ISSN: 0379-7112, https://doi.org/10.1016/j.firesaf.2005.07.004

[7] Ki-Il, S. – Gye-Chun, C. – Seok-Bue, C. – In-Mo, L. (2013): Beam–spring structural analysis for the design of a tunnel pre-reinforcement support system ,International Journal of Rock Mechanics and Mining Sciences, Vol. 59, pp. 139-150., ISSN: 1365-1609, https://doi.org/10.1016/j.ijrmms.2012.12.017

[8] Yong, Y. – Jianmin, Y. (2015): Some modifications to the process of discontinuous deformation analysis, Journal of Rock Mechanics and Geotechnical Engineering, Vol. 7, Issue 1, pp. 95-100., ISSN: 1674-7755, https://doi.org/10.1016/j.jrmge.2014.12.001

[9] Li, Z. – Kenichi, Z. – Fei, W. – Wright, P. – Kiwamu T., (2014): Behaviour of cast-iron tunnel segmental joint from the 3D FE analyses and development of a new bolt-spring model, Tunnelling and Underground Space Technology, Vol. 41, pp. 176-192., ISSN: 0886-7798, https://doi.org/10.1016/j.tust.2013.12.012

[10] Krivács, T. – Borbély, D. – Görög, P. (2015): Kőzetek rideg tönkremenetelének figyelembe vétele vágatstatikai számításokban. In: Török Á., Görög P., Vásárhelyi B. (szerk.), Mérnökgeológia - Kőzetmechanika 2015. 458 p., Budapest, Magyarország, 2015.02.04-2015.02.05., Hantken Kiadó, pp. 299-312., Mérnökgeológia - Kőzetmechanika Kiskönyvtár; 18, ISBN:978-615-5086-09-0

[11] Gál, E. – Görög, P. (2013): Lőttbetonos alagútfalazat és kőzet kapcsolatának vizsgálata gránitos kőzetkörnyezetben, In: Török Á, Görög P, Vásárhelyi B (szerk.), Mérnökgeológia-Kőzetmechanika 2013. 366 p. Budapest: Hantken Kiadó, 2013. pp. 165-176., Mérnökgeológia-Kőzetmechanika Kiskönyvtár; 16., ISBN:978-615-5086-06-9

[12] Fehérvári, S. (2007a): Alagúttüzek hatása a beton falazatra, Vasbetonépítés, Vol. 9.(2), pp. 56-62., ISSN 1419-6441, Onlie elérhetőség: http://www.fib.bme.hu/folyoirat/vb/vb2007_2.pdf

[13] Fehérvári, S. (2007b): Az alagúttüzek természetéről, Vasbetonépítés, Vol. 9.(1), pp. 13-17., ISSN 1419-6441, Onlie elérhetőség: http://www.fib.bme.hu/folyoirat/vb/vb2007_1.pdf

[14] Khattri, S. K. (2017): From small-scale tunnel fire simulations to predicting fire dynamics in realistic tunnels, Tunnelling and Underground Space Technology, Vol. 61, pp. 198-204, ISSN: 0886-7798, https://doi.org/10.1016/j.tust.2016.10.010

Ref.:
Csanády, Dániel – **Fenyvesi,** Olivér – **Megyeri,** Tamás: *Effects of tunnel-fire on load bearing capacity of tunnel-lining and surrounding rock mass. Part 2 (Sectional Calculation)*
Építőanyag – Journal of Silicate Based and Composite Materials, Vol. 72, No. 3 (2020), 99–105. p.
https://doi.org/10.14382/epitoanyag-jsbcm.2020.16

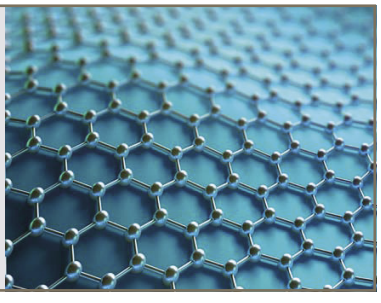

An investigation into practical values of sound transmission loss across natural luffa fibers

Hangátviteli veszteség gyakorlati értékeinek vizsgálata luffa szálakat tartalmazó közegben

Lamyaa Abd AL Rahman JAWAD
is a university teacher in Middle Technical University, Iraq. She has a Ph.D. in Mechanical Engineering from University Technology Malaysia. She teaches Vibration and Stress Analysis and has many researches in porous absorption materials and their acoustical characteristics.

Tawfeeq Wasmi M .SALIH
is a university teacher in Mustansiriyah University, Iraq. He has a Ph.D. in Mechanical Engineering. He teaches Insulation Materials and Heat Transfer and has many researches in renewable energies and energy efficient buildings.

Lamyaa Abd Alrahman JAWAD ▪ Health and Medical Technology College- Baghdad, Middle Technology University, Iraq ▪ lamyaeng@gmail.com
Tawfeeq Wasmi M. SALIH ▪ College of Engineering, Al-Mustansiriyah University, Iraq ▪ tawfeeqwesmi@gmail.com

Érkezett: 2019. 02. 29. ▪ Received: 29. 02. 2019. ▪ https://doi.org/10.14382/epitoanyag-jsbcm.2020.17

Abstract
Natural fibers could be used as sound insulation due to their advantageous acoustic properties. The main object of this study is to investigate the sound transmission loss (STL) of natural Luffa fibers (LF) due to their availability and sustainability where they would be a good choice instead of synthetic materials that have some health issues. The study has been done experimentally. The work has included a collection of LF from local gardens in Iraq, manufacturing of the specimens and measuring the STL using an impedance tube for selected samples: 20 mm of 970 kg/m3, 30 mm of 880 kg/m3 as well as 30 mm of 600 kg/m3. The effect of both thickness and density of the samples on the values of STL were studied. The results show that the increase of the thickness by adding 10 mm layer improved the STL value by 15-20 %. Also, the increasing of the density enhanced the sound insulation, where the STL value at 880 kg/m3 has improved by 30-40 % comparing to 600 kg/m3 for the same thickness (30 mm).
Keywords: sound transmission loss, acoustic insulation, natural fiber, luffa, sustainability
Kulcsszavak: hangátviteli veszteség, hangszigetelés, természetes szálak, luffa, fenntarthatóság

1. Introduction

Noise has many negative effects on humans including: nervous stress, sleep loss and hearing loss. In addition, acoustic waves may damage sensitive mechanical and electrical systems because of the corresponding vibration and fatigue. For these reasons, sound insulation materials are used to reduce the noise as well as to keep a certain range of calm.

There are two important terms describe the acoustic performance of a material which are the sound absorption and sound transmission loss. The sound absorption is the ability of a material to reduce sound reflections, reverberation, and echo within an enclosed space. While, the sound transmission loss (STL) is the ability of a material, panel, or wall to act as a barrier preventing airborne sound transmission from one space to another [1]. In this study, the sound transmission loss has taken into account where it provides an indication of the sound intensity stopped by a barrier for certain frequency. Insulation materials have the ability to reflect or absorb the sounds nearly at all frequencies [2-3].

Conventional acoustic insulators are evaluated depending on their fibrous construction and sizes of pores for their structure. Thus, most sound insulators are synthetic materials manufactured from combinations of minerals and plastics. Insulators made of synthetic materials, like glass wool, expanded polystyrene and polyurethane foams have many health side effects related to eyes and lungs. Hence, researchers have looked into natural materials and agricultural waste to find alternatives. These types of materials have many benefits as they are cheaper, nonabrasive and renewable. Also, organic substances impose less health and safety issues during processing [4, 5 and 6].

Luffa is a plant grows up in tropical and subtropical regions. It is available locally in Iraq and neighborhood countries, and the fruit is very fibrous so it is used as a scrubbing sponge, as shown in *Fig. 1*. In addition, Luffa usually grows up rapidly and profusely, where it requires 150 to 200 warm days to mature. The fibrous characteristic of Luffa is an encouraging factor of applying it as sound insulation and it would be a contribution to green technology.

Fig. 1 Luffa as a natural material: a) Local plant; b) Sponge shape of Luffa
1. ábra Luffa természetben megtalálható formái: a) termés; b) szivacsnak feldolgozva

2. Literature review

There is currently much interest in developing sustainable insulators, either from natural, biomass or even recycled materials. Natural materials, such as plant fibers could be used to satisfy comfortable environment free of undesired sounds. Many investigations have developed a wide range of natural porous materials, where these materials have shown a bunch of advantages such as availability and no side effects [6].

A study, conducted under the EU HOLIWOOD project a decade ago [7], has tested the performance of several possible absorbers made from natural materials like: cotton, flax and cellulose. Results were compared with those for conventional fiberglass, mineral wool and polymers where the natural materials show encouraged conclusions. The most effective natural absorber was the flax, while cotton fibers have very similar acoustic properties to fiberglass. Cellulose fibers are not attractive where they may be attacked by fungi and dampness.

Nor et al. [8] analyzed the effects of compressing porous layers of Coir fibers on its sound performance, which can be used for automotive applications. Moreover, Nor, et al. [9] investigated the effects of various factors of Coir fiber on acoustic absorption. The results indicated that layer thickness and fiber diameter have important effects on the absorptive behavior of Coir fibers.

Yang et al. [10] studied the acoustic performance of assembled fiber consisting of: cashmere, goose down and kapok. These natural materials had internal structures that influenced the sound absorption as measured against mass, air gap and sound frequency. These fibers showed a good performance at low to medium frequencies, where with low density and tiny diameter, these fibers have good absorption but their performance deteriorated at higher frequencies.

Deveikytė et al. [11] investigated the effectiveness of different configurations of straw and reeds with respect to frequency bands. In order to compare their effectiveness, the specimens of the same density had different thicknesses (5-20 cm). The noise reduction values were between (10-25 dB) within frequency bands range from (100-3150) Hz. The result indicated that thicker specimens have better sound insulation. However, straw and reeds are good at low frequencies, and they could therefore be used to make composite panels of both fibrous and porous panels [12].

Khair et al. [13] used Bamboo as natural material for sound absorption. The result revealed that it is a good sound absorber at high frequency above 3 kHz with a sample of 2 cm long. Improvement of absorption at lower frequency can be achieved by increasing the air gap at the back of the sample.

3. Experimental work

The experimental work included the collecting of LF from a local garden then using spinning machine to rip the fruit and product the raw material yarns. In order to manufacture the composite fibers, the raw material was grinded and peeled it to tiny strings and then mixed with the Urea-formaldehyde resin as a cohesive material. The additional mass due to the resin was 20% of the original mass for each sample. After mixing the fibers with the resin in a mold, the sample has been inserted in the compressing machine, where thermal treatment involving. The machine was running simultaneously to compact the composite under high temperature. The sample was covered by two plates upper and lower for an approximately 5-7 minutes under pressure of 170 kg/cm². *Fig. 2* shows the processes of the manufacturing.

Fig. 2 Processes of manufacturing the composite sample
2. ábra A kompozit anyag előállításának folyamata

Three typical samples have manufactured and tested according to ISO10534-2 in order to determine the effect of both density and thickness on the practical values of STL. The samples were: 20 mm of 970 kg/m³, 30 mm of 880 kg/m³ and 30 mm of 600 kg/m³, as shown in *Fig. 3*.

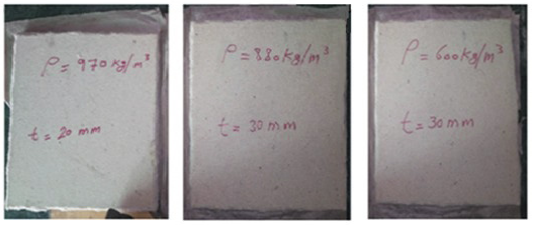

Fig. 3 Samples used in the study
3. ábra A kutatás során használt minták

Measurements of bulk density for the panels have evaluated by taking random set of individual fibers of Luffa and measuring the dimensions and physical properties using electronic microscopy of 50X magnification. Some captured photos of the selected fibers are shown in *Fig. 4*.

The selected panels have cut into circular shapes (100 mm and 28 mm for each panel) to fit the diameters of the impedance tubes, as shown in *Fig. 5*.

Measurements were conducted at Noise and Vibration Laboratory, UTHM University, Malaysia. The readings of STL values have obtained using an impedance tube instrument, as shown in *Fig. 6*. The device allowed the normal incidence acoustic field to flow through the fiber to reach a resonator. Each test was repeated three times to confirm the measurements data where the time that required acquiring the absorber's spectrum by the instrument took approximately 10 s with a resolution of 3.13 Hz. Furthermore, calibration process has been utilized for GRAS-42 AB microphone at calibrations sensitivity of 114 dB at 1 kHz.

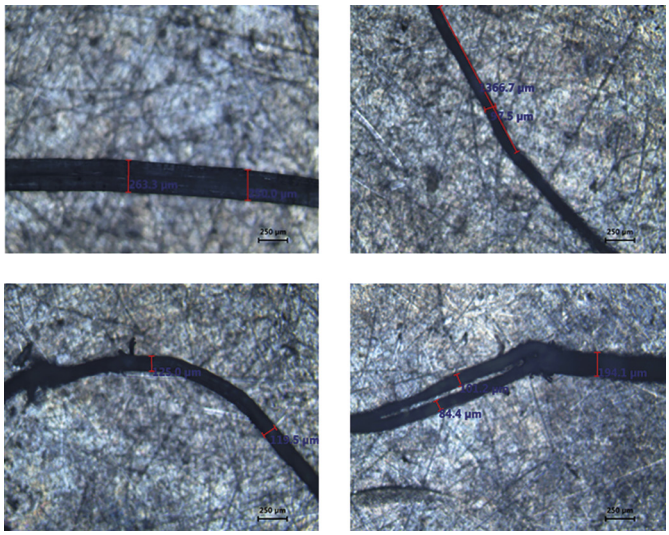

Fig. 4 Photos captured for some selected individual fibers
4. ábra Egyes kiválasztott szálakról készült felvételek

Fig. 5 Samples cut to circular shapes (100, 28 mm)
5. ábra Henger alakúra vágott minták (100 ill. 28 mm átmérő)

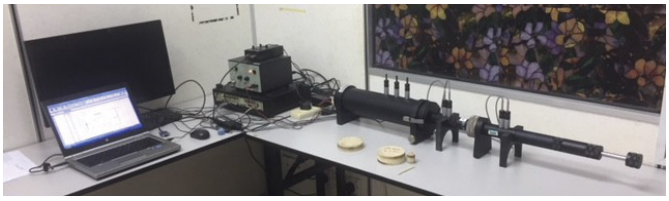

Fig. 6 Impedance tube instrument and setup system
6. ábra Impedancia meghatározására használt kísérleti összeállítás

4. Results and discussions

4.1 Effect of thickness

Fig. 7 illustrates the STL values of LF panels treated with Urea Formaldehyde for 20 mm (970 kg/m^3) and 30 mm (880 kg/m^3) at a range of frequencies from 50 Hz to 5000 Hz. The results show that the STL values of LF panels at 30 mm thickness shifted to up comparing to the 20 mm panel, thus indicated more reliability as a sound barrier. The 20 mm panel reached a maximum value of 24 dB at low frequencies (less than 1500 Hz) and 26 dB at high frequencies. The 30 mm panel (880 kg/m^3) reached a maximum value of 28 dB at low frequencies, and 30 dB at high frequencies. So in general, the increasing of the thickness improved the STL value by 15-20 %. A lack of measurement accuracy at frequencies between 1500 Hz and 2000 Hz was apparently marked, due to the combining of the data collected from both tubes in lower and higher frequencies that created unexpected sharp decline in STL curve. However, Luffa fibers (LF) may have less transmission loss in low to medium frequency ranges because the latex applied has not affected on the panel's inelasticity. The well mixing of fibers with sufficient amounts of air gaps may improve this problem to some extent [14].

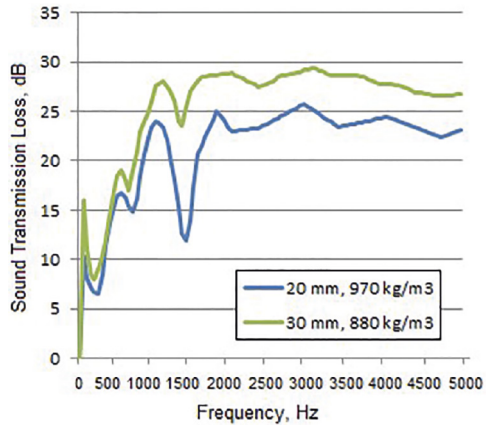

Fig. 7 Comparison of STL values for the effect of thickness
7. ábra Minta vastagság hatása az STL-értékekre

4.2 Effect of density

The STL values from experimental test for the densities (600 and 880 kg/m^3) of the same thickness panels (30 mm) are shown in *Fig. 8*. Maximum STL values at low frequencies were 19 dB and 28 dB for densities of 600 and 880 kg/m^3, respectively. Maximum STL values at high frequencies were 22 dB and 30 dB for densities of 600 and 880 kg/m^3, respectively. Thus, the STL values have been increased by increasing the value of the density, and in general, the increasing in STL value was 30-40% for current samples. In frequency ranges less than 500 Hz, the difference in STL values between the panels is unrecognized and that is attributed to the high acoustic resistance which leads to diminish sound transmission. Whereas at high frequencies, the improvement was recognized due to lose the ability of dissipation the high sound power.

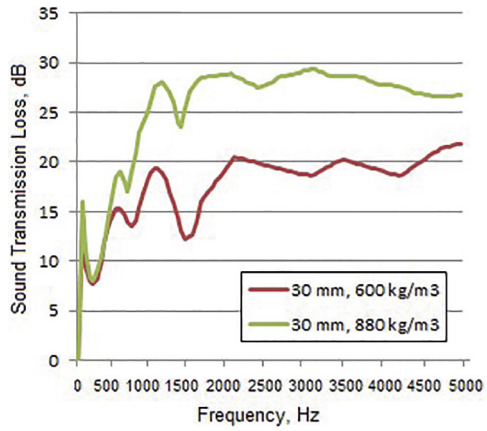

Fig. 8 Comparison of STL values for the effect of density
8. ábra Minta sűrűségének hatása az STL-értékekre

4.3 Sound transmission class

Plots of sound transmission loss are complex and are usually reduced to single number represent the sound transmission class (STC). To determine STC, the values of STL across a barrier could be compared at various frequencies, between 125 to 4000 Hz, to a standard contour. Then a standard curve could be plotted according to ASTM E413 over STL values where the value at 500 Hz is assigned as the STC [15]. The higher STC

value the better sound barrier. *Figs. 9*, *10* and *11*) show the STC values of the selected panels, where the results show that value of STC has increased from 13 dB to 15 dB due to the increasing of the thickness from 20 mm to 30 mm. Evidently, STC value for the higher density of 30 mm panel is increased comparing with the less density one, where it was 11 dB for 600 kg/m^3 panel and became 15 dB for 880 kg/m^3 panel.

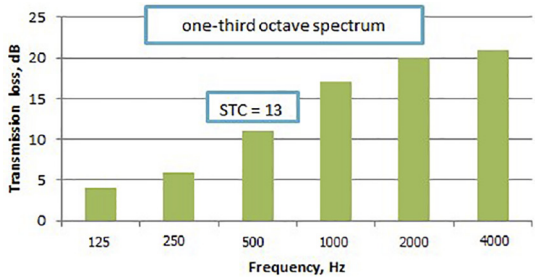

Fig. 9 STC for (20 mm, 970 kg/m^3) panel
9. ábra STC értékek a 20 mm vastag, 970 kg/m^3 sűrűségű minta esetén

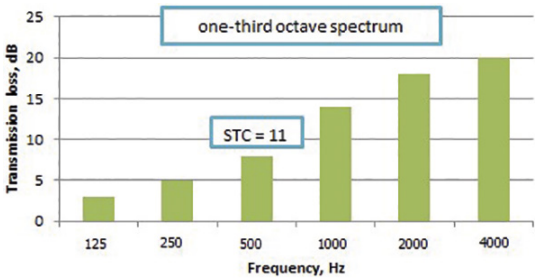

Fig. 10 STC for (30 mm, 880 kg/m^3) panel
10. ábra STC értékek a 30 mm vastag, 880 kg/m^3 sűrűségű minta esetén

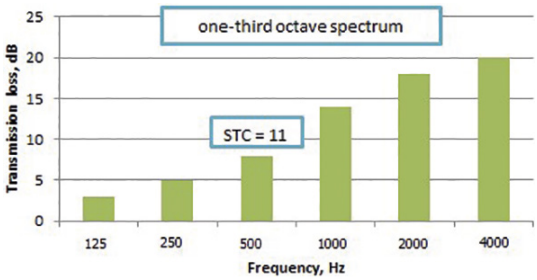

Fig. 11 STC for (30 mm, 600 kg/m^3) panel
11. ábra STC értékek a 30 mm vastag, 600 kg/m^3 sűrűségű minta esetén

5. Conclusions

The environmental concerns due to the utilization of petroleum resources, called to employ new eco-friendly materials for many applications. Among various natural materials, Luffa fibers (LF) have introduced as a matrix for sound insulation panels, where they have less environmental impacts, more economic advantage and no health side effect. The study has done experimentally by manufacturing Luffa composite panels and testing the sound transmission loss (STL) for selected samples. The effect of both density and thickness of the samples on the values of STL were studied. The results show that by increasing the thickness from 20 to 30 mm, the STL was improved by 15-20%. Also, the increasing of the density increases the STL value, where the STL value for 880 kg/m^3 panel improving by 30-40% comparing to 600 kg/m^3 panel for the same thickness (30 mm).

Acknowledgments

Author is grateful to all support given by: Malaysian Palm Oil Board (MPOB), Noise and Vibration Laboratory, Faculty of Mechanical and Manufacturing Engineering, UTHM University, Malaysia.

References

[1] Long, M. (2014): Architectural Acoustics. Second Edition, Academic Press; 2014.
[2] Rajiv, P. – Rajkishore, N. (2016): Acoustic Textiles, Springer, 2016
[3] Anand, N. – Kiran, M. C. – Varadarajulu, K. Ch. (2017): Influence of Density on Sound Absorption Coefficient of Fibre Board. Scientific Research Publishing, Open Journal of Acoustics, 7, 1-9, 2017, https://www.scirp.org/html/1-1610168_73876.htm.
[4] Ravindran, A. (2007): Investigation of Inverse Acoustical Characterization of Porous Materials Used in Aircraft Noise Control Application. Wichita State University, 2007, https://www.semanticscholar.org/paper/Investigation-of-inverse-acoustical-of-porous-used-Ravindran/43a31f27e399508e9fcd9f24d05158824af4ba37.
[5] Wang, C. N. – Torng, J. H. (2001): Experimental Study of the Absorption Characteristics of Some Porous Fibrous Materials, Applied Acoustics, 62(4): pp. 447-459, 2001, https://doi.org/10.1016/S0003-682X(00)00043-8.
[6] SCU (2011): Science for Environment Policy - Sustainable natural materials can be used for noise insulation. European Commission DG Environment News Alert Service, University of the West of England, 2011.
[7] Oldham, D. J. – Egan, C. A. – Cookson, R.D. (2011): Sustainable acoustic absorbers from the biomass. Applied Acoustics, 72: 350-363, 2011, https://doi.org/10.1016/j.apacoust.2010.12.009.
[8] Nor, M.J. et al. (2010): Effect of Compression on the Acoustic Absorption of Coir Fiber. American Journal of Applied Sciences, 7(9): pp. 1285, 2010, http://dx.doi.org/10.3844/ajassp.2010.1285.1290.
[9] Nor, M. J. et al. (2010): Effect of Different Factors on the Acoustic Absorption of Coir Fiber. Journal of Applied Sciences, 10: pp. 2887-2892, 2010, http://dx.doi.org/10.3923/jas.2010.2887.2892.
[10] Yang, S. – Yu, W. – Pan, N. (2011): Investigation of the Sound-Absorbing Behavior of Fiber Assemblies. Textile Research Journal, 81(7): pp. 673-682, 2011, http://dx.doi.org/10.1177/0040517510385177.
[11] Deveikytė, S. – Mažuolis, J. – Vaitiekūnas, P. (2012): Experimental Investigation into Noise Insulation of Straw and Reeds. Science–Future of Lithuania/Mokslas–Lietuvos Ateitis, 4(5): pp. 415-422, 2012, http://dx.doi.org/10.3846/mla.2012.67.
[12] Yang, H.-S. – Kim, D.-J. – Kim, H.-J. (2003): Rice Straw–Wood Particle Composite for Sound Absorbing Wooden Construction Materials. Bioresource Technology, 86(2): pp. 117-121, 2003, https://doi.org/10.1016/S0960-8524(02)00163-3.
[13] Khair, F. A. et al. (2014): Preliminary Study on Bamboo as Sound Absorber. Applied Mechanics and Materials, Trans Tech Publ., 2014, https://doi.org/10.4028/www.scientific.net/AMM.554.76.
[14] Ayub, M. et al. (2009): Analysis on Sound Absorption of Natural Coir Fiber Using Delany-Bazley Model", Proceedings of the International Conference on Mechanical Engineering, Dec. 2009, https://www.researchgate.net/profile/Md_Ayub/publication/283359223_Analysis_on_sound_absorption_of_natural_coir_fiber_using_delany-bazley.
[15] Khedari, J. et al. (2004): New Low-Cost Insulation Particleboards from Mixture of Durian Peel and Coconut Coir. Building and Environment, 39(1): pp. 59-65, 2004, https://doi.org/10.1016/j.buildenv.2003.08.001.

Ref.:
Jawad, Lamyaa Abd Alrahman – **Salih**, Tawfeeq Wasmi M.: *An investigation into practical values of sound transmission loss across natural luffa fibers*
Építőanyag – Journal of Silicate Based and Composite Materials, Vol. 72, No. 3 (2020), 106–109. p.
https://doi.org/10.14382/epitoanyag-jsbcm.2020.17

A comparative study of the modified phyllosilicate group of minerals isoprene for a new nanocomposite preparation

Izoprén ásványok módosított rétegszilikát csoportjának összehasonlító vizsgálata új nanokompozit fejlesztéséhez

Fayq Hsan JABBAR ▪ Department of Renewable Energy, College of Energy and Enviroment Science, Alkarkh University of Science, Iraq

Emad Abbas Jaffar AL-MULLA ▪ College of Health and Medical Techniques, Al-Furat Al-Awsat Technical University, Iraq

Wisam Hindawi HOIDY ▪ Department of Chemistry, College of Education, University of Al-Qadisiyah, Iraq ▪ wisam.hoidy@qu.edu.iq

Érkezett: 2019. 03. 09. ▪ Received: 09. 03. 2019. ▪ https://doi.org/10.14382/epitoanyag-jsbcm.2020.18

Abstract

In this study, new nanocomposites of biopolymers were prepared. Sunflower oil synthesized fatty amides (FA_{SF}), used as an organic compound to change the natural group of mineral clay phyllosilicate, sodium montmorillonite (Na- MMT) and potassium illite (K- ILT). The clay modification was accomplished by stirring the clay particles in an aqueous (FA_{SF}) solution which increases the clay layer distance from 1.28 to 2.79 nm of MMT and 1.18 to 1.33 nm of ILT because the action exchange capacity Na- MMT is much greater than the low cation exchange capacity K- ILT. The improved Na-MMT was then used as a natural rubber (NR) nanocomposite isoprene preparation. The modifier's interaction in the clay layer was defined by X- ray diffraction (XRD). The nanocomposite was synthesized through melt mixing of modified clay (MMT) and NR by a traditional method. Using XRD, transmission electron microscopy (TEM) and thermogravimetric analysis (TGA), the nanocomposite was characterized. The results of XRD and TEM verified nanocomposite growth. Compared to pure NR, NR modified MMT nanocomposites show higher thermal stability. FA_{SF} as a vegetable oil derivative to modify clay will reduce dependence on surfactants based on petroleum. Such nanocomposite is considered environmentally friendly in addition to renewable resources.

Keywords: natural rubber, nanocomposite, fatty amides, phyllosilicate

Kulcsszavak: természetes gumi, nanokompozit, zsírsavamidok, rétegszilikát

Fayq Hsan Jabbar

is a lecturer at College of Energy and Enviroment Science, Al-Karkh University for Science, Iraq; He has worked as a director of Research & Development and director of Graduate Studies at the above University, he has received his PhD from Sudan University of Science & Technology, Sudan in 2015. Previous positions: lecturer at Al- Mustansiriya University, Iraq, lecturer at Universities in Libya and director of the Consulting office in the Baghdad Provincial Council, Iraq ; main fields of interest : composite materials, biopolymer nano-composites, corrosion of metals, nanomaterials,; He has more than 5 publised papers in Scopus journals ; his H-Index = 4 according to Scopus database.

Emad Al-Mulla

is a Professor at College of Health and Medical Techniques, Al-Furat Al-Awsat Technical University, Iraq; He is currently Dean of Babylon Technical Institute at above University. He has received his PhD from University Putra Malaysia, Malaysia in 2010, He was a Post Doctoral researcher at the same University from April 2012 to April 2013; main fields of interest: biopolymer nano-composites, bioorganic synthesis, nanomaterials,; He has more than 60 published papers in Scopus and ISI journals; his H-Index = 16 according to Scopus database.

Wisam Hindawi Hoidy

is a Lecturer at Chemistry Department, College of Education, University of Al-Qadisiyah, Iraq;. He has received his Msc from University Putra Malaysia, and Ph.D from University of Al Qadisiyah; main fields of interest: Biochemistry, genetics, cancer, biopolymer nano-composites and bioorganic synthesis; He has more than 15 published papers in Scopus and ISI journals; his H-Index = 7 according to Scopus database.

1. Introduction

Thermoplastic elastomers are a class of rubber-like polymers, but can be treated as a thermoplastic polymer [1]. When combining rubbers and plastics, the most impressive results were obtained by the thermoplastic elastomers. The most suitable type of rubber for natural rubber producing countries are thermoplastic natural rubber among the different nonplastic rubbers. There have been several studies on processability and rheological properties in this field [2]. Clay (mineral phyllosilicate group) is one of the most commonly used non-black rubber fillers. It is a cheap natural mineral that was an important part of the rubber industry, it is used as an economical filler to adjust the processing and performance of natural and synthetic rubbers, but due to its large particle size and law surface operation, the strengthening ability of clay is small. The clay particles in the polymer matrix could only be spread on the microscale even though the clay consisted of layers of silicate with a planar structure of 1 nm thickness [3-4]. Through general methods of polymer production, the layers can not be isolated from each other. The most recent way to improve clay's enhancement potential is achieved by adjusting clays hydrophilic form to organophilic. This is achieved by replacing clay interlayer cations with organic cations like alkylammonium. Some researchers have been able to intercalate different polymers in the clay interlayer using modified clay to prepare polymer/clay nanocomposites [5,6]. For modification of Na- MMT and K-ILT, mixed fatty amides (FA_{SF}) synthesized with vegetable (sunflower) oil were used. Modified Na- MMT was used to prepare new nanocomposite rubber/clay and modified K-ILT was used to prepare new traditional composite rubber/clay. In this study, two forms of rubber composite's properties have been explored using the above group of minerals of phyllosilicate. With FA_{SF} as a modifier for production of rubber/MMT nanocomposite and rubber/ILT traditional composite [7], rubber/modified Na-MMT is more thermal stability was observed compared to those used rubber/ modified K-ILT.

2. Materials and Methods

2.1 Materials

Sunflower was obtained from Ngo Chew Hong Oils and Fats(M) Sdn. Phyllosilicate was from Novo Nordisk, Denmark's. Urea, sodium hydroxide, and hexane were purchased from Merck, Germany. The Malaysian Rubber Board (MRB),

Malaysia, kindly provided the natural rubber (NR) of SMR (CV60) grade. Both chemicals used were available in the highest purity.

2.2 Preparation of organoclay

Organoclay was made with a method of cationic exchange, where was Na^+, triacylglyceride synthesized (FA_{SF}) alkylammonium ion was shared in the MMT. The procedure was prepared as mentioned by Al-Mulla et al. [7,8]. In a watery solution, in 600 ml of hot distilled water, sodium montmorillonite (Na-MMT) (4.00 g) was vigorously stirred for 1 hour to form a clay suspension [9,10]. FA_{SF} (4.50 g) was then dissolved in 400 ml of hot water and concentrated hydrochloric acid (16.00 ml). After being vigorously stirred at 80 °C for 1 hour, the organoclay suspension was filtered and washed with distilled water until a 1.0M silver nitrate solution. It was dried for 72 hours at 60 °C. The mixture was ground until the particle size was 100 ml before the nanocomposite was prepared [11-13].

2.3 Preparation of NR/ modified clay

An internal mixer (Haake Poldrive) prepared the planned quality of NR. For the first time, the NR was softened for 1 minute and blended in the second and third minutes with the required amount of modified clay. The compounds were then molded for 10 minutes with a pressure of 150 Kg/cm^2 in an electrically heated hydraulic press at 130 °C. The compounds were immediately cooled for 5 minutes at the end of the molding cycle [14]. *Table 1* lists the quantity of NR and the modified clay used in this analysis.

Sample identity	Weight of NR (g)	Weight of modified clay (g)
NR modif.0	30.00	0.00
NR modif.1	29.70	0.30
NR modif.2	29.40	0.60
NR modif.3	29.10	0.90
NR modif.4	28.80	1.20
NR modif.5	28.50	1.50
NR modif.6	28.20	1.80

Modif.0, modif.1, modif.2, modif.3, modif.4 , modif.5 and modif.6 = 0, 1, 2, 3, 4 , 5 and 6 phr, respectively.

Table 1 *Weight of modified NR and clay (modified Na-MMT and K-ILT)*
1. táblázat *Természetes gumi és agyag (módosított Na-MMT és K-ILT) aránya az egyes mintákban*

2.4 Characterization

2.4.1 X-Ray diffraction (XRD) analysis

X-ray diffraction study was conducted using Shimadzu XRD 6000 diffractometer with CuK (k= 0.15406 nm) radiation.

2.4.2 Thermogravimetric analysis (TGA)

A Perkin Elmer model TGA7 Thermgravimetry analyzer was used to test the thermal stability of the samples. The samples were heated from 35 to 800 °C with a 10 °C/min heating rate under the atmosphere of nitrogen with 20 ml/min nitrogen flow rate.

2.4.3 Transmission electron microscopy (TEM)

The dispersion of clay has been analyzed using electron microscopy (EFTEM) for energy filtering transmission. TEM images were taken in a 120 KeV acceleration voltage LEO 912 AB EFTEM. The specimens were made using a cryomicrotome Ultracut E (Reichert and Jung). With a diamond knife at 120 °C, thin pieces of about 100 nm were sliced [7].

3. Results and discussion

3.1 X-ray diffraction measurements

X–ray diffraction technique was used to measure the distance of the silicate layers from the clay and alkyl ammonium cations from the interlayer. This has also been used to calculate the distribution of modified clays in the NR matrix by the silicate layers. *Table 2* indicates the alkylammonium (FA_{SF}-MMT and poorly modified FA_{SF}–ILT) interlayer gap of natural clay (Na-MMT) and modified clays [15]. The interlayer gap of Na- MMT for FA_{SF} – ILT and FA_{SF} – MMT has been extended from 1.18 nm to respectively 1.32 and 1.28 to 2.79 nm.

Type of clay	Exchange cation	2Ø (degree)	d-Spacing (nm)
Na-MMT	Na^+	6.88	1.28
FA_{SF} -MMT	$RCO\text{-}NH_3^+$	3.36	2.79
K-ILT	K^+	7.80	1.18
FA_{SF} –ILT	$RCO\text{-}NH_3^+$	6.45	1.32

Table 2 *X-ray diffractometer of unmodified MMT, ILT and modified MMT, ILT*
2. táblázat *Röntgen diffraktométeres mérési eredmények módosított és módosítatlan MMT és ILT esetén*

Table 3 summarizes the intercalated silicate layer in NR / unmodified MMT and NR / modified MMT nanocomposites obtained from the XRD study.

Composite/ clay	d-Spacing (nm)					
	1 phr	2 phr	3 phr	4 phr	5 phr	6phr
NR/Na-MMT	1.35	1.37	1.34	1.32	1.30	1.29
NR/ FA_{SF}-MMT	3.05	3.19	3.34	3.21	2.98	2.85
NR/K-ILT	1.22	1.23	1.25	1.21	1.20	1.19
NR/ FA_{SF}-ILT	1.36	1.37	1.38	1.39	1.36	1.33

Table 3 *XRD analysis of composites of NR / unmodified MMT, ILT and NR / modified MMT, ILT*
3. táblázat *Röntgendiffrakciós analízis eredményei: természetes gumi és módosítatlan MMT, ILT kompozitok valamint természetes gumi és módosított MMT, ILT kompozitok*

3.2 Thermo gravimetric analysis (TGA)

Fig. 1 shows the weight loss curves for K- ILT, Na- MMT, FA_{SF} – ILT, FA_{SF}–MMT, NR. NR/ 3phr K- ILT, NR/2phr Na- MMT and NR/ 4phr FA_{SF}–ILT microcomposite, NR/ 3phr FS_{SF}-MMT nanocompoositecontainingwaterduetohydratedsodiumcation (Na^+) intercalated inside the clay layers. The main difference between the unmodified clay thermogram and the organoclay thermogram is that the organic components in the organoclay decompose between 200 and 500 °C. As temperature rises 165 to 610 °C, the FA_{SF} decomposed. The cycle of decomposition at about 320 °C (*Fig. 1c*). It can be found that FA_{SF}–MMT decomposition temperatures (*Fig. 1e*) are higher than K- ILT (*Fig. 1a*), Na- MMT (*Fig. 1b*), pure FA_{SF} (*Fig. 1c*) and FA_{SF}- ILT

(*Fig. 1d*) temperatures. The increase in FA_{SF} decomposition temperatures in organoclays suggests a strong intermolecular interaction between the cations of alkylammonium and the clay. In other words, their decomposition temperature increases after the FA_{SF} ion is intercalated and bound to the clays silicate layers. Thermo gravimetric analyzes were also performed on the microcomposite NR / 3 phr K- ILT (Fig.1g), NR / 2 phr Na- MMT (Fig. 1h), NR / 4 phr FA_{SF} – ILT (Fig. 1i) and NR / 3 phr FA_{SF} – MMT (Fig. 1j) nanocomposite to assess the effect of unmodified nanocomposite, poorly changed clay (poor organoclay FA_{SF}–ILT) and altered clay material (organoclay FA_{SF} MMT) in the thermal properties rubber matrix, the TGA results are shown in (*Fig. 1f, g, h, i, j*). The onset of nanocomposite degradation is higher for NR containing FA_{SF} – MMT (*Fig. 1j*) at 375 °C compared to pure NR (Fig. 1f), NR / 3phr K- ILT (*Fig. 1g*), NR /2 phr Na- MMT (*Fig. 1h*), NR / 4 phr FA_{SF} – ILT (*Fig. 1i*) microcomposite, respectively at 265, 270, 285 and 290 °C.

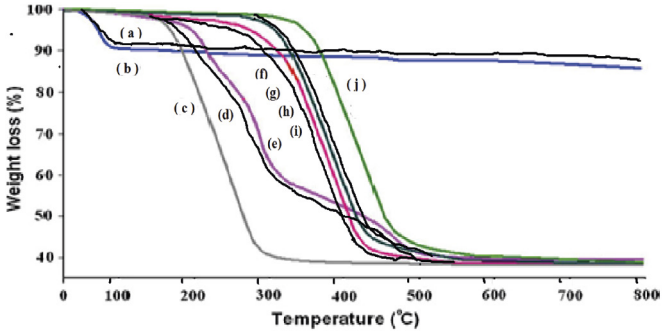

Fig. 1 TGA thermograms of (a): K-ILT, (b): Na-MMT, (c): FA_{SF} (d): FA_{SF}-ILT, (e): FA_{SF}-MMT, (f):NR, (g): NR/3phr K-ILT, (h): NR/2 phr Na-MMT , (i): NR/4 phr FA_{SF} –ILT, (j):NR/3 phr FA_{SF} –MMT

1. ábra Termogravimetriai vizsgálatok eredményei (TGA): (a): K-ILT, (b): Na-MMT, (c): FA_{SF} (d): FA_{SF}-ILT, (e): FA_{SF}-MMT, (f):NR, (g): NR/3phr K-ILT, (h): NR/2 phr Na-MMT , (i): NR/4 phr FA_{SF} –ILT, (j):NR/3 phr FA_{SF} –MMT

The results show that the thermal stability improves in (*Fig. 1j*) with the addition of the FA_{SF}–MMT, up to 3 phr loadings, and an increase above this percentage does not boost thermal stability. The presence of homogeneously dispersed silicate in the polymer surface obstructs the permeability of volatile degradation products from the substrate and helps to prolong nanocomposite degradation [16,17].

3.3 Transmission electron microscopy (TEM)

Fig. 2 shows transmission electron microscopy micrographs of NR composites supported by 4 phr FA_{SF} –ILT and 3 phr FA_{SF} –MMT. The FA_{SF} –ILT micrograph of NR/4 phr reveals that stack morphology is completely preserved in the NR matrix due to the incompatibility of both components (*Fig. 2a*). Dark bundles are the thickness of each layer of clay or agglomerates. Image, *Fig. 2b* shows TEM images of nanocomposites NR / 3 phr FA_{SF} –MMT showing good properties and composite effects. The dark bundles of the changed clay are scattered with an intercalated state in the NR matrix, which can be seen in the pictures [18]. *Table 3* displays the silicate interlayer gap of the clay layer from the XRD study .

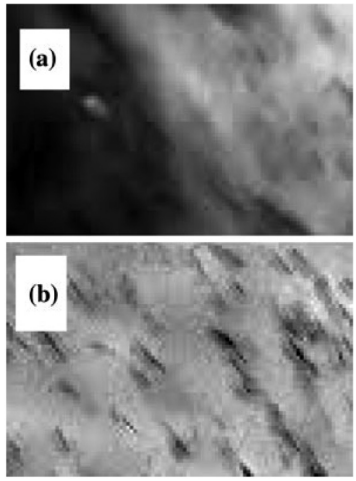

Fig. 2 TEM micrographs of (a): NR/4 phr FA_{SF} –ILT microcomposite and (b): NR/3 phr FA_{SF}-MMT nano-composite

2. ábra Transzmissziós elektronmikroszkóppal készített felvételek: (a): NR/4 phr FA_{SF} –ILT mikrokompozit és (b): NR/3 phr FA_{SF}-MMT nanokompozit

4. Conclusions

Sunflower oil synthesized fatty amides (FASF) have been used as an organic compound to modify the natural group of mineral clay phyllosilicates (Na-MMT & K-ILT). The presence of long chain fatty acids in FASF suggests that they should only be useful as surfactants to modify Na- MMT. Using modified MMT, new rubber / clay nanocomposites (nano- NR) were prepared. Rubber nanocomposites developed using FASF as a modifier display more thermal stability compared to microcomposites produced on the basis of poorly configured ILT with NR, these are considered environmentally friendly nanocomposites.

References

[1] Bohmic, A. K. – Stephens, H. L. (2001): Handbook of Elastomers. Marcel Dekker, New York.

[2] Homkhiew, C. –Rawangwong, S. – Boonchouytan, W. – Thongruang, W. – Ratanawilai, T. (2018): Composites from Thermoplastic Natural Rubber Reinforced Rubberwood Sawdust: Effects of Sawdust Size and Content on Thermal, Physical, and Mechanical Properties. Int J Polym Sci 1: 1-11. https://doi.org/10.1016/S0167-2738(99)00101-0

[3] Al-Mulla, E. A. J. (2011a): Polylactic acid/epoxidized palm oil/fatty nitrogen compounds modified clay nanocomposites: preparation and characterization. Korean J Chem Eng 28: 620–626. https://doi.org/10.1007/s11814-010-0373-6

[4] Al-Shemmari, F. H. J. – Al-Mulla, E. A. J. – Rabah, A. A. (2014): A comparative study of different surfactants natural rubber clay nano-composite. Rend Fis Acc Lincei 25: 409–413. https://doi.org/10.1007/s12210-014-0307-z

[5] Masoud, F. – Susan, D. – Zahra, S. – Mohsen, N. (2006): Gas barrier properties of PP/EPDM blend nanocomposites. J Mem Sci 282:142–148. https://doi.org/10.1016/j.memsci.2006.05.016

[6] Al-Mulla, E. A. J. (2011b): Preparation of new polymer nanocomposites based on poly (lactic acid)/fatty nitrogen compounds modified clay by a solution casting process. Fiber Polym 12: 444–450. https://doi.org/10.1007/s12221-011-0444-2

[7] Al-Mulla, E. A. J. – Yunus, W. M. Z. – Ibrahim, N. A. – Rahman, M. Z. (2010): Enzymatic synthesis of fatty amides from palm olein. J Oleo Sci 59: 59–64. https://doi.org/10.5650/jos.59.59

[8] Al-Shemmari, F. H. J. – Rabah, A. A. – Al-Mulla, E. A. J. – Abd Alrahman, N. O. M. (2013): Preparation and characterization of natural rubber latex/modified montmorilloniteclay nano-composite. Res Chem Intermed 39: 4293–4301. https://doi.org/10.1007/s11164-012-0946-6

[9] Hoidy, W. H. – Ahmad, M. B. – Al-Mulla, E. A. J. – Ibrahim, N. A. (2010): Chemical Synthesis and Characterization of N - hydroxy - N - methyl Fattyamide from Palm Oil. Orient J Chem 26(2):369-372. https://doi.org/10.1007/s10924-010-0240-x

[10] Hoidy, W. H. – Al-Mulla, E. A. J. (2013): Study of preparation for co-polymer nanocomposites using PLA/LDPE/CTAB modified clay. Irq Nat J Chem 79: 61-72. https://doi.org/10.1007/s10924-010-0240-x

[11] Al-Mulla, E. A. J. – Yunus, W. M. Z. – Ibrahim, N. A. – Ab Rahman, M. Z. (2010a): Epoxidized palm oil plasticized polylactic acid/fatty nitrogen compound modified clay nanocomposites: preparation and characterization. Polym Comp 18(8): 451–460. https://doi.org/10.1177/096739111001800806

[12] Al-Mulla, E. A. J. – Yunus, W. M. Z. – Ibrahim, N. A. – Rahman, M. Z. (2010b): Difatty acyl urea from corn oil: synthesis and characterization. J Oleo Sci 59(3):157–160. https://doi.org/10.5650/jos.59.157

[13] Hoidy, W. H. – Ahmad, M. B. – Al-Mulla, E. A. J. – Ibrahim, N. A. (2010b): Modification of montmorillonite by Difattyacyl thiourea using cation exchange process. Orient J Chem 26 (2): 409-414. https://doi.org/10.1007/s10924-010-0240-x

[14] Hoidy, W. H. – Al-Mulla, E. A. J. – Essa, S. M. (2019): Mechanical and Thermal Properties of Natural Rubber/Poly Lactic Acid/dioctadecyldimethylammonium bromide Modified Clay Nanocomposites. J Phys Conf 1234 (1): 1-12. https://doi.org/10.1088/1742-6596/1234/1/012085

[15] Al-Mulla, E. A. J. – Jabbar, F. H. – Kadhim, Z. J. – Abdullah, A. A. – Wadday, A. G. – Mlkat, S. M. (2017): Epoxized palm oil plasticized polycaprolactione nanocomposites preparstion. Nano Biomed Eng 9(3): 214-220. https://doi.org/10.5101/nbe.v9i3.p214-220

[16] Al-Mosawy, M. G. A. – Al-Mulla, E. A. J. – Mohamad, M. J. (2017): Bentonite-based organoclays using chalcone and azo dye as organophilic reagents. Építőanyag JSBCM 69(2): 49-54. https://doi.org/10.14382/epitoanyag-jsbcm

[17] Al Mutoki, S. M. M. – Al-Ghzawi, B. A. K. – Samir, A. M. – Al-Mulla, E. A. J. (2017): Raman shift of silicon rubber-nano titania PMNC. Építőanyag JSBCM 69(1): 20-23. https://doi.org/10.14382/epitoanyag-jsbcm

[18] Vu, Y. T. – Mark, J. E. – Pham, L. H. – Engelhardt, M. (2001): Clay nanolayer reinforcement of cis-1,4-polyisoprene and epoxidized natural rubber. J Appl Polm Sci 82: 1391–1403. https://doi.org/10.1002/app.1976

Ref.:
Jabbar, Fayq Hsan – **Al-Mulla**, Emad Abbas Jaffar – **Hoidy**, Wisam Hindawi: *A comparative study of the modified phyllosilicate group of minerals isoprene for a new nanocomposite preparation*
Építőanyag – Journal of Silicate Based and Composite Materials, Vol. 72, No. 3 (2020), 110–113. p.
https://doi.org/10.14382/epitoanyag-jsbcm.2020.18

Szomorú szívvel tudatjuk mindazokkal, akik ismerték és szerették,
hogy életének 93. évében elhunyt

Dr. Boksay Zoltán

kémikus, nyugalmazott egyetemi tanár,
az ELTE Természettudományi Kar egykori oktatási dékánhelyettese.

1927-ben született Budapesten. Középiskolai tanulmányait Kaposvárott és Budapesten végezte, majd 1950-ben szerzett okleveles vegyész diplomát az Eötvös Loránd Tudományegyetemen, ahol 1948-tól már hallgatóként is oktatott. 1971-1997 között egyetemi tanár, közben négy éven át dékánhelyettes az ELTE Természettudományi karán.

1953-tól 1973-ig fizikus hallgatóknak kémia főkollégiumot tartott, majd 1973-tól 1997-es nyugdíjazásáig vegyész hallgatóknak általános kémiát. Közben 1966-tól több speciális kollégiumi előadáson adta át tudását részben saját kutatási területéről, részben a kémia elvi problémáinak köréből választott témákban. Sok SZTE tagunk emlékezik nagy nosztalgiával a Veszprémi Egyetem 1981-1983. közötti szakmérnöki képzésére, melyen „Az üveg szerkezete és tulajdonságai" című nagysikerű előadássorozatával egy életre elhivatottá tette többségünket az üvegtudomány iránt.

1960-ban az MTA kémiai tudományok kandidátusa, majd 1970-ben az MTA doktora címet szerzett. Behatóan foglalkozott a középiskolai és az egyetemi kémiaoktatás összehangolásával és a permanens egyetemi reformokkal. Nyolc éven át volt az Oktatási Minisztérium Vegyész Szakbizottságának titkára. A hetvenes évektől nyugdíjazásáig az ELTE kémiatanári államvizsga bizottságának elnöke. A középiskolai kémiaoktatást a tanárok továbbképzésével és tankönyvírással segítette. Az Országos Középiskolai Tanulmányi Verseny Kémiai Bizottságának évtizedeken át volt elnöke.

Tudományos munkásságában különösen az üvegelektródokkal és az üveg elektromos vezetésének elméleti és kísérleti tanulmányozásával ért el nemzetközileg is számottevő eredményt.

Kezdetektől tagja volt az MTA Szilikátkémiai és az Elektroanalitikai Munkabizottságának. A tudományos minősítési eljárásokban gyakran szerepelt bíráló bizottsági tagként vagy elnökként, legtöbbször azonban opponensként.

78 cikkben foglalkozott kutatási eredményeivel, 1971-1996. között 26 tudományos beszámolót készített az üvegipar és üvegfelhasználók számára. 29 kémiai és oktatási tárgyú, továbbá 9 magyar nyelvészeti cikket írt. Egy szakkönyv és több tankönyv szerzője.

Számos kitüntetés birtokosa, köztük az ELTE Pro Universitate emlékérme és a Magyar Professzorok Világtanácsa Pro Universitate et Scientia kitüntetése is.

1999. óta a Szilikátipari Tudományos Egyesület örökös tagja, évtizedeken át, 2010-ig az Építőanyag folyóirat szerkesztőbizottságát segítette szaktudásával. Egyesületünk a Szilikátiparért Emlékérem adományozásával ismerte el kiemelkedő munkásságát.

2020. május 19-én búcsúzott el szeretett családjától.

Nyugodjék békében!
Emlékét szeretettel őrizzük szívünkben.

SZTE

GUIDELINE FOR AUTHORS

The manuscript must contain the followings: title; author's name, workplace, e-mail address; abstract, keywords; main text; acknowledgement (optional)**; references; figures, photos with notes; tables with notes; short biography** (information on the scientific works of the authors).

The full manuscript should not be more than 6 pages including figures, photos and tables. Settings of the word document are: 3 cm margin up and down, 2,5 cm margin left and right. Paper size: A4. Letter size 10 pt, type: Times New Roman. Lines: simple, justified.

TITLE, AUTHOR

The title of the article should be short and objective.

Under the title the name of the author(s), workplace, e-mail address.

If the text originally was a presentation or poster at a conference, it should be marked.

ABSTRACT, KEYWORDS

The abstract is a short summary of the manuscript, about a half page size. The author should give keywords to the text, which are the most important elements of the article.

MAIN TEXT

Contains: materials and experimental procedure (or something similar), results and discussion (or something similar), conclusions.

REFERENCES

References are marked with numbers, e.g. [6], and a bibliography is made by the reference's order. References should be provided together with the DOI if available.

Examples:

Journals:

[6] Mohamed, K. R. – El-Rashidy, Z. M. – Salama, A. A.: In vitro properties of nano-hydroxyapatite/chitosan biocomposites. *Ceramics International.* 37(8), December 2011, pp. 3265–3271, http://doi.org/10.1016/j.ceramint.2011.05.121

Books:

[6] Mehta, P. K. – Monteiro, P. J. M.: Concrete. Microstructure, properties, and materials. *McGraw-Hill*, 2006, 659 p.

FIGURES, TABLES

All drawings, diagrams and photos are figures. The **text should contain references to all figures and tables**. This shows the place of the figure in the text. Please send all the figures in attached files, and not as a part of the text. **All figures and tables should have a title**.

Authors are asked to submit color figures by submission. Black and white figures are suggested to be avoided, however, acceptable.

The figures should be: tiff, jpg or eps files, 300 dpi at least, photos are 600 dpi at least.

BIOGRAPHY

Max. 500 character size professional biography of the author(s).

CHECKING

The editing board checks the articles and informs the authors about suggested modifications. Since the author is responsible for the content of the article, the author is not liable to accept them.

CONTACT

Please send the manuscript in electronic format to the following e-mail address: femgomze@uni-miskolc.hu and epitoanyag@szte.org.hu or by post: Scientific Society of the Silicate Industry, Budapest, Bécsi út 122–124., H-1034, HUNGARY

We kindly ask the authors to give their e-mail address and phone number on behalf of the quick conciliation.

Építőanyag – *Journal of Silicate Based and Composite Materials*, Quarterly peer-reviewed periodical of the Hungarian Scientific Society of the Silicate Industry, SZTE.
http://epitoanyag.org.hu

European Materials Research Society

E-MRS now has more than 4,000 members from industry, government, academia and research laboratories, who meet regularly to debate recent technological developments of functional materials. The E-MRS differs from many single-discipline professional societies by encouraging scientists, engineers and research managers to exchange information on an interdisciplinary platform, and by recognizing professional and technical excellence by promoting awards for achievement from student to senior scientist level. As an adhering body of the International Union of Materials Research Societies (IUMRS), the E-MRS enjoys and benefits from very close relationships with other Materials Research organizations elsewhere in Europe and around the world.

23 RUE DU LOESS, BP 20 - 67037
STRASBOURG CEDEX 02, FRANCE
EMRS@EUROPEAN-MRS.COM
WWW.EUROPEAN-MRS.COM